

ANALYSIS OF FILM BREAK-UP AND DRY PATCH STABILITY

by

SARA GERSBERG de RODRIGUEZ

Lic. in Physics, University of Buenos Aires, 1969

A THESIS SUBMITTED IN PARTIAL FULFILMENT OF
THE REQUIREMENTS FOR THE DEGREE OF
MASTER OF APPLIED SCIENCE

in the Department

of

Mechanical Engineering

We accept this thesis as conforming to the
required standard

THE UNIVERSITY OF BRITISH COLUMBIA

August 1975

In presenting this thesis in partial fulfilment of the requirements for an advanced degree at the University of British Columbia, I agree that the Library shall make it freely available for reference and study. I further agree that permission for extensive copying of this thesis for scholarly purposes may be granted by the Head of my Department or by his representatives. It is understood that copying or publication of this thesis for financial gain shall not be allowed without my written permission.

Department of Mech. Engineering

The University of British Columbia
2075 Wesbrook Place
Vancouver, Canada
V6T 1W5

Date September 16, 1975

ABSTRACT

The stability of stationary dry patches in a thin, heated liquid film was analyzed according to previous models and compared with recent experimental data. Previous analysis indicate that dry patch stability is expressed in terms of a balance of forces at the upstream edge of the dry patch: a pressure force tends to rewet the dry patch, and the surface tension and thermocapillary forces causes the dry patch to spread. Roughly, the models are reduced to two types, the first evaluates pressure force applying a Bernoulli-type equation to the center-streamlines, the second uses the control-volume approach. The former method gives half the pressure force predicted by the second model; in both analyses the flow is considered one-dimensional. In the present study the contradiction was clarified by applying the control volume technique to a two-dimensional flow. Both methods give equivalent results for the limiting case of control volume coinciding with the center streamline.

When experimental data are used the model that proposes a Bernoulli-type equation to find pressure force best describes the balance of forces, specially for low Reynolds numbers. For high Reynolds numbers pressure forces depart significantly from surface forces.

In the present study the force balance criterion for stability of dry patches was extended to the case of a wavy film. Kapitza's analysis for surface waves on thin film was used and the bi-dimensional character of the flow was considered through the introduction of a coefficient whose value was assumed equal to the steady case. Results show that a body force must be included together with pressure force to balance surface tension force. A better description of the flow field is needed since Kapitza's analysis is not valid near the dry patch.

A further model is presented by means of which film profiles and pressure forces can be evaluated. The goal was to describe flow behaviour of a thin heated film around a dry patch. Due to the complexity of the problem different assumptions at various stages were made. The problem was divided into two regions, similar to a boundary layer method. In the outer region surface tension effects were neglected and the patch acts like a solid object for the flow. Increases in stagnation pressure are balanced by changes in hydrostatic pressure. In the inner region surface tension effects predominate over inertial effects. The free surface profiles, valid for a narrow range of low Reynolds numbers, are wedge-shaped and different from measured profiles. In future work surface tension effects in the outer region must be included and the solution extended to a larger range of Reynolds numbers.

TABLE OF CONTENTS

Chapter		Page
1.	INTRODUCTION	1
2.	REVIEW OF LITERATURE	5
	2.1 General	5
	2.2 Thin Film Flow	5
	2.2.1 Laminar Film Flow	6
	2.2.2 Turbulent Film Flow	7
	2.2.3 Wavy Film Flow	8
	2.3 Stability of Dry Patches	11
	2.3.1 Steady Case	11
	2.3.2 Unsteady Case	20
	2.4 Contact Angle	24
3.	COMPARISON WITH EXPERIMENTS OF PREVIOUS STABILITY MODELS AND SOME SIMPLE EXTENSIONS	28
	3.1 Discussion of McAdam's Experiments	28
	3.2 Relationship Between Various Models	30
	3.3 Comparison of Previous Models With Data	31
	3.3.1 General	31
	3.3.2 Low Re	34
	3.3.3 High Re	37
	3.4 Simple Extensions	39
	3.4.1 Simple 2-D Extensions	39

Chapter	Page
3.4.2 Re-laminarization Effects	41
3.5 Discussion	42
3.5.1 Balance of Forces	42
3.5.2 Role of Thermocapillarity	44
3.6 Summary	46
4. UNSTEADY EFFECTS	48
4.1 Evaluation of α	52
5. A RATIONAL TWO-DIMENSIONAL MODEL	56
5.1 General	56
5.2 Solution	58
5.2.1 Outer Region	58
5.2.2 Inner Region	66
5.3 Discussion	69
6. SUMMARY AND CONCLUSIONS	73
FIGURES	76
REFERENCES	103
APPENDIX A - EVALUATION OF THE SHEAR FORCE AND BODY FORCE FOR A KAPITZA VELOCITY PROFILE	107
APPENDIX B - DEVELOPMENT OF THE SIMPLIFIED NAVIER-STOKES EQUATIONS USED IN CHAPTER 5	112
APPENDIX C - PROPERTIES OF CARBON DIOXIDE	120

LIST OF TABLES

Table		Page
3.1	Evaluation of Pressure Forces and Surface Forces according to Zuber & Staub at low Re	34
3.2	Evaluation of Pressure Forces According to Ponter <i>et al.</i> at low Re	35
3.3	Evaluation of Pressure Force, Body Force and Surface Tension Force According to Wilson	35
3.4	Evaluation of Pressure Forces and Surface Forces at High Re	38
3.5	Evaluation of Pressure Forces and Surface Forces When the 1/7 Power Law is Used at Low Re	42
4.1	Evaluation of Pressure Force and Surface Tension Force When the Control-Volume Method is Applied to a Wavy Liquid Film	53
4.2	Evaluation of Pressure Forces and Surface Forces When the Thickness Criterion is Applied to a Wavy Film	54
5.1	Evaluation of Pressure Force According to Model Described in Chapter 5	71

LIST OF FIGURES

Figure	Page
1. Some mechanisms of film break-up	76
2. Nuclear power plant	77
3. Flow boiling regimes, upward flow	78
4. Dry patch on a solid surface	79
5. Forces acting at a dry patch (Ref. 22)	80
6. Annular flow with waves (Ref. 26)	81
7. Triple front position during two waves for different values of heat fluxes (Ref. 26)	82
8a. A liquid drop on a horizontal plate	83
8b. Hysteresis of the contact angle.	83
9. A drop on a tilted plate	84
10. Variation of apparent contact angle due to surface roughness	85
11. Film profiles for different times, $T=2^{\circ}\text{C}$, $Re=185$, (Ref.1). .	86
12. Contact angle variation with time, $T=2^{\circ}\text{C}$, $Re=185$, (Ref.1). .	87
13. Film profiles for different times, $T=2^{\circ}\text{C}$, $Re=310$, (Ref.1). .	88
14. Contact angle variation with time, $T=2^{\circ}\text{C}$, $Re=310$, (Ref.1). .	89
15. Film profiles for different times, $T=2^{\circ}\text{C}$, $Re=940$, (Ref.1). .	90
16. Contact angle variation with time, $T=2^{\circ}\text{C}$, $Re=940$, (Ref.1). .	91
17. Average contact angle versus input Reynolds No.	92
18. Average contact angle versus local Reynolds No.	93
19. Scheme of a two dimensional flow around a dry patch. The dash lines indicate the control volume used	94

Figure	Page
20. Pressure forces according to different models	95
21. Comparison of the total surface force ($F_o + F_{th}$) according to Zuber and Staub with the surface force without thermal effects (F_o)	96
22. Difference between pressure force and surface force according to Zuber and Staub model for low Re (circles). Difference between pressure force and surface forces when the 1/7 power law is used as a velocity profile (squares).	97
23. Difference between pressure force and surface forces for high Re	98
24. Comparison of the pressure force according to the two dimensional model with Zuber and Staub criterion, Inlet temperature = 2°C	99
25. Scheme of the film surface profile in the vicinity of a dry patch on an inclined plate	100
26. Film thickness profile according to model described in Chapter 5	101
27. Film thickness profile according to model described in Chapter 5	102
28. Density of saturated CO ₂ liquid versus temperature	120
29. Density of saturated CO ₂ vapor versus temperature	121
30. Thermal conductivity CO ₂ versus temperature	122
31. Surface tension of liquid CO ₂ versus temperature	123
32. Dynamic viscosity of CO ₂ versus temperature	124
33. Latent heat of CO ₂ versus temperature	125
34. Vapor pressure of CO ₂ versus temperature	126

ACKNOWLEDGEMENTS

I would like to express my sincere thanks and appreciation to my supervisor, Dr. E.G. Hauptmann for his help and advice throughout the project. Also I would like to thank Dr. D.W. McAdam for sharing with me his experimental data and his knowledge of the subject.

This work was sponsored by the National Research Council of Canada.

NOMENCLATURE

a	distance from origin to source and sink, (m)
a_c	radius of collar, (m)
A	aspect ratio of body
b	width of body, (m)
c	thickness of a collar, (m)
C	phase velocity, (m/s)
d	width of a collar, (m)
F_B	body force, (N/m)
F_p	pressure force, (N/m)
F_s	shear force, (N/m)
F_σ	surface tension force, (N/m)
F_{th}	thermocapillary force, (N/m)
Fr	Froude number, $\frac{\bar{u}}{(\rho g)^{1/2}}$
g	acceleration due to gravity, (m/s^2)
h	film thickness in presence of waves, (m)
$h_{\ell g}$	latent heat of vaporization, (J/kg)
h_0	average thickness of a wavy film, (m)
h_p	wave peak thickness, (m)
k	wave number, $\frac{2\pi}{\lambda}$, (m^{-1})
k_t	thermal conductivity, ($W/m \cdot ^\circ C$)
K	total radius of curvature, (m)
l	heated plate length, (m)
L	length of body, (m)

m	source and sink strength, (m^2/s)
p	pressure, (N/m^2)
p_B	pressure at the bottom of the plate, (N/m^2)
Q	heat flux, (W/m^2)
r	dimensional coordinate (m)
r^*	dimensionless coordinate
R	radius of curvature of dry patch, (m)
Re	Reynolds number, $\frac{\rho \bar{u} \delta}{\mu}$
Re_i	input Reynolds number
t	time, (s)
T	temperature, ($^{\circ}C$)
T_i	interface temperature, ($^{\circ}C$)
T_p	plate temperature, ($^{\circ}C$)
u, v, w	dimensional velocities, (m/s)
u^+	u/u^x dimensionless velocity
u^x	$\sqrt{\tau_0/\rho}$, (m/s)
u^*, v^*, w^*	dimensionless velocities
\bar{u}	average velocity, (m/s)
u_1, v_1, w_1	reference velocities, (m/s)
u_T, w_T	maximum velocities at $y = \delta$, (m/s)
u_0	velocity at average stream cross-section h_0 , (m/s)
\bar{U}	uniform velocity equal to the average velocity of a parabolic profile, (m/s)
U_T	uniform velocity equal to the maximum velocity of a parabolic profile, (m/s)

We	Weber number, $\rho u^2 \delta / \sigma$
x, y, z	dimensional coordinates, (m)
x^*, y^*, z^*	dimensionless coordinates
x_s	coordinate of stagnation point, (m)
y^+	dimensionless coordinate, $\frac{y u^x}{\nu}$
z_0	width of control volume, (m)

Greek Symbols

α	angle of inclination of the plate, ($^\circ$)
α (Chapter 4)	ratio of total momentum flux in the x direction to input momentum flux
δ	film thickness, (m)
δ_c	critical film thickness, (m)
δ_M	maximum film thickness, (m)
δ^+	dimensionless film thickness, $\frac{\delta u^x}{\nu}$
Γ	flow rate, (kg/m \cdot s)
Γ_c	critical flow rate, (kg/m \cdot s)
Γ_e	flow rate that evaporates, (kg/m \cdot s)
λ	wavelength, (m)
μ	dynamic viscosity (kg/m \cdot s)
ν	kinematic viscosity, (m ² /s)
ω	wave circular frequency, $\frac{2\pi}{T}$, (s ⁻¹)
ρ	liquid density, (kg/m ³)
ρ_v	vapour density, (kg/m ³)
σ	surface tension, (N/m)

θ	contact angle, ($^{\circ}$)
θ_A	static advancing contact angle, ($^{\circ}$)
θ_R	static receding contact angle, ($^{\circ}$)
θ'_A	contact angle at the leading edge of a drop, ($^{\circ}$)
θ'_R	contact angle at the rear, ($^{\circ}$)
τ	wave period, (s)
τ_i	shear stress at the interface, (N/m^2)
τ_0	shear stress at the wall, (N/m^2)

Supra Index

min	minimum
av	average
max	maximum

1. INTRODUCTION

In systems cooled with a fluid which can change phase, the wall-to-liquid heat transfer coefficient is high where the wall and liquid are in direct contact. Where this contact is not maintained the heat transfer coefficient may be considerably reduced causing a rise in the surface temperature. The rise in temperature can lead to melting or rupture of the metal surfaces. As the wettability of the surface by the liquid is of a critical importance, dry spot formation must be prevented.

There is little information concerning the detailed formation of dry spots or dry patches. One mechanism of dry patch formation is when the free surface is subject to a local temperature variation (Figure 1). Surface tension, σ , of the liquid changes from point to point and tangential forces may be exerted producing a bulk movement of the liquid from lower to higher surface tension regions (Marangoni effects). For example when film thickness is not uniform (due to waves) the surface temperature is higher in thinner regions and lower in thicker regions. Generally, for liquids surface tension decreases with temperature and there is a net motion of liquid from thinner regions (low σ) to thicker regions (high σ) and film destruction can occur. Even in case of evaporation at the interface, some departure from the thermodynamic equilibrium is possible, therefore, free surface temperature can be different from saturation temperature at that pressure, and Marangoni effects can still be present. In the case

of mass transfer, changes in concentration produce variations of surface tension which in turn can produce motion on the fluid leading to film destruction.

Nucleation (bubble formation) is another possible cause of film break-up. Film thickness underneath each bubble is reduced and locally destroyed. If the bubble stays on the wall for a sufficiently long time, the dry area at the base of the bubble spreads.

Liquid film break-up can be present in boiling water-cooled reactors (Figure 2). This phenomenon is called dryout. When a sub-cooled fluid enters a heated tube, a flow regime called annular flow can appear (Figure 3). In this regime the wall of tube is covered by a thin liquid film, while the centre of the tube has vapour moving at a higher velocity. If the film breaks up, dryout occurs with the consequent decrease in the heat transfer coefficient. As most reactor systems operate with constant heat flux, the resultant temperature rise is often sufficient to melt the fuel rod or induce corrosion.

McAdam [1] observed film break-up in a thin liquid film of CO_2 flowing under gravity over a heated plate. Thermocapillary effects (variation of σ with T) and evaporation at the interface were the main mechanisms for the formation of dry patches in his tests. Nucleation did not occur in these experiments because the system was not sufficiently superheated to produce bubbles.

In order to better understand how to prevent formation of dry patches, some workers have tried to describe the flow behaviour

around those dry areas. Some mathematical models are available in the literature describing the flow behaviour near the vertex of a dry patch (Figure 4). No consideration of the lateral flow, that is, the flow that diverts around the dry patch is taken into account. The "static" stability of a dry patch is expressed in terms of a balance of forces at the upstream edge of the dry patch: a pressure or stagnation force tends to rewet the dry patch, and the surface tension and thermocapillary forces cause the dry patch to spread.

The scope of the present study is to critically examine existing models to see how they agree with recent experimental data recorded by McAdam, and make some suggestions for a better understanding of the flow behaviour in order to prevent the formation of dry spots.

As a first step, Chapter 2 includes a review of literature of those aspects related to dry patch stability. Chapter 3 consists of a selection of criteria for stability of dry patches. McAdam's data are analyzed and the different criteria are checked. The results and limitations of the previous models are discussed. As a first modification to the previous models a new model is proposed to evaluate the magnitude and consequence of the flow that diverts around the dry patch. The model proposes an ideal flow around a body whose shape is similar to the shape of a dry patch so that velocities and pressure forces can be evaluated.

McAdam's results show that the contact angle and film thickness change with time even though the dry patch is stationary. Surface waves are responsible for this variation and can produce a range of

contact angles and film thicknesses before the patch rewets or retreats. This effect is not accounted for in previous models. The forces acting on the upstream edge of the dry patch in the presence of waves are evaluated using the momentum theorem in Chapter 4, assuming that the wave pattern can be described by Kapitza's analysis.

Chapter 5 presents an approximate solution for the increase in thickness which occurs just upstream of a dry patch. For simplicity the situation considered is a slightly inclined plate, with stagnation pressure balancing the increase in hydrostatic pressure arising from the increase of film thickness near the dry patch. For a vertical plate, increase in stagnation pressure is balanced by changes in curvature of the free surface. Although contact angles on an inclined plate are probably lower than those for an equivalent flow on a vertical plate the differences are expected to be small. Thus estimates of pressure forces from an inclined model may be used as a rough check against McAdam's data. A calculation of type is done and results are discussed.

2. REVIEW OF LITERATURE

2.1 General

The stability of a dry patch has been analyzed by several investigators to predict conditions under which the dry patch remains stable. This criterion is usually obtained by a force balance at the upstream stagnation point of a dry patch. The main forces are pressure force, surface tension force, and thermocapillary force developed as a result of the variation of surface tension with surface temperature. This approach takes into account the contact angle, the flow behaviour far from the dry spot, the thickness of the film, changes in temperature of the free surface and the physical properties of the liquid-vapour system. Details of the flow and temperature fields around the dry spot are not considered, except in the vicinity of the "nose" of the dry patch. Some papers deal with experimental observations of dry patches and their stability [2], [3], [4] others [5], [6] attempt theoretical descriptions, while some workers [7] [8] have tested the criteria against experimental data. In what follows, the fluid-flow regions are roughly classified for convenience as thin film, laminar, turbulent, and wavy flow.

2.2 Thin Film Flow

To understand the previous models it is necessary to review flow in thin films. Because of their many industrial applications

they are a subject of continuous study. Various regimes of thin film flow can be distinguished and because of the presence of a free surface, the classification of the regimes must take into account surface tension and viscous effects. Thus Reynolds number Re , Weber number We , and Froude number Fr , are the most useful dimensionless physical quantities for flow pattern classification. Film flow can be subdivided into laminar or turbulent regimes depending on whether Re is smaller or larger than a critical Re . In addition, the free surface may be smooth or wavy depending on Fr and We . It has been shown [9] that gravity waves first appear in a water film when $Fr = 1-2$ and capillary surface effects become important in the neighbourhood of $We = 1$. Thin film flow can be classified as follows [10]:

laminar without rippling	$Re < 1$ to 6
laminar with rippling	$6 < Re < 250$ to 500
turbulent	$Re > 250$ to 500 .

Studies [11,12] that are still the subject of discussion, indicate $Re = 0$ for inception of laminar instability during flow down a vertical surface. It should be noted that the presence of waves does not necessarily mean the flow is turbulent.

2.2.1 Laminar Film Flow

When a liquid film flows under gravity on a vertical plate shear forces at the interface can be neglected. Nusselt [13] obtained the fully developed velocity profile for a steady, viscous flow with no shear or wave motion at the free surface as

$$u = u_T \left(\frac{2y}{\delta} - \frac{y^2}{\delta^2} \right), \quad u_T = u(y = \delta) \quad \dots (2.1)$$

Under these approximations the flow rate

$$\Gamma = \rho \frac{2g\delta^3}{3\mu} \quad \dots (2.2)$$

These velocity profiles were confirmed by Dukler [14], Cook and Clark [15] among others.

If the width of the flow channel is finite, additional terms arising from viscous edge effects, drag and capillary forces modify the former simplified formulas.

2.2.2 Turbulent Film Flow

Although no theories exist on thin film flow for the turbulent regime, Dukler and Bergelin [14] developed a simplified relation between film thickness and pressure drop, assuming that the universal velocity profile developed by Von Karman for pipes applies to the liquid phase in two-phase film flow. Their results are

$$u^+ = y^+, \quad 0 < y^+ < 5 \quad (\text{laminar sublayer})$$

$$u^+ = -3.05 + 5.0 \ln y^+, \quad 5 < y^+ < 30 \quad (\text{buffer layer}) \quad \dots (2.3)$$

$$u^+ = 5.5 + 2.5 \ln y^+, \quad 30 < y^+ < \delta^+ \quad (\text{turbulent zone})$$

where $u^+ = u/u^x$

$$y^+ = yu^x/\nu$$

$$\delta^+ = \delta u^x/\nu \quad (\text{dimensionless film thickness})$$

and

$$u^* = (\tau_0/\rho)^{1/2} \quad (\text{friction velocity}).$$

By integrating the dimensionless velocities over the film thickness Dukler and Bergelin found the relationship between Re and δ^+ to be

$$Re = \delta^+(3 + 2.5 \ln \delta^+) - 64 \quad \dots (2.4)$$

For flow down a vertical plate without shear at the interface [14]

$$\delta^+ = \frac{g^{1/2} \rho \delta^{3/2}}{\mu} \quad \dots (2.5)$$

An expression [16] for the velocity profile in the turbulent zone that fits the experimental data well and is easier to handle is

$$u = u_T (y/\delta)^{1/7} \quad \dots (2.6)$$

2.2.3 Wavy Film Flow

Between the smooth laminar and turbulent regimes the flow is characterized as laminar flow with surface waves. This region has been studied by many workers [11], [17], [18]. Determining the Re for the inception of wavy flow is the subject of study of many investigators [19]. For vertical plates, the onset of waves occurs at very low Re . The Kapitza [17] treatment of wavy film flow predicts an inception $Re = 5.8$ for water on a vertical wall, but is only valid

for long wavelengths with respect to mean film thickness.

Benjamin [11] presented a detailed treatment of the onset of a two-dimensional (2-D) instability in thin film flow considering capillary effects. He found that for vertical plate the inception Reynolds number is equal to zero. Castellana and Bonilla [12] also found Reynolds number is equal to zero for wave inception.

For the case of a wavy film flow on a vertical wall, Levich [18] has shown that the complete Navier-Stokes equations can be reduced to the familiar form of the boundary layer

$$\frac{\partial u}{\partial t} + u \frac{\partial u}{\partial x} + v \frac{\partial u}{\partial y} = -\frac{1}{\rho} \frac{\partial p}{\partial x} + \nu \frac{\partial^2 u}{\partial y^2} + g \quad (\text{a})$$

$$\frac{\partial p}{\partial y} = 0 \quad (\text{b}) \quad \dots \dots (2.7)$$

$$\frac{\partial u}{\partial x} + \frac{\partial v}{\partial y} = 0 \quad (\text{c})$$

At $y = h(x)$ the boundary conditions at the free surface must be satisfied

$$p = p_{\sigma} \approx -\sigma \frac{\partial^2 h}{\partial x^2} \quad \dots \dots (2.8)$$

$$\mu \frac{\partial u}{\partial y} = 0 \quad \dots \dots (2.9)$$

At the solid wall $y = 0$

$$u = v = 0 \quad \dots \dots (2.10)$$

As $v \sim \frac{\partial h}{\partial t}$ at the free surface the continuity equation can be expressed

$$\frac{\partial h}{\partial t} = - \frac{\partial}{\partial x} \left(\int u dy \right) \quad \dots (2.11)$$

Kapitza was the first to attempt a solution of this system. In his analysis the term $v \frac{\partial u}{\partial y}$ in equation (2.7a) was omitted. It was assumed that the velocity distribution in the film could be given by the usual parabolic expression of the form

$$u = 3 \bar{u}(x,t) \left\{ \frac{y}{h} - \frac{y^2}{2h^2} \right\} \quad \dots (2.12)$$

Here $\bar{u}(x,t)$ is the average velocity over the cross-section and is a function of the position along the film and time. Kapitza assumed that film thickness could be represented by $h = h_0 + h_0 \psi$, where h_0 is the average film thickness and $h_0 \psi$ is the deviation of the surface from that average. He also assumed that for undamped waves, quantities like film thickness and average liquid velocity are functions of the argument $(x - Ct)$ where C is the phase velocity of the waves. With these conditions, by substituting u in Equations (2.7a) and (2.11) Kapitza obtained a first, undamped approximate solution for the thickness h_0 closely related to Nusselt's formula for laminar flow. In this approximation the phase velocity is $C = 3 u_0$ where u_0 is the velocity at average stream cross section h_0 . In a second approximation Levich [18] followed Kapitza's method and carried out an analysis of the wavy flow to determine the condition under which the energy supplied

to the film by gravity forces was balanced by the dissipation of energy by viscous forces. In this context it was found

$$h_p = h_0 \quad (1.46)$$

h_p : thickness of a peak

$$C = 2.4 u_0$$

$$\frac{h_0}{\delta} = 0.93$$

h_0 : mean film thickness with waves

δ : smooth film thickness at the same flow rate.

$$\lambda = \frac{2\pi}{u_0} \left\{ \frac{\sigma h_0}{\rho \cdot 2.1} \right\}^{1/2}$$

The expression for the velocity field was found to be

$$u(x,y,t) = 3 u_0 [1 + 0.6 \sin(kx-\omega t) - 0.3 \sin^2(kx-\omega t)] \left(\frac{y}{h} - \frac{y^2}{2h^2} \right) \dots (2.13a)$$

$$v(x,y,t) = -1.8 u_0 k \cos(kx-\omega t) [1 - \sin(kx-\omega t)] \left(\frac{y^2}{2h} - \frac{y^3}{6h^2} \right) \dots (2.13b)$$

Both Kapitza's and Levich's results are valid under the condition that $\lambda > 13.7 h_0$. This corresponds to $Re \approx 50$ for a vertical water or CO_2 film.

2.3 Stability of Dry Patches

2.3.1 Steady Case

Bankoff [20], postulated two stages of film break-up. An initial stage in which thin spots are produced in the film by growth

of an unstable surface wave, and a second stage, "break-up stage," in which liquid is displaced from the solid surface. In the first stage wettability properties of the system measured through the contact angle do not play a role, while in the second stage the contact angle is the major factor influencing stability of dry spots. Hartley and Murgatroyd [5] have considered the specific case of an isothermal film flowing under gravity in the presence of a dry patch. They considered a patch of the shape shown in Figure 4 and assumed that the liquid in the central stream segment, AB, stagnates, while the remaining flow follows the stream lines shown. A cross section of the liquid near the dry patch is shown in Figure 4. They considered that the free surface acts like a membrane and a dry patch is stable when the meniscus (curved region of the film) is in mechanical equilibrium. In their analysis they equated "upstream" surface tension force (due to the interaction of the liquid-vapour system with the rest of the liquid and with the plate) to "downstream" pressure force (that force required to bring the liquid at B to rest from its velocity in the undisturbed film at A). The upstream force, assuming that curvature of the meniscus (Figure 4, plane x,y) is larger than the curvature of the patch (Figure 4, plane x,z)(true for thin films), has two components; σdz represents the force that the rest of the fluid applies to the membrane, and $\sigma \cos \theta dz$ represents the force that the plate applies to the membrane (θ is the contact angle, see Figure 4). The total upstream surface tension force for an isothermal flow is $\sigma(1-\cos \theta) dz$. The downstream force was found by Hartley and Murgatroyd applying the Bernoulli equation to the thin viscous liquid flowing over a vertical plate

$$\frac{p}{\rho} + \frac{1}{2} u^2(y) = \frac{p_B}{\rho} + \frac{1}{2} v_B^2, \quad v_B = 0 \quad \dots (2.14)$$

$$F_p = \rho \int_0^{\delta} \frac{u^2}{2} dy, \quad \dots (2.15)$$

where F_p = pressure force per unit width.

No explanation is given about the validity of a Bernoulli-type equation. Probably the workers assumed that the work done by the gravity force equals the work done by the shear force. This is a good assumption far from the dry patch but not in the vicinity near the dry patch where the fluid is slowed down. Hartley and Murgatroyd evaluated the Equation (2.15) for an isothermal, steady laminar film with no shear at the interface. The velocity profile is parabolic (Equation 2.1) and the equilibrium of forces can be expressed in terms of thickness δ as

$$\frac{1}{15} \rho^3 \frac{g^2}{\mu^2} \delta^5 = \sigma(1 - \cos \theta). \quad \dots (2.16)$$

They found a minimum, or critical film thickness of (2.16).

$$\delta_c = 1.72 \left[\sigma \left(\frac{1 - \cos \theta}{\rho} \right) \right]^{1/5} \left[\frac{\mu}{\rho g} \right]^{2/5}. \quad \dots (2.17)$$

In terms of mass flow rate this becomes,

$$\Gamma_c = 1.69 \left(\frac{\mu}{\rho g} \right)^{1/5} \left[\sigma(1 - \cos \theta) \right]^{3/5}.$$

According to this formula if the thickness of the film is larger than δ_c , the patch rewets, while for film thicknesses smaller than δ_c dry patches can be established. The existence of a dry patch is an essential condition in the analysis as the film could quite possibly be thinner without breakdown of the film if the surface is already wetted. As another application of their criterion Hartley and Murgatroyd considered the case of a laminar or turbulent film motivated by surface shear only. They also postulated that the sum of the kinetic and surface energy of the unbroken film was minimized at the critical thickness for stability. This gives a different critical thickness δ'_c called "minimum thickness from power criterion" although (except for the contact angle) the same parameters are involved

$$\delta'_c = 1.34 (\sigma/\rho)^{1/5} (\mu/\rho g)^{2/5} .$$

Bankoff [21] assumed that the liquid film will break up into rivulets when the total mechanical energy (kinetic plus surface) per unit area is the same in the two configurations. For low flow rates, energy considerations favour a break-up into parallel rivulets. The minimum film thickness δ_c found is a function of the contact angle formed between the rivulet and the solid surface.

$$\delta_c = 1.72 \left(\frac{\sigma}{\rho}\right)^{1/5} (\mu/\rho g)^{2/5} f(\theta) \quad \dots (2.18)$$

The function $f(\theta)$ is a function of contact angle and geometry of the rivulets. This contact angle is not subject to the same conditions of forces as contact angle at the stagnation point.

It is interesting to note that contact angle was not experimentally measured in these works, so Hartley and Murgatroyd [5] could only work with the power criterion. They used other workers' experimental results to evaluate their analytical criterion, with varying degrees of success. Hewitt and Lacey [4] designed an experiment to specifically test dry patch stability. They found that the upstream surface tension force was about eight times the pressure force using a sessile drop value of θ . Ponter *et al.* [7] presented a model to predict liquid film breakdown in the presence of mass transfer. They assumed a dry patch of the same shape as Hartley and Murgatroyd (Figure 4). If the dry patch is stable surface force along AB must balance the fluid force brought about by the loss in momentum in bringing the liquid to rest at B. According to Ponter the balance of forces is represented by

$$\int_0^{\delta} u^2 dy = \sigma(1 - \cos \theta) \quad (2.19)$$

For a steady, laminar flow without waves or shear at the interface

$$u = u_T \left(\frac{2y}{\delta} - \frac{y^2}{\delta^2} \right) \quad (2.1)$$

Substitution into Equation 2.19 gives

$$\frac{2}{15} \rho^3 \frac{g \delta^5}{\mu^2} = \sigma(1 - \cos \theta) \quad \dots (2.20)$$

Note that the left hand side of this equation is two times that evaluated by Hartley and Murgatroyd (see 2.16). Critical thickness is then given by

$$\delta_c = 1.495 \left[\sigma \frac{(1 - \cos \theta)}{\rho} \right]^{1/5} [\mu / \rho g]^{2/5} \quad \dots (2.21)$$

or in terms of the mass flow rate (Equation 2.2)

$$\Gamma_c / \mu = 1.116 (1 - \cos \theta)^{0.6} \left(\frac{\rho \sigma^3}{\mu^4 g} \right)^{1/5}$$

Γ_c / μ defines the minimum liquid flow rate or minimum wetting rate to sustain a stable dry patch. Ponter [7] measured mass flow rate, contact angle and surface tension during absorption to test the validity of the model. Close agreement was found between contact angles measured under flow conditions and those measured from a sessile drop under the same conditions. Data for water films in the presence of a saturated alcohol-air mixture are reported and show good agreement between the observed and predicted minimum wetting rates.

Zuber and Staub [6] extended the Hartley and Murgatroyd analysis [5] to the case with heat transfer and proposed two additional forces due to thermal effects; thermocapillary force, due to a non-uniform temperature at the free surface and vapour thrust, due to change in momentum flux experienced by the fluid particles when they pass from liquid to vapour phase. They

assumed a linear temperature profile and approximated the meniscus by a wedge shape to simplify calculations. Their conditions for a stable dry shape to simplify calculations. Their conditions for a stable dry patch is

$$\frac{\rho}{15} \left(\frac{g\Delta\rho}{\rho v} \right)^2 \delta_c^5 = \sigma(1-\cos\theta) + \frac{d\sigma}{dT} \delta_c \frac{Q}{k_t} \cos\theta + \rho_v \left(\frac{Q}{\rho_v h_{lg}} \right)^2 \frac{\Delta\rho}{\rho} \cos^2\theta \delta_c .$$

where $\Delta\rho = \rho - \rho_v$ (2.22)

The minimum film thickness δ_c will permit the wetting of the entire surface. In this analysis as well as the previous ones it appears that only one value of δ is possible for each value of θ . McPherson [22] deals with a horizontal film with a shear stress at the interface. He also presents the picture of a meniscus as a physical surface, and equilibrium of forces at the vertex of the dry patch implies that the patch may be "quasi-stable". Unbalance of forces corresponds to a situation where the patch grows either upstream or downstream. He includes the forces considered by Zuber and Staub [6], as well as vapour shear at the film vapour interface, hydrostatic head from the liquid film, and drag at the small step in the film. The heated length upstream of the dry patch edge (see Figure 5) is divided into a region (l-m) over which the film is being decelerated and diverted with no change in thickness and a region (m) over which evaporation reduces the thickness to zero. The velocity profile in the evaporation length (m) does not change and is identical to that at m. To evaluate the vapour thrust force he considered a non-constant heat flux due to conduction in the wall from the dry to the wet region. Thermocapillary effect is considered together with surface tension force in the expression

$$F_{\sigma} = \sigma(T_i) - \sigma(T_p) \cos \theta \quad \dots (2.23)$$

where $\sigma(T_i)$ is the surface tension evaluated at the interface and $\sigma(T_p)$ is the surface tension evaluated at the point where the liquid, vapour and plate are in contact. The resultant force acting on the vertex of the dry patch is the sum of the stagnation force, vapour thrust, shear force, surface force, body force, and drag force.

McPherson applied his analysis to a known case of dryout taken from experiments conducted at Harwell [22]. He concluded that for a steam-water system the most important forces are upstream surface tension force F_{σ} , (thermal effects included), downstream deceleration F_p and interfacial shear forces F_s

$$F = F_{\sigma} + F_p + F_s$$

If

$$F = 0 \quad \text{stable dry patches}$$

$$F > 0 \quad \text{film rewets}$$

$$F < 0 \quad \text{dry patch grows upstream.}$$

Using a linear velocity profile

$$F = \sigma(T_i) - \sigma(T_p) \cos \theta + \frac{2}{3} \rho \delta (u_{L\infty}^2 - u_{Le}^2) + \tau_i \left(\frac{1+m}{2} \right) \left(1 - \frac{u_{Le}}{u_{L\infty}} \right) \quad \dots (2.24)$$

McPherson also proposed a mechanism for maintaining a "quasi-stable" dry patch. According to McPherson when a dry patch is first formed the upstream surface force will decelerate the approaching film causing a

downstream force. If F_p is negligible, F_s must balance F_σ . As no measurements of contact angle were recorded at Harwell, McPherson shows that for every possible contact angle there is some shear force which will balance the surface force (or shear plus pressure force in case the latter is not negligible). He suggested that a self-adjusting process will occur, but if upstream forces are larger than downstream forces for all degrees of deceleration, the patch will move upstream. On the other hand, once a "quasi-stable" dry patch is formed, rewetting is only possible through some perturbation of the system such as an increased film flow or droplet deposition rate.

In a recent paper, Wilson [23] considers an isothermal liquid film flow down a vertical plate where a dry patch has already formed. The flow is assumed to be undisturbed by the dry patch except in a thin region around its boundary called the "collar". The thickness of the collar can be predicted and according to the theory developed is almost three times the thickness of the liquid far from the patch. It is proposed that the collar resembles a boundary layer in which surface tension forces replace the familiar viscous drag.

It is interesting to point out that the pressure balance at the apex of dry patch is

$$\sigma \left(\frac{1}{a_c} - \frac{\sin \theta}{R} \right) = \frac{2}{15} \frac{g^2}{\mu^2} \rho^3 \frac{\delta^5}{c} + 2 \rho g d, \quad \dots (2.25)$$

where

a_c = radius of collar

c = thickness of collar

R = radius of curvature of dry patch boundary

d = width of collar .

Wilson assumed a collar whose cross section is an arc of a circle making the appropriate angle with the solid boundary so that d , a_c , and c can be related. Equation 2.25 states that pressure inside the meniscus, $\frac{\sigma}{K}$ is represented by two terms. The first, (right hand side Equation 2.25) represents stagnation pressure assuming a laminar velocity profile (in terms of a force is equal to Ponter's pressure force) and the second term, represents the pressure due to a body force. Wilson's paper is the first to formally analyze an increase in thickness near the dry spot. This bulge or collar was observed experimentally by Hewitt [4], Ponter [7] and McAdam [1].

2.3.2 Unsteady Case

As was explained in the review of thin liquid films, surface waves are present for vertical flows at all Re . The effect of waves on the process of rewetting has only recently been considered. Hsu and Simon [24] stressed the importance of waves in producing temperature differences at the free surface. These in turn are capable of sustaining steady surface tension force differences which distort the film and make it thinner, leading to formation of a dry patch. Simon and Hsu in another paper [25] conducted an experimental and analytical investigation of the breakdown due to heating of a falling subcooled liquid film. Two flow regimes, the capillary wave and roll wave regimes were found. Capillary waves are weak so that if a dry patch is formed the surface remains dry and is not rewetted because pressure force is not large enough to overcome surface forces. They found a

constant value of We during experiments with water and water-glycerol flow down a heated vertical plate. Simon and Hsu [25] assumed that a constant We is the quantity controlling stability of a dry patch and found a critical thickness after rearrangement of We :

$$\delta_c = 0.66 \left[\frac{\sigma}{\rho} \right]^{1/5} [\mu/\rho g]^{2/5} \dots (2.26)$$

This formula does not include contact angle or heating effects. It is consistent with the assumptions made by Simon and Hsu [25] that minimum film thickness when breakdown occurs is independent of the process through which this film thickness is reached and is the same as the isothermal case.

The roll wave regime occurs at a higher flow rate and in this regime the film breakdown oscillates between a dry and a wetted surface condition. Dryout occurs at wave troughs, however, wave crests have enough momentum to rewet a dry patch. According to Simon and Hsu, the rewetting process is determined by heat flux and other parameters not involved in the capillary-wave regime. Thompson [8] tried to find the effect of surface waves in the presence of a dry patch by evaluating the pressure force using liquid film thickness at the wave hollow, average, base of surface waves, and wave peak. He considered a water film driven by steam flow and evaluated the surface, thermo-capillary and vapour thrust forces with Zuber and Staub's [6] formulae for three dryout conditions.

The interfacial shear term was obtained from McPherson's equation by assuming that stagnation occurs over a distance l equal to total heated length (see Figure 5). Pressure force is found by adopting either a logarithmic or linear velocity profile. Thompson's results show that vapour thrust, body and drag forces are several orders of magnitude smaller than the pressure and surface tension forces, while interfacial shear and thermocapillary forces are only one order of magnitude smaller. He concludes that stability of a dry spot depends on the relative magnitude of the pressure and surface tension forces (as would be the case for an isothermal flow). Although no stable dry patches were observed, in at least two of three cases examined his calculations give $F_{\sigma} > F_p$ (evaluated for an average thickness). However, Thompson [8] found that F_p using the peak thickness is an order of magnitude larger than F_{σ} . In this case the dry patch is unstable, as was observed experimentally. The main conclusions of his paper are:

1. stability of a dry patch will be governed by F_{σ} and F_p ,
2. effective kinetic energy of surface waves is much greater than the average kinetic energy of the film.
Stable dry patches cannot exist when surface waves are present.
3. contact angle of a stationary interface under flow conditions is nearly the same as the static angle of a sessile drop, and
4. nucleating is the main thermal instability.

McAdam [1] makes some observations about the role of waves in the rewetting process: although waves were present in most of his experiments, their effect was not always to rewet the dry patch. He presented a sequence of photographs showing that waves caused distortion of the stagnation point and narrowing of the dry patch but did not result in complete rewetting.

Mariy *et al.* [26] also stress the importance of waves in the rewetting process in a study of the motion of the 3-phase front (point where the liquid, the vapour and the solid are in contact). They analyzed flow in a horizontal tube, with a thin liquid film driven by its own vapour, with the following assumptions: the dry patch behaves like the edge of an annular liquid film at the end of the 2-phase flow; the film front in the absence of waves is stable and of thickness δ_c , the heat supplied being just sufficient to evaporate the incoming liquid at the triple phase front; for each contact angle there is a unique value of the critical thickness δ_c , (Equation 2.15) and rewetting occurs if the fluid becomes thicker than δ_c . They considered the flow perturbed with waves called "harmonics". The flow model consists of a mass of liquid moving at the average velocity, plus an excess of liquid moving as a rigid body at the phase velocity (Figure 6).

Mariy *et al.* [26] suggest film thickness increases at the 3-phase front when waves approach, so downstream forces overcome upstream forces and the triple phase front moves forward. The subsequent advance and retreat of the front depends on whether the excess liquid is evaporated before the next wave arrives, in proper circumstances

the front will move forward and rewet the surface. Continuity and energy equations based on the model of "waves" are solved to determine movement of the stagnation point. Dryout data recorded by Barnet *et al.* [27] and Thompson and Macbeth [28] were used to show the dependence of positions of the stagnation point on parameters such as flow rate and heat flux. Their results are shown in Figure 7. When surface heat flux is less than or equal to the dryout value excess liquid due to the "waves" is not evaporated and the 3-phase front moves forward. If heat flux is high enough to evaporate more than the incoming fluid the 3-phase front recedes. No general criterion can be extracted from their paper, as movement of the 3-phase front is strongly dependent on the model of waves used. Mariy's [26] work will not be considered elsewhere in the present study.

2.4 Contact Angle

A free liquid drop or a drop in contact with a solid will assume a shape which minimizes the free energy (Helmholtz function) of the system. In absence of gravity this is equivalent to minimizing the surface area of the drop [29]. For a two-dimensional system (Figure 8a), the minimization of the free energy is represented by Young's equation:

$$\sigma_{lg} \cos \theta = \sigma_{sg} - \sigma_{sl} \quad \dots (2.27)$$

where

σ_{ij} = interfacial energies or surface tension

lg = refer to liquid-vapour

sg = refer to solid-vapour

sl = refer to solid-liquid interfaces

θ = angle of contact.

Equation (2.24) is satisfied when surface tensions vary smoothly and the surface of the solid is smooth and rigid. In a real system these conditions are difficult to satisfy.

Young's equation predicts one and only one stable contact angle for a given system. However, experimental evidence suggests a characteristic of wetting is the ability of a liquid drop to have many different stable angles on a solid surface (hysteresis effect). For example, if a droplet of the same liquid is added to drop "a" to make a larger drop "b" (or withdrawn to form droplet "c") the base of the drop usually stays constant and the contact angle changes (Figure 8b). Two relatively reproducible angles are the larger angle (in drop "b"), called advancing static angle and the smaller (drop in "c"), called the receding static angle. The difference $\theta_A - \theta_R$ is called contact angle hysteresis. It has been shown [29] that for a drop on an inclined plate (Figure 9) equilibrium of forces is represented by the equation

$$mg \sin \alpha = w \sigma_{lg} (\cos \theta'_R - \cos \theta'_A)$$

α = angle of inclination of the plate

w = width of drop

θ'_R = contact angle at rear

θ'_A = contact angle at the leading edge.

The angle α can be increased as long as $\theta'_R \neq \theta_R$ and $\theta'_A \neq \theta_A$. However, when $\theta'_R = \theta_R$ (minimum angle) and $\theta'_A = \theta_A$ (maximum angle), equilibrium of forces cannot be satisfied and the drop will roll. If there were no hysteresis (unique value of contact angle) the drop would roll on the plate for any angle " α ," [29]. In the case of a dry patch the liquid meniscus can be assimilated to a large drop. However, stagnation of the flow increases the pressure inside the drop and the system is removed from the conditions of equilibrium for which Young's equation is valid. Therefore, because of hysteresis effects stable dry patches can exist.

One of the earliest explanations of hysteresis suggested that the receding angle would be smaller than the advancing because the surface had been wetted by the advancing liquid. Other explanations for hysteresis are based on roughness and heterogeneity of the solid surface. Johnson and Dettre [29, 30], explicitly show the effect of roughness on wetting (see Figure 10). These observations on contact angle correspond to the case where the common line (L V S) does not move.

Ponter [31] and Thompson [8] measured contact angles under flow conditions as well as contact angles of a sessile drop and claimed good agreement. Nevertheless, it could be argued that while both values are close, they are not equal. These arguments can explain the discrepancy found by Hewitt [1] when θ is replaced by the equilibrium value in the balance of forces for the stability of a dry patch. A proper measurement of the contact angle under flow conditions is necessary to test the criterion for dry patch stability.

McPherson [22] suggested that sinusoidal roughness of the heater may be a factor affecting dry patch stability. This results in a larger force which tends to hold back an advancing film and a smaller force which tends to reduce the force on a receding film. Hysteresis effects were not considered in the previous models [5,6] in the sense that the thickness criterion for rewetting is no longer valid. The flow rate can be increased and the dry patch remains stationary. In the present study this effect is called "anchoring". Observations made by McAdam [1] agree with this concept. When the common line moves along the solid, the contact angle formed between the liquid and the solid is called "dynamic" contact angle. Movement of the common line would appear to be a contradiction of no slip conditions at the solid wall. Some papers [32, 33] try to explain how the 3-phase front might actually move but these studies are beyond the scope of the present investigation. McAdam [1] measured dynamic contact angles and found the common line oscillates even for stable dry patches due to the presence of waves.

Ponter *et al.* [34] developed an experimental method to measure contact angle of a water drop on a smooth copper surface under either isothermal or heat transfer conditions. For the isothermal case, the variation of θ with temperature is almost linear and the slope of the curve is negative. For the non-isothermal case they found only small differences in the initial contact angle and the equilibrium contact angle under isothermal conditions. Ponter *et al.* [34] also reported results of water breakdown on a copper surface. They compared experimental values of minimum wetting rates with those predicted by Zuber and Staub and found good agreement for high temperature differences between the surface and inlet water temperature.

3. COMPARISON WITH EXPERIMENTS OF PREVIOUS STABILITY MODELS AND SOME SIMPLE EXTENSIONS

3.1 Discussion of McAdam's Experiments

A liquid CO₂ film under gravity flow over a heated glass plate was used by McAdam [1] to study film break-up under boiling conditions. The total length of the heated plate was 163 mm and was designed so that the bottom 25 mm section of the plate could be observed. Constant heat was supplied to the plate and dryout data were obtained by setting the flow rate while raising the heat flux until a dry patch was observed. Film break-up occurred when Re based on film thickness ranged from 185 to 1000. System inlet pressures and temperatures correspond to saturation conditions and ranged from 2°C to 18°C. A specially designed schlieren system was developed to obtain quantitative measurements. Photographs of film break-up were taken with a movie camera and the frames were individually analyzed. Once the data were processed, information on contact angle under flow conditions and liquid film profile upstream of the tip of dry patch was obtained. Some of the data from McAdam's thesis are plotted in Figures 11 to 16. The inlet temperature was 2°C and Re = 185,310,940. McAdam observed stationary patches (Figures 11 & 15), dry patches growing upstream or receding (Figure 13) and growing downstream or advancing (Figure 13). The representation of the film thickness and of the contact angle (Figures 12, 14, 16) shows a variation with time even if the dry patch was classified as stationary.

In the present study attention was focussed on stationary dry patches since this case is the most important one for stability considerations. The receding and advancing cases should include new forces that were not considered in any of the previous models, nor in the present research. Variation with time of contact angle and thickness near the dry patch is attributed to perturbations or waves in the flow. In order to apply the previous criteria an average stationary contact angle and an average thickness was used.

In Figure 17, θ (average contact angle) is plotted versus Re input numbers for all the stationary dry patches analyzed in the present study. Heat fluxes and temperatures are also indicated. Generally the heat flux necessary for formation of a dry patch increases when initial flow rate increases at constant bulk temperatures (Figure 17). For almost constant Re (~ 700) the heat flux is constant ($\sim 24000 \text{ W/m}^2$), however, for $Re \sim 900$ the required heat flux ranges from 30000 to 63000 W/m^2 . The contact angle decreases for most saturation temperatures when input Re and heat fluxes increase. This is in agreement with the fact that generally contact angle decreases with temperature of the solid surface [34]. Since Hartley and Murgatroyd predict that in isothermal flow the contact angle increases with increasing Re , the results shown in Figure 17 indicate that thermal effects might be very important in determining dry patch stability.

3.2 Relationship Between Various Models

As a first step in comparing the previously discussed models with experiments, it can be shown that in some cases these models are related to each other. For example, Hartley and Murgatroyd [5] and Zuber and Staub's [6] criteria are equal when the dry patches are formed in isothermal liquid films flowing over unheated surfaces. McPherson's [22] analysis can easily be converted to the Zuber and Staub criterion for the case of a draining liquid film flowing over a heated plate. In this case $F_s = 0$ (Equation 2.24) and the criterion for dry patch stability reduces to

$$\frac{\rho}{2} \int_0^{\delta} (u_{L\infty}^2 - u_{Le}^2) dy = \sigma(T_i) - \sigma(T_p) \cos \theta \quad \dots (3.1)$$

where

$u_{L\infty}$ = is the velocity upstream of the dry patch

u_{Le} = is the velocity at the edge of the dry region.

Assuming a parabolic velocity profile (McPherson assumed a linear profile) and that the fluid stagnates completely $u_{Le} = 0$, the inertia term reduces to the same expression used by Zuber and Staub. Although McPherson presented the surface force as an alternative to the upstream force proposed by Zuber and Staub it is in fact the same expression. If the term $\sigma(T_i) \cos \theta$ is added and subtracted to the right hand side of Equation (3.1) then

$$\begin{aligned} & \sigma(T_i) - \sigma(T_p) \cos \theta + \sigma(T_i) \cos \theta - \sigma(T_i) \cos \theta \\ & = \sigma(T_i)[1 - \cos \theta] + [\sigma(T_i) - \sigma(T_p)] \cos \theta . \end{aligned}$$

Multiplying and dividing by $\Delta T = T_p - T_i$, this becomes

$$\sigma(T_i)[1 - \cos \theta] + \frac{\sigma(T_i) - \sigma(T_p)}{T_p - T_i} (T_p - T_i) \cos \theta .$$

As the variation of σ with T is approximately linear

$$\sigma(T_i)[1 - \cos \theta] + \left| \frac{\Delta \sigma}{\Delta T} \right| \Delta T \cos \theta .$$

Assuming a linear temperature profile as did Zuber and Staub, the upstream forces can be expressed as

$$\sigma(T_i)(1 - \cos \theta) + \left| \frac{\Delta \sigma}{\Delta T} \right| \frac{\delta Q}{k_t} \cos \theta .$$

This is the same as right hand side of Equation 2.22 when vapour thrust effects are negligible. Ponter's Equation (2.20) for the pressure force is twice the pressure force found by Zuber and Staub, this difference is discussed later in Section 3.4.

3.3 Comparison of Previous Models With Data

3.3.1 General

After studying the different models that analyzed dry patch stability through an equilibrium of forces, Zuber and Staub, Ponter

et al., and Wilson's criteria were selected to be tested with McAdam's data. From different approaches Bankoff [21] and Simon and Hsu [25] presented minimum film thicknesses for the formation of dry patches. With these film thicknesses, pressure forces are evaluated and compared to the surface forces proposed by Zuber and Staub. In order to check any of the previously discussed models the data needed are local data near the dry patch, but not perturbed by its presence. For example McAdam measured Re at the top of the heated plate, (input Reynolds numbers, Re_i) but dry patches were observed and recorded in any position of the bottom 25 mm of the plate. Evaporation along the plate might affect the input Re and consequently the input thickness of the liquid film. Thus local Re and local film thicknesses corrected for evaporation are considered in order to check the previous criteria.

Under steady conditions, and as the temperature of the free surface is at saturation temperature, it is assumed that the heat supplied to the plate is equal to the heat flux at the interface and equal to the heat absorbed by vaporization. The thickness changes because of evaporation, and as the temperature of the interface does not vary there is a temperature gradient along the plate. Under the conditions just described

$$\frac{\Gamma_e}{\Gamma_i} = x = \frac{Q_1}{\mu Re h_{lg}}$$

where

Q = heat supplied to the plate

Γ_e = flow rate that evaporates

Γ_i = input flow rate

h_{lg} = latent heat of vaporization

l = length of heated plate where evaporation occurs before a dry patch is formed

μ = viscosity.

$$\Gamma = (1 - x) \Gamma_i ,$$

Γ = liquid flow rate after evaporation.

Local Reynolds number,

$$Re = \frac{\Gamma}{\mu} .$$

As the dry patches appear randomly in the last 25 mm of the plate it was considered that an average $l = (163 - \frac{25}{2})$ mm). It was assumed that the liquid film thickness will not experience appreciable further changes by evaporation.

Figure 18 shows average contact angles as a function of the local Re. The same general features described in Figure 17 are observed. When Re increases the heat fluxes increase, while contact angle decreases when heat flux increases, except for a saturation temperature = 18°C. In the latter case the degree of evaporation is very high (89%). This is due to the fact that the latent heat at $T = 18^\circ\text{C}$ is much less than at lower temperatures. To dissipate a constant amount of heat (65000 W/m^2) more fluid must evaporate. The assumption that the heat supplied to the plate is equal to the heat of vaporization might be incorrect. Local Re less than 270 are classified as low Re (Re input = 185, 310, 420), while local Re larger than 270 are classified as high Re.

3.3.2 Low Re

Zuber and Staub's expression (Equation 2.22) for dry patch stability reduces to

$$\frac{1}{15} \frac{\rho^3 \delta_c^5 g^2}{\mu^2} = \sigma(1 - \cos \theta) + \frac{d\sigma}{dT} \frac{\delta_c Q}{k_t} \cos \theta + \rho_v \left[\frac{Q}{\rho_v h_{fg}} \right]^2 \cos^2 \theta \delta_c \dots (3.2)$$

when $\rho_v \ll \rho$.

Table 3.1 shows the magnitude of the different forces.

Vapour thrust effects were found negligible for all cases.

TABLE 3.1

Evaluation of Forces According to Zuber & Staub at Low Re

T(°C)	Re _i	Re	$\delta_c \times 10^5$ (m)	$F_p \times 10^5$ (N/m)	$F_\sigma \times 10^5$ (N/m)	$F_{th} \times 10^5$ (N/m)	$F_\sigma + F_{th} \times 10^5$ (N/m)
2	185	144	7.8	158	146	43	189
2	310	221	9.0	319	109	121	230
9	420	269	9.2	382	88	175	263

As indicated previously, the pressure force proposed by Ponter [7] is two times the pressure force presented by Zuber and Staub [6]. For a laminar velocity profile, using McAdam's data, the magnitude of the forces are shown in Table 3.2.

TABLE 3.2

Evaluation of Pressure Forces According to Ponter *et al.* at Low Re

Re	$F_p \times 10^5$ (N/m)
144	316
221	638
269	764

Similarly, Wilson's [23] analysis (for unheated flow) was applied to $Re_i = 185$ at the lowest heat flux. The balance of pressure at the apex is expressed by

$$\sigma \left(\frac{1}{a_c} - \frac{\sin \theta}{R} \right) = \frac{2}{15} \frac{\rho g^2}{\mu} \frac{\delta^5}{c} + 2 \rho g d. \quad (2.25)$$

If R is very large and c is taken as the experimental thickness equal to 15×10^{-5} m, a_c and d can be evaluated through the collar model proposed by Wilson. The results are tabulated below.

TABLE 3.3

Evaluation of Forces According to Wilson

Re	$\delta_c \times 10^5$ (m)	$F_p \times 10^5$ (N/m)	$F_B \times 10^5$ (N/m)	$F_\sigma \times 10^5$ (N/m)
144	7.8	316	180	140

Although heat transfer was present, the heat flux was only 5500 W/m^2 and Wilson's balance can be applied to McAdam's data as a first

approximation. Therefore, the increase of upstream forces due to heating effects would be insufficient to balance the pressure plus body forces. Bankoff [21] using a criterion of equating the total energy (kinetic plus surface) of a continuous film to the energy of a film that breaks up into rivulets, determines a minimum film thickness for the equilibrium situation.

For the lower heat flux that corresponds to $Re_i = 185$,

$$\delta_c = 1.73 \times 10^{-5} \text{ m} .$$

The pressure force is far smaller than the surface forces when δ_c and a parabolic velocity profile is used. The Simon and Hsu [25] criterion to evaluate the minimum film thickness is independent of the heat flux and only depends on the fluid properties:

$$\delta_c = 0.666 \left(\frac{\sigma}{\rho}\right)^{1/5} \left(\frac{\mu}{\rho g}\right)^{2/5} . \quad (2.26)$$

For

$$T = 2^\circ\text{C}$$

$$\delta_c = 3.5 \times 10^{-5} \text{ m} .$$

A pressure force evaluated with this film thickness and a parabolic velocity profile gives about 4×10^{-5} N/m. This value is two orders of magnitude less than the upstream forces. Equation (2.26) was deduced by Simon and Hsu [25] taking a constant Weber number equal to 0.0145 for water and water-glycerol. As their criterion is independent

of heat flux it is interesting to compare their expression with Hartley and Murgatroyd. The Hartley and Murgatroyd criterion based on a We can be expressed as

$$We = 1.67 (1 - \cos \theta) .$$

This expression depends on the contact angle and is equal to 0.55 when θ equals 48° , the contact angle observed for $Re = 185$. Both criteria [5] and [25] are different. Actually, Simon and colleagues made measurements on a system of water and water-glycerol and extension of their conclusions to another system is not justified. In any case absence of the contact angle indicates that their analysis should be improved in order to consider this fundamental parameter in the stability of dry spots.

3.3.3 High Re

For high Re velocity profiles are described by the universal velocity profile (Equation 2.3) or by a power law such as seventh-root law (2.6). The Zuber and Staub criterion may be used for high Re by replacing the parabolic velocity profile with the $1/7$ power law in the pressure force, $F_p = \rho \int \frac{u^2}{2} dy$. The upstream forces (F_σ , F_{th}) can be added and expressed as a unique force (see 3.2) equal to

$$\sigma(T_i) - \sigma(T_p) \cos \theta .$$

When the increase in temperature of the plate is evaluated near the dry patch using a linear temperature profile, the temperature at the point where the solid, liquid and vapour are in contact is larger than the critical temperature for CO_2 . This would mean a separating surface between liquid and vapour could not exist. Since dry patches were observed, it is believed that the temperature of the plate at 3-phase front must be less than the critical temperature. Therefore the linear temperature profile is not a good assumption even for thin film. When the temperature of the plate equals the critical temperature $\sigma(T_p)=0$, so that upstream forces have a maximum limit equal to $\sigma(T_i)$.

Table 3.4 summarizes the different forces for 6 cases using the assumption above for maximum upstream force.

TABLE 3.4

Evaluation of Forces at High Re

T(°C)	Re _i	Re	$\delta_c \times 10^5$ (m)	$F_p \times 10^5$ (N/m)	$F_\sigma \times 10^5$ (N/m)	$(F_\sigma + F_{th})^{MAX} \times 10^5$ (N/m)	T _p (°C)*
2	940	470	13.0	860	80	425	78
9	700	453	11.9	700	58	305	41
13	750	477	12.1	679	89	250	44
	855	531	12.5	817	61	250	55
18	750	450	10.8	463	43	170	48
	1050	116(lam.)	6.5	76	50	170	67

*The temperatures were evaluated through a linear profile.

Vapor thrust effects were found negligible relative to the magnitude of the other forces. As far as the previous models are concerned

(see Table 3.1 to 3.4) no stable dry patches can exist, as in most of the cases pressure force exceeds the surface force.

3.4 Simple Extensions

3.4.1 Simple 2-D Extensions

The pressure force presented by Zuber and Staub is half the pressure force used by Ponter *et al.* Zuber and Staub calculated the pressure force by applying the Bernoulli equation to the center-stream line. This increase in pressure times the normal area yields the force. Actually this is not a proper procedure since only the center-streamlines stagnate.

If a pressure force has to be found, the entire pressure distribution along the meniscus should be known. Ponter applied the momentum equations to a control volume and considered the flow one-dimensional, although it is well known that the flow is at least 2-D in the plane of the plate near the dry patch. The difference between these two approaches in the evaluation of the pressure force can be understood if the momentum theorem is applied to a control volume shown in Figure 19.

Considering the flow bidimensional in the vicinity of the dry patch, the complete steady expression for the x component force acting on the control volume is

$$\int_{s_0} \rho u [u dy dz + w dx dy] = \int F_x dz ,$$

$$F_x = F_B + F_s + F_\sigma + F_{th} \quad \text{total force per unit width}$$

$$F_B = \text{body force per unit width}$$

$$F_s = \text{shear force at the wall per unit width.}$$

In the approximation that $F_B = -F_s$,

$$\int_{s_0} \rho u^2 dy dz + \rho w dx dy = \int (F_\sigma + F_{th}) dz \quad \dots (3.3)$$

The first term of the pressure force is the same as that used by Ponter. However, there is a second term because the flow decelerates and diverts around the dry patch. This term has a sign opposite to the first, giving a pressure force smaller than the one predicted by Ponter. A complete velocity field must be known in order to evaluate the right pressure force. As an attempt to find the contribution to the pressure force due to the lateral flow the velocity field for an infinite ideal flow around an obstacle is proposed. The obstacle is a Rankine half body whose shape is similar to the inverted U-shape of the theoretical dry patch, with velocity components

$$u = \bar{U} + m \frac{x}{x^2 + z^2}, \quad w = m \frac{z}{x^2 + z^2},$$

where

\bar{U} = average velocity of the parabolic profile

m = source strength related to the width of the

dry patch and the velocity through the

relation $\frac{b\bar{U}}{2\pi}$

- b = width of dry patch measured on the movie film
 x_s = coordinate of the stagnation point = $\frac{m}{U}$
 z_0 = width of control volume.

The width of the control volume (Figure 19) is chosen in a way that the contour of the dry patch can be considered plane. This width is much smaller than size of the dry patch. The force per unit width becomes

$$F_x = \rho \bar{U}^2 \delta - \rho \delta \bar{U} \frac{m}{z_0} \left(\frac{\pi}{2} - \arctan \left(\frac{x_s}{z_0} \right) + \frac{\delta \rho m^2}{2} \left(\frac{1}{x_s^2 + z_0^2} \right) \right) \dots (3.4)$$

When the width of the control volume tends to zero, Equation (3.4) reduces to

$$F_x = (\rho/2) \bar{U}^2 \delta, \quad z_0 \rightarrow 0$$

which is the same pressure force obtained by Zuber and Staub. In this context it can be seen that Zuber and Staub's pressure force represents a limiting case, while Ponter's force does not take lateral flow into consideration. Some evaluations of the pressure force using Equation (3.4) are shown in Figure 24.

3.4.2 Re-laminarization Effects

The previous history of the liquid film probably determines the velocity profile near the dry patch. For example, if a dry patch is formed when a thin liquid film draining by gravity breaks-up, most

likely the velocity profile in the vicinity of the patch is parabolic. On the other hand, if a dry patch is formed in a thick and turbulent flow, although the film gets thin near the dry patch the flow might remain turbulent and not re-laminarize. The free surface can be smooth as McAdam [1] observed but the nature of the bulk fluid can be still turbulent. For these reasons, the 1/7 power law was used to evaluate the pressure force for local $Re = 221$ and 269 , $Re_i = 310$ and 420 respectively. Table 3.5 shows the results of the calculations.

TABLE 3.5

Evaluation of Forces When the 1/7 Power Law is Used at Low Re

Re	$\delta_c \times 10^5$ (m)	$F_p \times 10^5$ (N/m)	$F_\sigma + F_{th} \times 10^5$ (N/m)
221	9.1	265	230
269	9.55	308	263

The pressure forces evaluated through the 1/7 power law are lower than when the parabolic velocity profile is used (Table 3.1). This could be an indication that although the film is very thin near the dry patch it might not relaminarize.

3.5 Discussion

3.5.1 Balance of Forces

Figure 20 shows the pressure force predicted according to Zuber and Staub [6], Ponter *et al.* [7] and Wilson [23], and includes

low Re as well as high Re cases. Figure 21 shows the total surface forces (surface force plus thermocapillary force) and the surface force alone (isolated from the thermal effects).

In general the estimate pressure forces are larger than surface forces and best results are obtained using Zuber and Staub's model. Figure 22 (circle points) and Figure 23 show the difference between the pressure and surface forces evaluated according to Zuber and Staub.

Surface forces become larger than pressure forces for $Re_1 = 185$, and $Re_1 = 1050$. For the last case the degree of evaporation was found to be very high (assuming that the heat supplied to the plate equals the heat absorbed by vaporization). For low Re (Figure 22, circles) the agreement between the absolute value of the forces is reasonable. The trend shows a departure of the balance of forces for increasing Re. At higher Re, (Figure 23) the pressure force exceeds the surface force by a factor of 3. This is possibly due to the fact that the assumptions made in the development of the previous models are not valid for high Re. The thicknesses estimated for low and high Re are smaller than the experimental thicknesses measured by McAdam [1]. If the experimental thicknesses are used to evaluate pressure force it becomes far larger than the surface forces for any Re. McAdam measured film thickness close to the dry patch and it is possible that the presence of a collar [23] results in a larger measured thickness.

Figure 24 shows the pressure forces according to Zuber and Staub criterion as well as the 2-D model. All

forces are larger than the surface forces also shown in Figure 24, however, the pressure force evaluated through the momentum theorem improves the agreement slightly. The simple 2-D model has some serious limitations. The flow decelerates and diverts around the dry patch implying a continuous increase in pressure. As the liquid has a free surface the curvature and thickness must change near the dry patch which is not accounted for by the model. In addition, the assumption that the body force is equal and opposite to the shear force on the wall is poor near the dry patch where the liquid is slowed down appreciably. Nevertheless the model is useful to distinguish between Zuber and Staub, and Ponter's formalism, and shows why Wilson's model gives a larger pressure force. Wilson considered that the flow is disturbed by the dry patch only in a thin region around its boundary. Actually the disturbance is more extended, affecting the flow field and leading to a decrease in pressure force. The results of estimating the pressure force considering that the liquid might not re-laminarize are shown in Figure 22 (squares). The difference between the pressure and surface force diminishes but more data are needed.

3.5.2 Role of Thermocapillarity

Figure 21 shows the total upstream force (surface plus thermocapillary forces). It also illustrates the surface force $\sigma(1 - \cos \theta)$ without thermocapillary effects. For a temperature, $T = 2^\circ\text{C}$, three cases were analyzed:

$Re_i = 185, Re = 144; Re_i = 310, Re = 221; Re_i = 940, Re = 470.$

When the local Reynolds number increases the contact angle and therefore the surface force decreases. At first sight this behaviour, also observed by Ponter [7], is in contradiction with the fact that when Re increases, the contact angle must increase as Hartley and Murgatroyd predict. This, however, ignores thermocapillary effects, which are also important for dry patch stability. When Reynolds number increases, heat flux and the total upstream force also increase (Figure 21). Therefore the thermocapillary force increases with Re to stabilize the dry patches. Thompson [8] did not consider thermocapillary effects as important as in the present research.

The thickness estimated for the flow depends on the velocity and temperature profile. At high Reynolds number the $1/7$ power law and linear temperature profile give estimates of the temperature of the plate ($T > 31^\circ\text{C}$) that do not agree with the observations of stationary dry patches. If a dry spot is formed the temperature of the plate at the triple contact point cannot exceed the critical temperature of CO_2 ($T = 31^\circ\text{C}$). If the difference in temperature between fluid and plate is limited by the critical temperature, the temperature profile can not be linear. Alternately, the thickness evaluated assuming a $1/7$ power law velocity profile is not the actual thickness of the film. It may also be possible that thermocapillary effects are present in an extended region well upstream of the dry patch, so that local thickness is smaller than estimated, leading to a smaller value of the pressure force. This is a very complex problem with flow and heat effects combined, and a deeper analysis is necessary in order to understand the formation and stability of dry patches.

3.6 Summary

Ponter's and Wilson's criteria do not describe the stability of dry patches measured by McAdam as well as Zuber and Staub's. The criterion of equal Weber number [25] is discarded in view of its lack of generality. The criterion of equating the energy for a continuous film to the energy of a configuration of rivulets gives a minimum film thickness almost 4 orders of magnitude less than the measured thickness (corrected for evaporation). The pressure force so evaluated is 3 orders of magnitude less than surface forces. The energy criterion is strongly dependent on the density and shape of rivulets and does not appear equivalent to a force balance criterion applied to the apex of an isolated dry patch.

For low Re , Figure 22 (circles) shows a relatively good agreement of forces, while at high Reynolds number (Figure 23) the pressure force calculated through a $1/7$ power velocity law is nearly three times the total upstream forces. The $1/7$ power law velocity profile and linear temperature profile do not describe the fact that stationary dry patches were observed. The temperature of the plate is over-evaluated and as a limit was assumed to be equal to the critical temperature of CO_2 . This implies that no increase in upstream forces can be expected.

Two simple extensions were proposed based on a more complete analysis of the problem, the 2-D extension and the re-laminarization effects [Figure 24 and Figure 22 (squares)].

However, agreement between pressure force and surface forces improved only slightly with these extensions. Although limitations on the two-dimensional model are severe (for example, it does not consider that the liquid has a free surface), the description of some aspects of the flow behaviour is more realistic than Zuber and Staub's.

The thicknesses measured by McAdam exceed the thicknesses estimated by any previous models. It is felt his measurements apply to the thickness of a "collar", an effect not described by the simple extensions.

4. UNSTEADY EFFECTS

McAdam's [1] measurements of the contact angle show a dependence with time even though dry patches were stationary. The fact that dry patches stand still and the contact angle changes with time in a rather periodic way suggests the idea that waves of fairly regular shape are responsible for the variation in the contact angle. When these waves change to a more irregular pattern (such as roll waves), increases in amplitude and rewetting might be possible. Hysteresis plays an important role by allowing larger contact angles before the dry patch becomes unstable.

Kapitza [17] and Levich [18] presented comprehensive studies of wave motion in thin liquid isothermal layers. Their studies enable the wavelength, frequency and amplitude of wave motion to be calculated. The treatment is limited to wavelengths greater than $14 h_0$ (h_0 = mean film thickness), which means Re numbers less than 50. As an attempt to analyze the unsteady effects the force criterion balance for stability of dry patches can be extended using Kapitza's expression for the velocity field. A control volume is chosen in the same way as for the steady case and an integral equation of motion is proposed. The forces acting on the volume are pressure force, surface tension force, viscous force and gravity and are now all functions of time. The control volume is fixed to the plate and the dry patch is assumed to be a solid object in the flow (Figure 19). The flow stagnates, producing an oscillatory pressure force over the rigid surface that

represents the dry patch. In this approximation the details of the flow near the leading edge of the film are not considered, the contact angle does not enter the analysis. The model is the following: when a fluid with waves stagnates on the object, it exerts a force that changes with time. If the dry patch stands still the balance between pressure and upstream forces is satisfied for each instant. For example, the maximum pressure force must be equal to the maximum upstream force and the minimum pressure force is balanced by the minimum upstream force. The minimum and the maximum surface forces determine a range of contact angles. The patch will rewet when the pressure force is high (or low) enough to overcome the anchoring. Perturbations can alter the regular wave pattern described by Kapitza [17] and rewetting might be possible.

Taking a control volume from infinity to the edge of the patch, the balance of forces per unit width in the direction of the main flow is expressed as

$$\int_0^{n\lambda} \int_0^h \rho \frac{\partial u}{\partial t} dx dy + \int_0^h \rho u^2 dy - \int_0^{n\lambda} \int_0^h \rho u w dy dx - \int_0^h \rho u v dx = F_\sigma + \int_0^h \int_0^{n\lambda} \rho g dx dy + \int_0^{n\lambda} \tau_0 dx \quad \dots (4.1)$$

$n\lambda$ with n integer represents a distance far enough in order to assume that the flow is not perturbed from its condition at infinity. The components of velocity are

$$u(x,y,t) = 3u_0 [1 + 0.6 \sin(kx - \omega t) - 0.3 \sin^2(kx - \omega t)] * \left(\frac{y}{h} - \frac{y^2}{2h^2} \right) \quad (2.13)$$

$$v(x,y,t) = -1.8 u_0 k \cos(kx-\omega t) [1 - \sin(kx-\omega t)] \left(\frac{y^2}{2h} - \frac{y^3}{6h^2} \right) \quad (2.13)$$

where

$$h = h_0 + h_0 0.46 \sin(kx-\omega t) .$$

Formula (4.1) can be simplified. The non-steady term is equal to zero when the integration is performed over an integer number of wavelengths. The 4th term of the left hand side is zero because no flow crosses the top face of the control volume, the evaporation is assumed to be negligible. Kapitza's [17] treatment is for undamped waves: the energy dissipated by wave motion must be balanced by the work done by gravity, which means that viscous shear and gravity forces cancel each other over one wavelength. A detailed calculation of the shear and gravity force is carried out in Appendix A.

The balance of forces without heat addition is, after simplification:

$$\int_0^h u^2 dy - \int_0^{n\lambda} \int_0^h \rho u w dx dy = \sigma(1 - \cos \theta) . \quad (4.2)$$

The second term of the left hand side represents the contribution of the lateral flow to the pressure force. This term is unknown beforehand because w , that is the component of velocity that appears due to the presence of a dry patch, is zero because Kapitza's model is one-dimensional. The second term is evaluated through an approximation: The balance of forces is expressed as

$$\alpha \int_0^h \rho u^2 dy = \sigma(1 - \cos \theta) \quad \dots (4.3)$$

where

$$\alpha \text{ is defined as } \left[1 - \frac{\iint \rho u w dx dy}{\int \rho u^2 dy} \right] \text{ steady case}$$

The term α represents a relationship between the lateral momentum flux and the incident momentum flux. It is assumed that this relationship is approximately equal to the steady case. Therefore α is evaluated for an ideal flow, steady, diverging and stagnating around an object whose shape is similar to the shape of the dry patch. Substituting (2.13) in formula (4.3)

$$F_p(t) = \alpha \frac{18}{15} \rho u_0^2 h_0 [1 + 0.6 \sin(kx - \omega t) - 0.3 \sin^2(kx - \omega t)]^2$$

for

$$x = 0$$

$$\begin{aligned} F_p(t) = & \alpha \frac{18}{15} u_0^2 \rho h_0 [1 + 0.36 \sin^2 \omega t + 0.09 \sin^4 \omega t - 1.2 \sin \omega t \\ & + 0.36 \sin^3 \omega t - 0.6 \sin^2 \omega t] - \alpha \frac{18}{15} 0.46 \rho u_0^2 h_0 [\sin \omega t \\ & + 0.36 \sin^3 \omega t + 0.09 \sin^5 \omega t - 1.2 \sin^2 \omega t + 0.36 \sin^4 \omega t \\ & - 0.36 \sin^3 \omega t] \end{aligned}$$

$$F_p(t = 0) = 1.2 \alpha \rho u_0^2 h_0$$

$$F_p(t = \tau/4) = 0.006 \alpha \rho u_0^2 h_0$$

$$F_p(t = \tau/2) = 1.2 \alpha \rho u_0^2 h_0$$

$$F_p(t = 3/4 \tau) = 3 \alpha \rho u_0^2 h_0$$

The average value of the pressure force is

$$\bar{F}_p = \frac{1}{\tau} \int_0^\tau F_p(t) dt$$

$$\begin{aligned} \bar{F}_p &= \frac{1}{\tau} \int_0^\tau \alpha 1.2 \rho u_0^2 h_0 [1 + 0.36 \sin^2 \omega t + 0.09 \sin^4 \omega t \\ &\quad - 0.6 \sin^2 \omega t] dt + \frac{1}{\tau} \int_0^\tau [-\alpha 1.2 0.46 \rho u_0^2 h_0 [-1.2 \sin^2 \omega t \\ &\quad + 0.36 \sin^4 \omega t] dt \end{aligned}$$

$$\bar{F}_p = \alpha 1.33 \rho u_0^2 h_0$$

4.1 Evaluation of α

A velocity profile that can describe a flow around an object whose shape is similar to a dry patch was proposed in Chapter 3.

$$\alpha = 1 - \frac{\rho \delta \bar{U} \frac{m}{z_0} \left(\frac{\pi}{2} - \arctan \frac{x_s}{z_0} \right) - \delta \rho \frac{m^2}{2} \left(\frac{1}{x_s^2 + z_0^2} \right)}{\rho \bar{U}^2 \delta}$$

$m, \delta, \bar{U}, x_s, z_0$ same as in Chapter 3.

In order to check the criterion for stability of dry patches, (Equation 4.3) experimental data for local Reynolds number equal to 144 ($Re_i = 185$) were used. A Reynolds number of 150 is three times larger than the maximum Reynolds number permitted for the complete validity of Kapitza's treatment, but measurements below $Re = 50$ were not available. In any case this analysis is intended only as a starting point for the considerations of the stability of dry patches when unsteady effects are important. For this case (low heatflux) heating effects can be neglected. For dry patch stability

$$F_p^{\min} = F_{\sigma}^{\min}$$

$$F_p^{\text{av}} = F_{\sigma}^{\text{av}}$$

$$F_p^{\max} = F_{\sigma}^{\max}$$

Table 4.1 shows the results of the calculations.

TABLE 4.1
Evaluation of Forces For a Wavy Liquid Film

T(°C)	Re_i	Re	α		$F_p \times 10^5$ (N/m)	$F_{\sigma} \times 10^5$ (N/m)	θ (°) experimental
2	185	144	0.47	min.	0.79	104	41
				av.	159	141	48
				max.	396	181	55

The average and maximum pressure force are larger than the average and maximum surface forces, while the minimum pressure force is two orders of magnitude smaller than the surface force.

The fact that the body force compensates with the shear force over a distance equal to a wavelength does not hold near the dry patch. Kapitza's flow is distorted, the pressure increases and the sinusoidal pressure described by Kapitza transforms into an asymmetric pattern. The flow slows down and the balance between shear and body force does not hold any more. As a result of this a net body force which also changes with time can be present in the equilibrium of forces.

The influence of the lateral flow evaluated through the coefficient α has the same limitations as was pointed out in Chapter 3. At this stage it is interesting to compare this simple model with some suggestions to treat unsteady effects made by Thompson [8]. If the pressure force is evaluated as Thompson did using a thickness equal to the average, minimum and maximum, but with a parabolic velocity profile (Thompson used a linear and a logarithmic velocity profile) the results are rather different (Table 4.2).

TABLE 4.2

Evaluation of Forces (Thickness Criterion) For A Wavy Film

	$F_p \times 10^5$ (N/m)	$F_\sigma \times 10^5$ (N/m)
min.	5	104
av.	109	141
max.	728	181

The results of Table 4.1 and Table 4.2 indicate that the evaluation of forces through the momentum theorem and through the thickness criterion are not equivalent. The maximum pressure force evaluated through the thickness criterion is significantly larger than the surface tension force. Thompson [8] found the same relationship for unstable dry patches, but in the present analyzed case the dry patch is stationary. Neither of these criteria give a good agreement with experimental data. Nevertheless, the control volume method of finding the pressure force is well founded while the thickness criterion to evaluate the force in the presence of waves is not justified. The disagreement between the downstream force evaluated through the momentum theorem and the upstream force for stationary dry patches is due to the fact that near the dry patch the flow is two dimensional and the internal pressure increases. These properties are not described by Kapitza's analysis.

5. A RATIONAL TWO-DIMENSIONAL MODEL

5.1 General

An exact solution of the fundamental equations of motion and energy equation would be desirable for dry patch stability studies. However, since these equations are non-linear and coupled, not only directly but through boundary conditions, it seems unlikely that complete solutions could be found for the general case.

The first useful approximation in order to get an indication of expected behaviour would be to consider an isothermal flow, the dry patch arising from some change in surface condition. However, the resulting Navier-Stokes equations for a viscous, free-surface flow around a dry patch of unknown shape are still unsoluble. This chapter suggests two further approximations in order to get the simplest model from which useful information can be obtained. First the flow is assumed steady, so that only "static" stability of the dry patch is determined. It is entirely possible that a "dynamic" stability analysis including surface waves might yield different results. However, the static model indicates some general features of the flow. Second, a procedure is employed analogous to that of using combinations of potential flow and boundary layer analysis to describe flow over a body. The dry patch is assumed to act as a solid body in the flow, and the flow patterns around it are determined by ignoring the boundary condition of prescribed contact angle at the edge of the patch (outer

region). This flow is "patched" to a second type which properly accounts for boundary conditions, but does not involve details of the flow away from the dry patch (inner region).

In the approximation of considering the dry patch as an obstacle for the flow, the idea is to find the flow behaviour of a liquid film with a free surface in the presence of an object. Lamb [36] showed (see also Schlichting [37]) that when a liquid between two plates is driven by a pressure gradient past a cylindrical closed body of arbitrary cross section placed between the plates, the resulting pattern of streamlines is identical with that in potential flow about the same shape. Hele-Shaw [38] used this method to obtain experimental patterns of streamlines in potential flow about arbitrary bodies. The present model is the following: a liquid film flowing along an inclined plate is forced by gravity past a solid body with the shape of a dry patch. The pressure increases and is taken into account hydrostatically by increasing the film thickness. The variation of thickness is gradual and curvature of the free surface is considered slight enough to neglect surface tension effects. The flow is perturbed as if an object of a size approximately equal to the size of a dry patch is placed between the free surface and the plate. When the fluid stagnates in front of the object the thickness of the liquid film is a maximum. In the second part of the model, surface tension effects are predominant and the thickness goes to zero and forms the contact angle θ with the plate (Figure 25). In this region inertial effects are neglected and the increase in pressure is hydrostatic. The difference between the inner

and external pressure at the free surface is equal to $\frac{\sigma}{K}$
(K = radius of curvature).

5.2 Solution

5.2.1 Outer Region

In the case of a slow liquid film flowing along an inclined plate forced by gravity past an obstacle the simplified equations of motion and continuity are (See Appendix B).

$$\frac{1}{\rho} \frac{\partial p}{\partial x} = \nu \frac{\partial^2 u}{\partial y^2} + g \sin \alpha \quad \dots (5.9)$$

$$\frac{1}{\rho} \frac{\partial p}{\partial y} = -g \cos \alpha \quad \dots (5.11)$$

$$\frac{1}{\rho} \frac{\partial p}{\partial z} = \nu \frac{\partial^2 w}{\partial y^2} \quad \dots (5.12)$$

$$\frac{\partial u}{\partial x} + \frac{\partial v}{\partial y} + \frac{\partial w}{\partial z} = 0 \quad \dots (5.13)$$

with the assumptions that

$$\delta_{\infty}/L \ll 1 ,$$

$$\left(\frac{\bar{u} \delta_{\infty}}{\nu}\right) \frac{\delta_{\infty}}{L} \ll 1 ,$$

$$\tan \alpha \sim \alpha \sim \delta_{\infty}/L .$$

The boundary conditions for this region are:

$$u(y = 0) = 0 \quad \left(\frac{\partial u}{\partial y}\right)_{y=\delta} = 0$$

$$w(y = 0) = 0 \quad \left(\frac{\partial w}{\partial y}\right)_{y=\delta} = 0$$

$$p(x, \delta(x, z), z) = 0 .$$

As the component v of the velocity appears only in the equation of continuity as a first approximation it is considered negligible. The set of equations is then

$$\frac{1}{\rho} \frac{\partial p}{\partial x} = v \frac{\partial^2 u}{\partial y^2} + g \sin \alpha \quad \dots \dots (5.9)$$

$$\frac{1}{\rho} \frac{\partial p}{\partial y} = -g \cos \alpha \quad \dots \dots (5.11)$$

$$\frac{1}{\rho} \frac{\partial p}{\partial z} = v \frac{\partial^2 w}{\partial y^2} \quad \dots \dots (5.12)$$

$$\frac{\partial u}{\partial x} + \frac{\partial w}{\partial z} = 0 \quad \dots \dots (5.14)$$

Integrating Equation 5.11,

$$p(x, y, z) - p_B(x, y = 0, z) = -\rho g \cos \alpha y ,$$

$$p(x, y, z) = p_B(x, z) - \rho g \cos \alpha y \quad \dots \dots (5.15)$$

Replacing the expression of the pressure in Equations 5.9 and 5.12

$$\frac{1}{\rho} \frac{\partial p_B}{\partial x} = \nu \frac{\partial^2 u}{\partial y^2} + g \sin \alpha \quad \dots (5.16)$$

$$\frac{1}{\rho} \frac{\partial p_B}{\partial z} = \nu \frac{\partial^2 w}{\partial y^2} \quad \dots (5.17)$$

If in Equation 5.16 it is defined

$$p'_B = p_B - \rho g \sin \alpha x \quad ,$$

then

$$\frac{1}{\rho} \frac{\partial p'_B}{\partial x} = \nu \frac{\partial^2 u}{\partial y^2} \quad \dots (5.16b)$$

$$\frac{1}{\rho} \frac{\partial p'_B}{\partial z} = \nu \frac{\partial^2 w}{\partial y^2} \quad \dots (5.17b)$$

Equations 5.14, 5.16b and 5.17b form a set of equations similar to the equations describing the Hele-Shaw experiments (Lamb [36], Schlichting [37]). A velocity field can then be defined

$$u = u_T(x, z) \left(\frac{2y}{\delta(x, z)} - \frac{y^2}{\delta^2(x, z)} \right) \quad ,$$

$$w = w_T(x, z) \left(\frac{2y}{\delta(x, z)} - \frac{y^2}{\delta^2(x, z)} \right) \quad .$$

According to the boundary condition

$$p(x, \delta(x, z), z) = 0 \quad ,$$

$$p_B = \rho g \cos \alpha \delta$$

from Equation (5.15). Then replacing u , w and p_B in Equations 5.16b, and 5.17b,

$$\frac{1}{\rho} \frac{\partial}{\partial x} (\rho g \cos \alpha \delta - \rho g \sin \alpha x) = -\nu \frac{2}{\delta^2} u_T ,$$

$$\frac{1}{\rho} \frac{\partial}{\partial z} (\rho g \cos \alpha \delta) = -\nu \frac{2}{\delta^2} w_T ,$$

$$\frac{\partial \delta}{\partial x} = -\frac{2\nu}{g\delta^2 \cos \alpha} u_T + \tan \alpha \quad \dots (5.18)$$

$$\frac{\partial \delta}{\partial z} = -\frac{2\nu}{g\delta^2 \cos \alpha} w_T \quad \dots (5.19)$$

$$\frac{\partial u}{\partial x} + \frac{\partial w}{\partial z} = 0 \quad \dots (5.20)$$

Equations (5.18 to 5.20) form a set of non-linear partial differential equations. If only a small increase in thickness is expected δ^2 can be put approximately equal to δ_∞^2 in the right hand side of Equations (5.18) and (5.19). Equation (5.20) becomes

$$\frac{\partial u_T}{\partial x} + \frac{\partial w_T}{\partial z} = 0 \quad \dots (5.21)$$

If this is done it can be shown that u_T and w_T are velocity components of a potential flow and that the velocity potential is

$$\Phi = \frac{\cos \alpha g \delta_\infty^2}{2\nu} (\delta(x,z) - (\tan \alpha) x) ,$$

For example, if $\delta = \delta_\infty$ in the right hand side of Equations 5.18 and 5.19, the equations become

$$\frac{\partial \delta}{\partial x} = - \frac{2\nu}{g \delta_\infty^2 \cos \alpha} u_T + \tan \alpha , \quad \dots \dots (5.22)$$

$$\frac{\partial \delta}{\partial z} = - \frac{2\nu}{g \delta_\infty^2 \cos \alpha} w_T . \quad \dots \dots (5.23)$$

Differentiating Equations (5.22) respect to x and Equation (5.23) respect to z and applying Equation (5.21),

$$\nabla^2 \delta(x,z) = 0 .$$

In addition, when Equation (5.22) is differentiated with respect to z and Equation (5.23) is differentiated with respect to x ,

$$\frac{\partial u_T}{\partial z} - \frac{\partial w_T}{\partial x} = 0 . \quad \dots \dots (5.24)$$

Then because of Equations 5.21 and 5.24, u_T and w_T are harmonic functions. If it is assumed that the object has the shape of a complete Rankine body whose size is approximately the size of the dry patch, u_T and w_T can be expressed as

$$u_T = U_T + m \left\{ \frac{x+a}{(x+a)^2 + z^2} - \frac{x-a}{(x-a)^2 + z^2} \right\},$$

$$w_T = m \left\{ \frac{z}{(x+a)^2 + z^2} - \frac{z}{(x-a)^2 + z^2} \right\},$$

where

m = source

a = distance from origin to source and sink

$U_T = \rho g \delta_\infty^2 \sin \alpha / 2\mu$ velocity for $x = \infty$.

Replacing u_T and w_T in Equations 5.22 and 5.23

$$\frac{\partial \delta}{\partial x} = \frac{-2\nu}{g \delta_\infty^2 \cos \alpha} \left\{ U_T + m \left(\frac{x+a}{(x+a)^2 + z^2} - \frac{x-a}{(x-a)^2 + z^2} \right) \right\} + \tan \alpha, \quad \dots (5.25)$$

$$\frac{\partial \delta}{\partial z} = \frac{-2\nu}{g \delta_\infty^2 \cos \alpha} m \left\{ \frac{z}{(x+a)^2 + z^2} - \frac{z}{(x-a)^2 + z^2} \right\} \quad \dots (5.26)$$

The boundary condition is that

$$\delta(-\infty, z) = \delta_\infty.$$

Substituting the value of U_T in Equation 5.25, the first term and third term of the right hand side cancel

$$\frac{\partial \delta}{\partial x} = - \frac{2\nu}{g\delta_\infty^2 \cos \alpha} m \left\{ \frac{(x+a)}{(x+a)^2 + z^2} - \frac{x-a}{(x-a)^2 + z^2} \right\} \dots (5.27)$$

Integrating 5.27

$$\delta = \frac{-2\nu}{g\delta_\infty^2 \cos \alpha} \frac{m}{2} \ln \left[\frac{(x+a)^2 + z^2}{(x-a)^2 + z^2} \right] + f(z) .$$

Integrating 5.26

$$\delta = \frac{-2\nu}{g\delta_\infty^2 \cos \alpha} \frac{m}{2} \ln \left[\frac{(x+a)^2 + z^2}{(x-a)^2 + z^2} \right] + f(x) .$$

Then

$$f(x) = f(z) = C ,$$

$$\delta(x, z) = - \frac{2\nu}{g\delta_\infty^2 \cos \alpha} \frac{m}{2} \ln \left[\frac{(x+a)^2 + z^2}{(x-a)^2 + z^2} \right] + C ,$$

$$\delta(-\infty, z) = \delta_\infty \dots C = \delta_\infty ,$$

$$\frac{\delta(x, z)}{\delta_\infty} = - \frac{\nu}{g\delta_\infty^3 \cos \alpha} m \ln \left[\frac{(x+a)^2 + z^2}{(x-a)^2 + z^2} \right] + 1 .$$

For $z = 0$

$$\frac{\delta(x,0)}{\delta_\infty} = - \frac{2\nu}{g\delta_\infty^3 \cos \alpha} m \ln \left| \frac{x+a}{x-a} \right| + 1 .$$

From the geometry of the Rankine body [35]

$$m = \frac{bU_T}{2 \arctan (a/b)} = \frac{bg \sin \alpha \delta_\infty^2}{2 \nu 2 \arctan a/b} ,$$

$$\left(\frac{a}{b}\right)^2 + \frac{a/b}{\arctan (a/b)} = A^2$$

where

$A =$ aspect ratio of the body $= L/b$

$L =$ length

$b =$ width .

Then

$$\frac{\delta(x,0)}{\delta_\infty} = \tan \alpha \frac{b}{\delta_\infty} \frac{1}{2 \arctan (a/b)} \ln \left| \frac{x/b - a/b}{x/b + a/b} \right| + 1 .$$

The maximum thickness occurs at $x = -L$

$$\frac{\delta_M(-L,0)}{\delta_\infty} = \tan \alpha \frac{b}{2\delta_\infty \arctan (a/b)} \ln \left| \frac{-A - a/b}{-A + a/b} \right| + 1 . \quad (5.28)$$

The ratio of the maximum thickness to the thickness at infinity is proportional to $Re^{-1/3}$.

5.2.2 Inner Region

In this region the flow is considered at rest and the Navier-Stokes equations are expressed as

$$\frac{1}{\rho} \frac{\partial p}{\partial x} = g \sin \alpha$$

$$\frac{1}{\rho} \frac{\partial p}{\partial y} = -g \cos \alpha$$

$$\frac{1}{\rho} \frac{\partial p}{\partial z} = 0 .$$

Integrating

$$p(x,y) = \rho g \sin \alpha x - \rho g \cos \alpha y + C .$$

The system of co-ordinates is located now at the surface of the imaginary body. If the boundary condition,

$$p(x = 0, y = \delta_M) = 0 \quad \dots \dots (5.29)$$

is chosen, then

$$p(x,y) = \rho g \sin \alpha x + \rho g \cos \alpha (\delta_M - y) . \quad \dots \dots (5.30)$$

The difference between the internal pressure (liquid pressure) and external pressure being the surface tension divided by the curvature

$$p = p_i - p_e = \sigma/K .$$

The curvature is expressed by

$$\frac{1}{K} = \frac{-\frac{d^2y}{dx^2}}{[1 + (\frac{dy}{dx})^2]^{3/2}} \approx -\frac{d^2y}{dx^2}$$

Equation (5.29) can be written as

$$\rho g \sin \alpha x + \rho g \cos \alpha (\delta_M - y) = -\sigma \frac{d^2y}{dx^2} .$$

The boundary conditions are

$$y(x=0) = \delta_M , \quad \frac{dy}{dx}(x=d) = -\tan \theta .$$

If the variable r is introduced equal to $\delta_M - y$

$$\frac{d^2r}{dx^2} - n^2 r = \frac{\rho g (\sin \alpha) x}{\sigma} , \quad n = \sqrt{\frac{\rho g \cos \alpha}{\sigma}} \dots (5.31)$$

A nondimensional form of the Equation (5.31) can be formed by choosing the dimensionless variables

$$x^* = \frac{x}{d}$$

$$r^* = \frac{r}{\delta_M} = 1 - \frac{y}{\delta_M}$$

so that

$$\frac{d^2 r^*}{dx^{*2}} - (n^2 d^2) r^* = (n^2 d^2) \left(\frac{d}{\delta_M} \right) (\tan \alpha) x^* \quad \dots \dots (5.32)$$

The boundary conditions in terms of the dimensionless variables are

$$r^*(x^* = 0) = 0 ,$$

$$\frac{dr^*}{dx^*}(x^* = 1) = \tan \theta \frac{d}{\delta_M} .$$

The solution of (5.32) is

$$r^* = A \cosh(ndx^*) + B \sinh(ndx^*) - \frac{d}{\delta_M} (\tan \alpha) x^* .$$

The first boundary condition implies that the coefficient A is equal to zero, while the second boundary condition determines B.

Thus

$$ndB \cosh nd - \frac{d}{\delta_M} \tan \alpha = \tan \theta \frac{d}{\delta_M} ,$$

and

$$B = \left(\frac{d}{\delta_M} \right) \frac{\tan \theta + \tan \alpha}{(nd) \cosh nd} = \frac{1}{\delta_M} \frac{(\tan \theta + \tan \alpha)}{n \cosh nd} ,$$

$$r^* = \frac{d}{\delta_M} \frac{(\tan \theta + \tan \alpha)}{(dn) \cosh nd} \sinh (ndx^*) - \frac{d}{\delta_M} (\tan \alpha)x^* \dots (5.33)$$

When $x^* = 1$, $r^* = 1$, these conditions define an equation for d :

$$1 = \frac{1}{\delta_M} (\tan \theta + \tan \alpha) \tanh nd - \frac{d}{\delta_M} \tan \alpha .$$

In terms of y , Equation (5.32) can be expressed as,

$$\frac{y}{\delta_M} = 1 - \frac{d}{\delta_M} \frac{(\tan \theta + \tan \alpha)}{(dn) \cosh nd} \sinh (ndx^*) - \frac{d}{\delta_M} (\tan \alpha)x^* .$$

This model also predicts a pressure force

$$F_p = \int_0^{\delta_M} \rho g \cos \alpha (\delta_M - y) dy = \frac{\rho g \cos \alpha \delta_M^2}{2} \dots (5.34)$$

5.3 Discussion

Figure (26) and (27) show the thickness profile for two Reynolds numbers when the plate inclination $\alpha = 2^\circ$. The contact angle, the width of the patch and the aspect ratio were chosen arbitrarily equal to 35° , 100×10^{-5} m and 2 respectively. The model gives an increase in thickness near the dry patch as was expected. The representation of the thickness for the inner region is almost

a straight line. This is due to the low pressure generated relative to the surface tensions according to this model. At each point of the curve the radius of curvature is much larger than the thickness. The matching of the solutions is not smooth because the effect of surface tension was neglected in the outer region. It should be mentioned at this point that if instead of the boundary conditions (5.29) a different constant is chosen different curvatures at the maximum thickness will result. The model permits the evaluation of a pressure force (Equation 5.34). Experimental data available correspond to observations of dry patches formed on a vertical plate. However, when the hysteresis in contact angle is small it is expected that surface force for a patch formed on an inclined plate will be similar to that on a vertical plate. Thus their pressure forces will be similar. For this reason McAdam's data were used to evaluate a pressure force according to the present model.

The model is valid for $(\text{Re} \frac{\delta_{\infty}}{L}) \ll 1$. McAdam's lowest Reynolds number corresponds to 185. If the length of the patch is chosen ten times larger than the width, the product $(\text{Re} \frac{\delta_{\infty}}{L})$ is of the order of 15, actually out from the range of validity of the model. Nevertheless, the pressure force was calculated to be 44×10^{-5} N/m. The surface force was evaluated according to previous models, $(F_{\sigma} = \sigma(1 - \cos \theta))$. Table 5.1 shows the results of the calculations.

TABLE 5.1

Evaluation of Pressure Force According to Model Described in Chapter 5

Re_i	$\theta(^{\circ})$	$\alpha(^{\circ})$	A	$b \times 10^5 (m)$	$\delta_{\infty} \times 10^5 (m)$	$\delta_M \times 10^5 (m)$	$F_p \times 10^5 (N/m)$	$F_{\sigma} \times 10^5 (N/m)$
185	48	2	10	100	27.4	31.64	44	146

If the surface force is correct, the requirement of equilibrium means the model underestimates the pressure force. The simplifications of the present approach introduce important limitations to the model. For example, the dependence of thickness on Reynolds number: if the patch dimensions don't depend strongly on Re, when Re increases the relative increase of thickness decreases; when Reynolds number decreases, the relative increase of thickness increases. This gives a contradictory result in the limit of zero Reynolds number since the increase in thickness should go to zero.

Perhaps the main restriction of this analysis was equating thickness with thickness at infinity in the right hand side of Equations (5.18 and 5.19). This restriction means that the absolute increase in thickness has to be considerably smaller than the initial thickness. With that condition it was found that absolute increase does not depend on initial thickness, but only on the geometry of the patch. As $Re = C \delta_{\infty}^3$, then $Re \gg C \Delta \delta^3$ (where C = constant, and $\Delta \delta$ is increase in thickness), while on the other hand $(Re \frac{\delta_{\infty}}{L}) \ll 1$. Thus there must be a range of Re where the results of the model describe the actual flow behaviour well. For example if $\alpha = 2^{\circ}$, $A = 2$, $b = 100 \times 10^{-5} m$ then $0 \ll Re \ll 16$.

Further measurements of patches in the range where the present model is valid are needed to compare the film profiles and pressure force with the actual behaviour and real forces.

6. SUMMARY AND CONCLUSIONS

A study has been carried out on the break-up of thin liquid films and the stability of dry patches formed on a heated plate. Recent experimental data [1] have been used to check previous analysis of dry patch stability. The different stability criteria are usually obtained by a force balance at the upstream stagnation point of a dry patch. They consider the principal forces to be pressure, surface tension and thermocapillary forces. The previous models differ mainly in evaluation of the pressure force: some workers [4][6] follow Hartley and Murgatroyd [5] and apply a Bernoulli-type equation to the center streamlines to find the pressure force; others [23] follow Ponter *et al.* [7] and use a control-volume approach. In both analysis the flow is considered one-dimensional and both methods give different results. In the present study the contradiction is clarified by using a control-volume technique applied to a two-dimensional flow. In such a case both methods give equivalent results in the limit, when the control volume coincides with the center streamline.

The experimental parameters used to check the previous models were heat flux, contact angle and Reynolds number. McAdam's thickness data were not used as they probably relate to a "collar" region [23], where the thickness is larger than the thickness further upstream. When these thicknesses are used in the previous criteria, the forces which tend to rewet the dry patch are much, much larger

than those which tend to spread the patch. For this reason upstream thickness corrected for evaporation was used to evaluate the forces.

Zuber and Staub's [6] criterion of force balance best describes the stability of "stationary" dry patches observed and measured by McAdam. At low Re , the balance between the pressure or stagnation force and surface forces is reasonable. At high Re the pressure forces depart significantly from surface forces. Therefore, according to previous models no stable dry patches can exist!

For all Re , the thermocapillary forces have an important role since the measured contact angles decrease with Re for each saturation temperature.

The main failure of previous models is that they are one-dimensional. As a first (and simplest) extension the present study considered an ideal flow around a body whose shape was similar to the shape of a dry patch. The pressure force evaluated by this model is still larger than the surface force, although smaller than the force evaluated for the one-dimensional case. The model was useful in clarifying discrepancies between previous criteria.

A second model to account for unsteady effects was proposed using the wave description for thin films presented by Kapitza [17]. Kapitza analyzed a one-dimensional flow in the plane of the plate, but in the present study the bi-dimensional character of the flow was considered. A coefficient evaluated for the steady two-dimensional case was applied using a control volume technique.

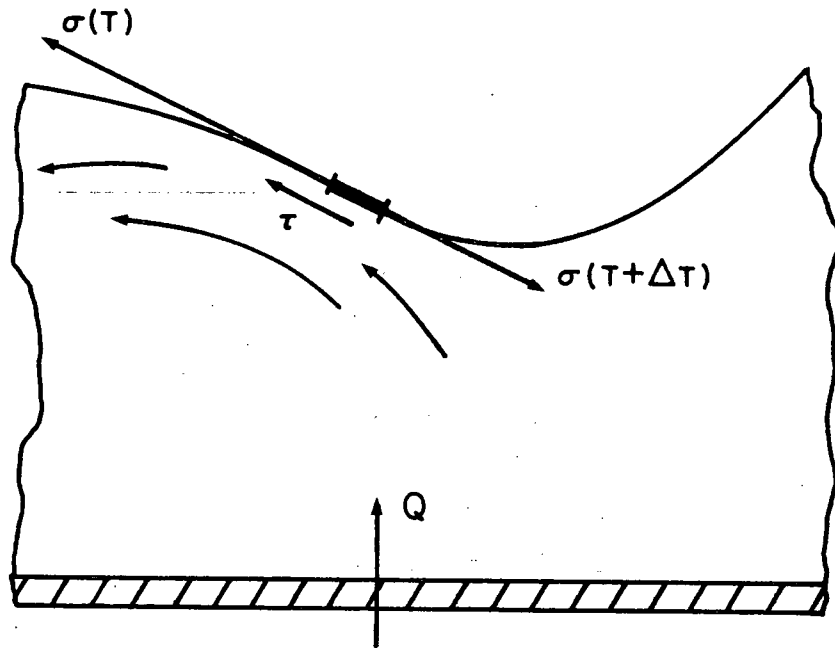
Pressure forces evaluated by the control-volume technique are compared with forces estimated when the thickness criterion [8] is applied to the same waves. Although results are not very different, the present model can be improved since Kapitza's analysis is not valid near the dry patch.

The most important limitation of the simple two-dimensional model is that changes in curvature and thickness of the free surface near the dry patch are not considered. The model presented in Chapter 5, describes the behaviour of a thin liquid film flowing by gravity on an inclined plate where a patch has formed. The problem was divided into two regions, "outer" and "inner". In the outer region increases in hydrostatic pressure arising from the increase of film thickness near the dry patch balance stagnation pressure. The solution obtained is valid for a narrow range of low Reynolds numbers. In the inner region the flow was assumed at rest, and the increase in pressure is compensated for by changes in curvature of the free surface (surface forces).

The estimated profiles are wedge-shaped and different from measured profiles. However, the flow behaviour should not be compared directly with experimental film profiles since they correspond to liquid films at higher Re .

In future work, assumptions made in the development of the present model such as neglecting surface tension effects in the outer region must be alleviated. Thermal effects should also be included, so that at each step a better description of the actual problem is obtained.

THERMOCAPILLARITY



EVAPORATION

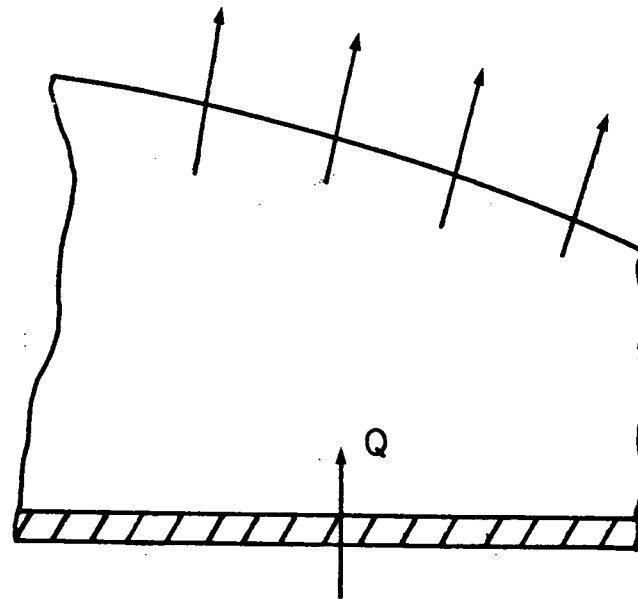


Figure 1 Some mechanisms of film break-up

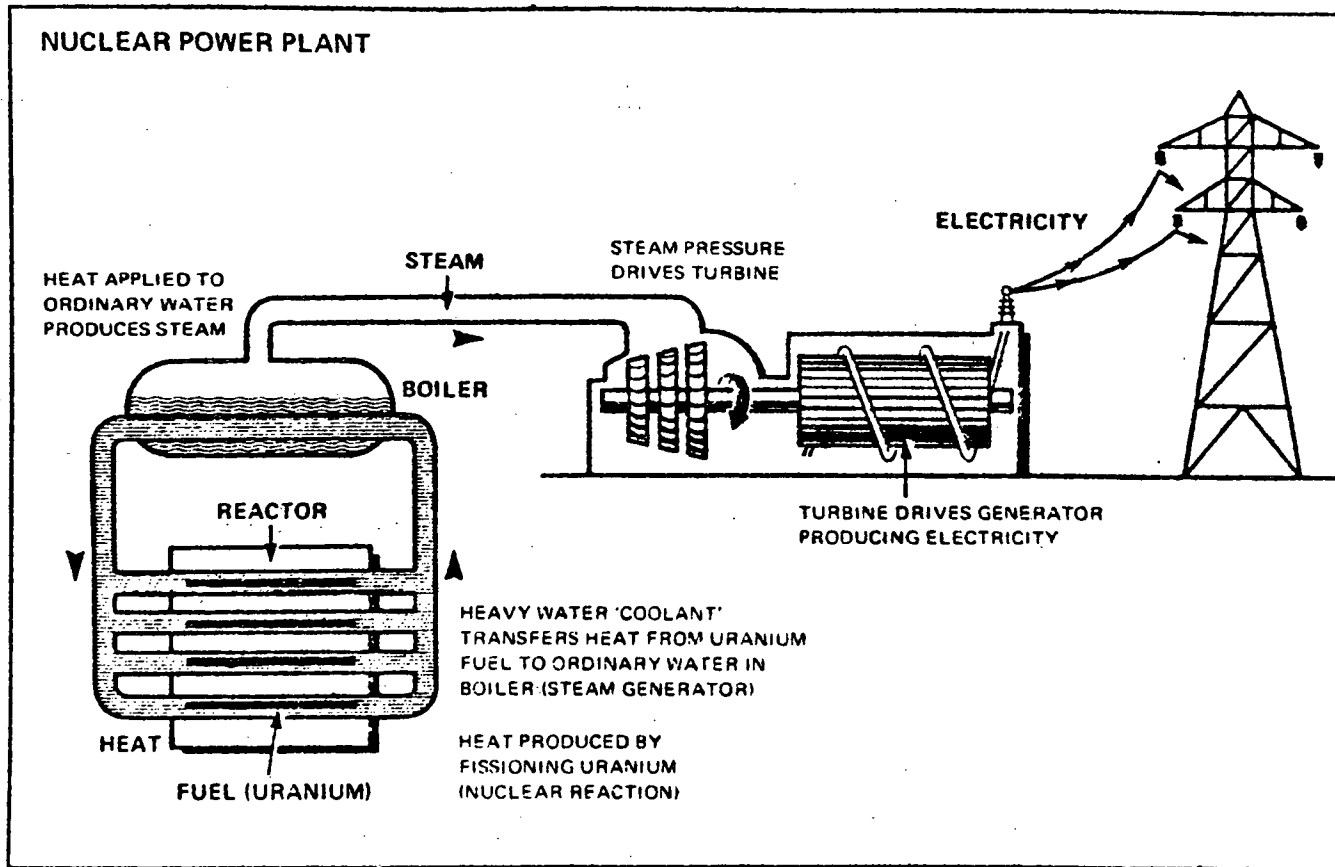


Figure 2 Nuclear power plant

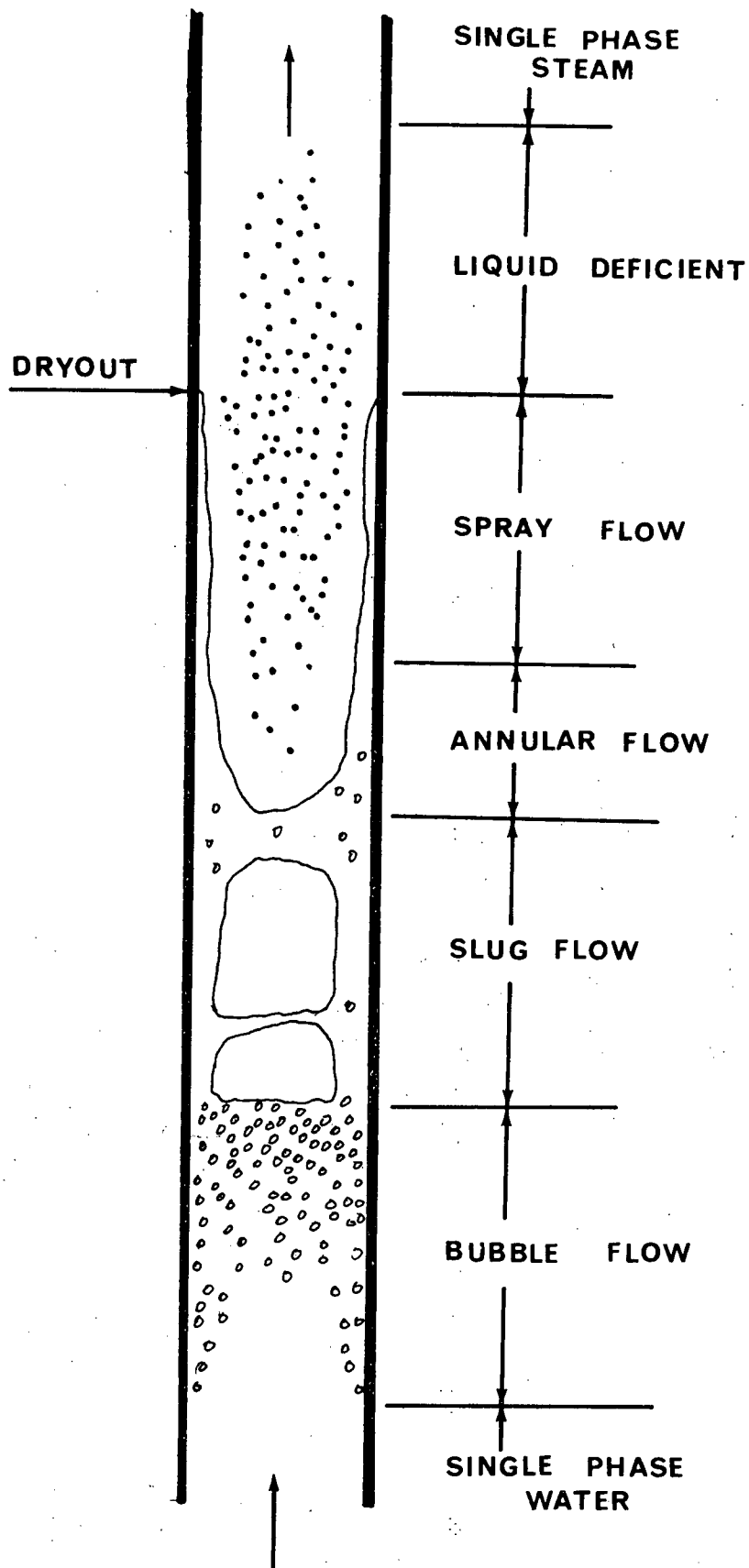


Figure 3 Flow Boiling Regimes, Upward Flow

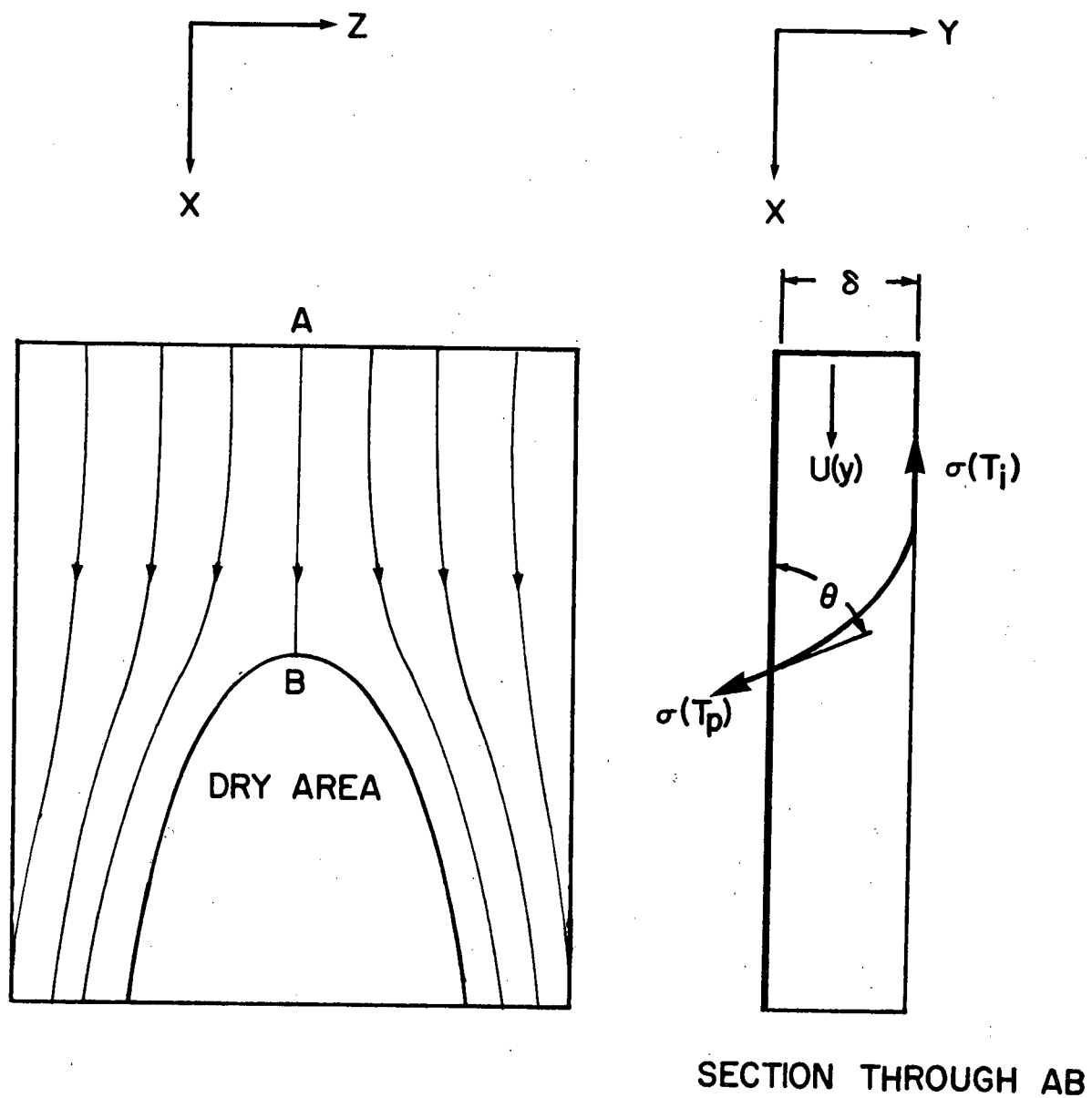
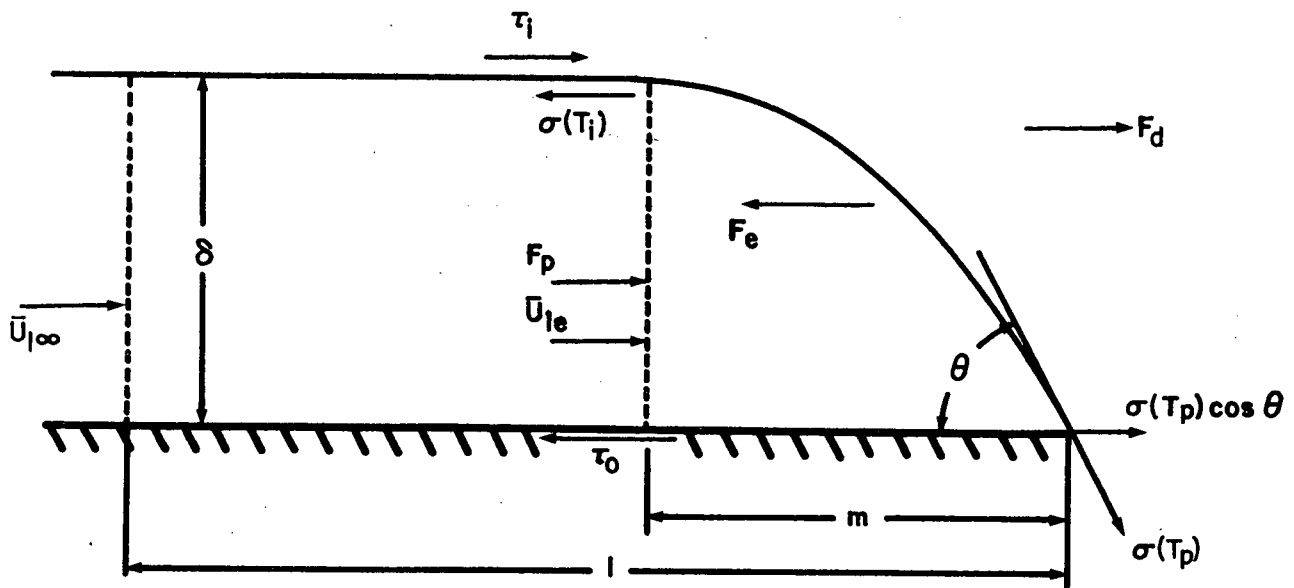


Figure 4 Dry patch on a solid surface



- F_e = FORCE DUE TO VAPOUR THRUST
 F_d = DRAG FORCE OVER STEP IN FILM
 F_p = PRESSURE FORCE
 F_σ = SURFACE FORCE $\sigma(T_1) - \sigma(T_p)\cos\theta$

Figure 5 Forces acting at a dry patch (Ref. 22)

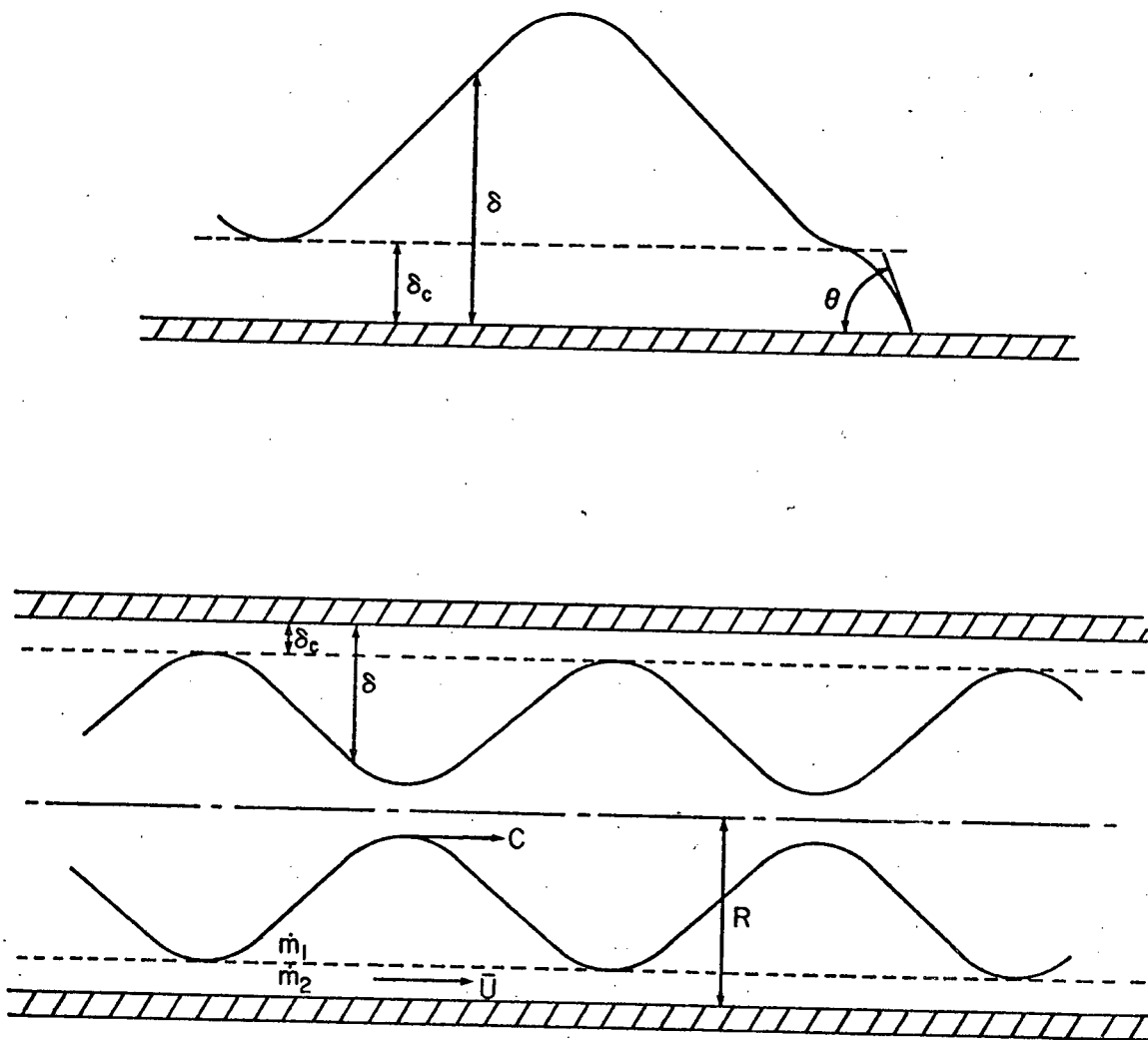


Figure 6 Annular flow with waves (Ref. 26)

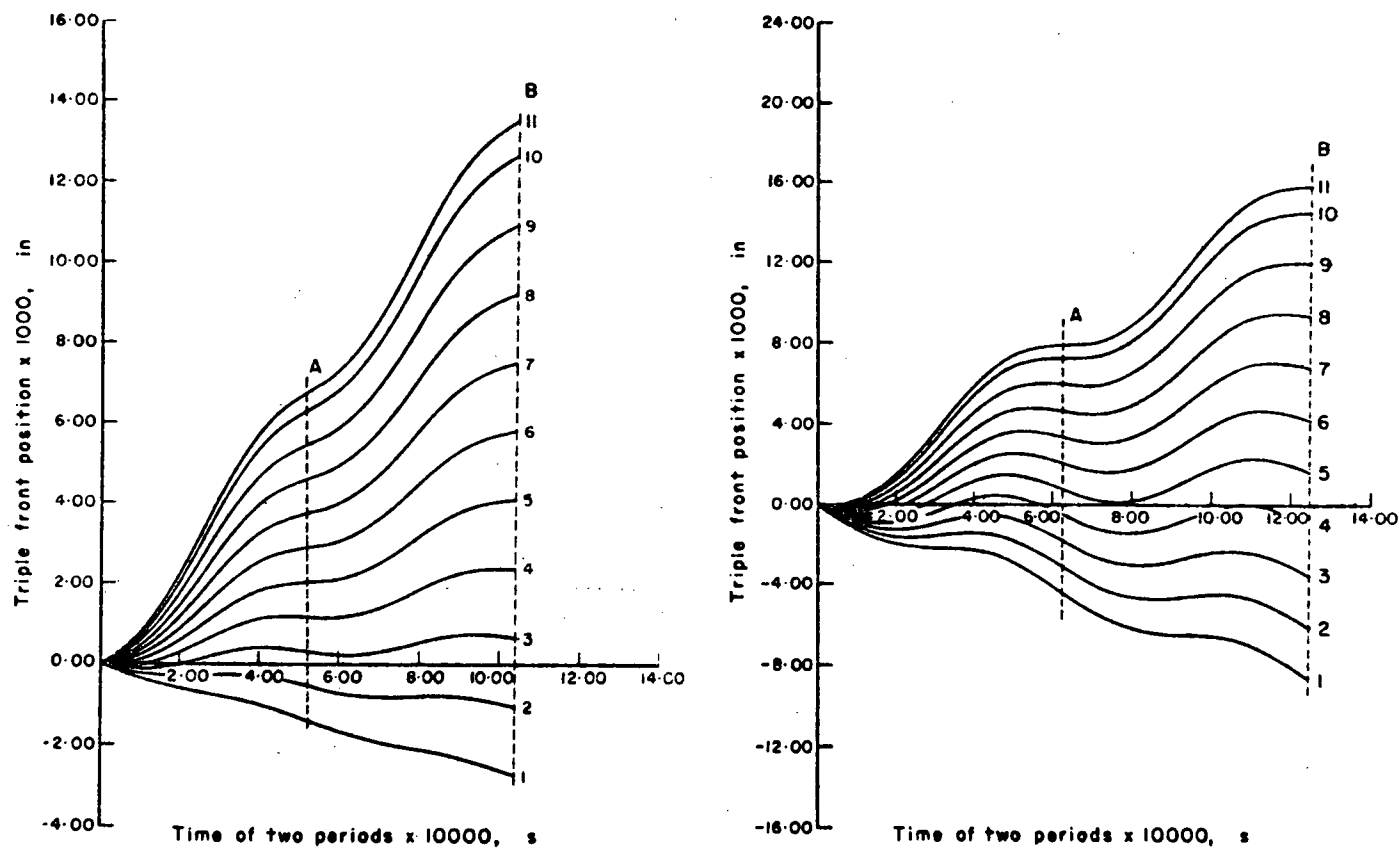
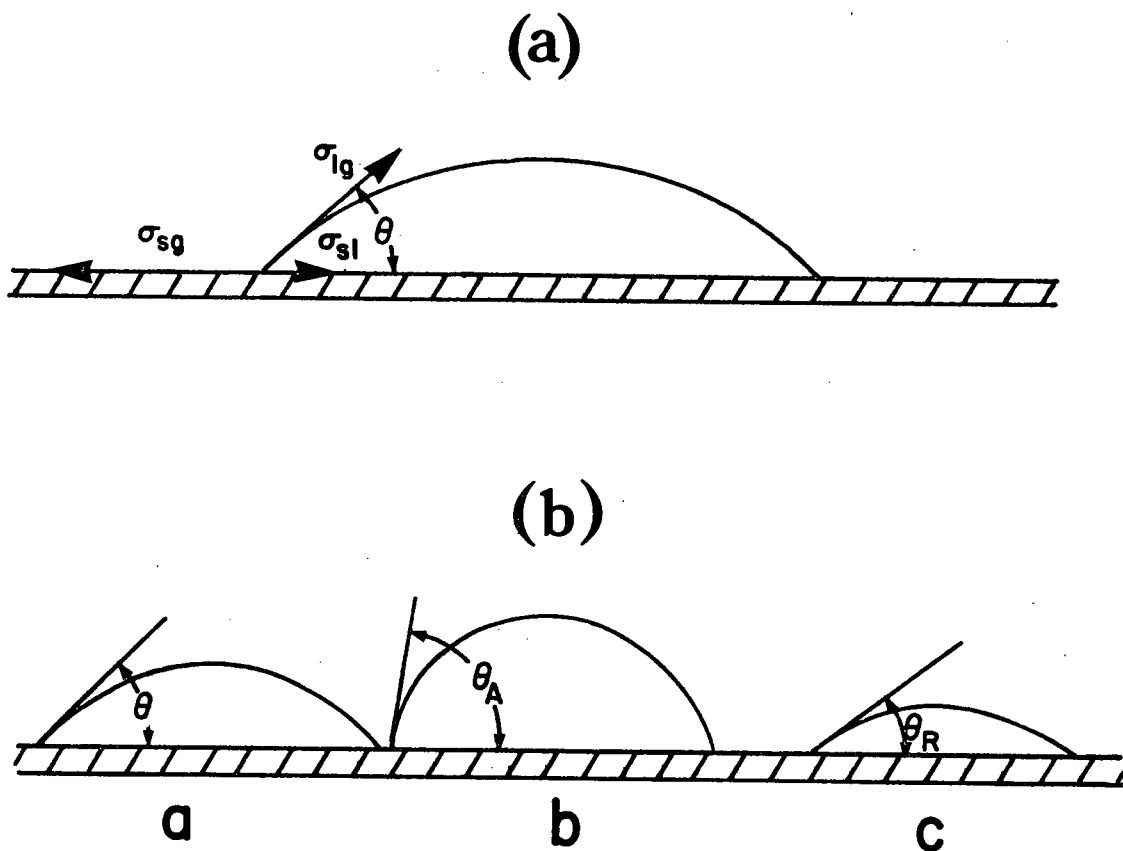


Figure 7 Triple front position during two waves for different values of heat fluxes (Ref. 26)



θ : CONTACT ANGLE IN EQUILIBRIUM

θ_A : STATIC ADVANCING ANGLE

θ_R : STATIC RECEDING ANGLE

Figure 8 (a) A liquid drop on a horizontal plate
(b) Hysteresis of the contact angle

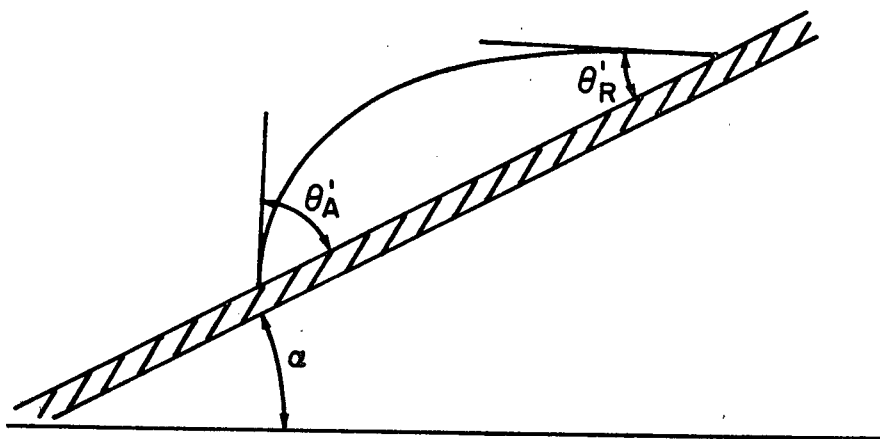
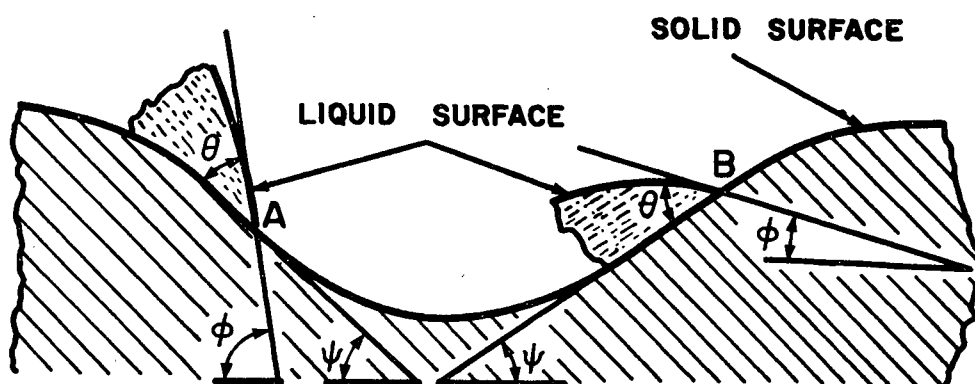


Figure 9 A drop on a tilted plate



AT A,
APPARENT CONTACT ANGLE $\phi = \theta + \psi$

AT B,
APPARENT CONTACT ANGLE $\phi = \theta - \psi$

Figure 10 Variation of apparent contact angle due to surface roughness

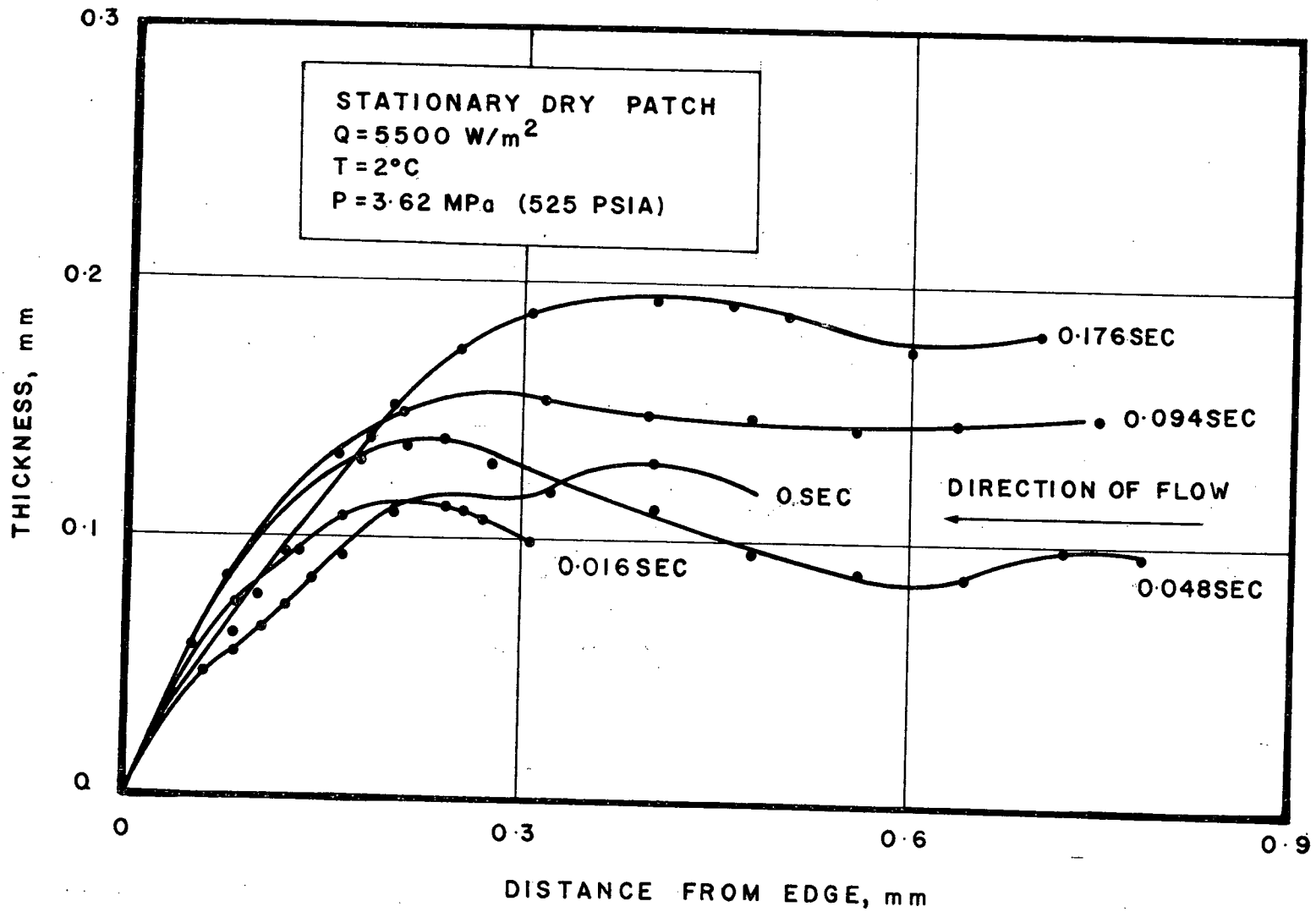


Figure 11 Film profiles for different times, (Ref. 1)

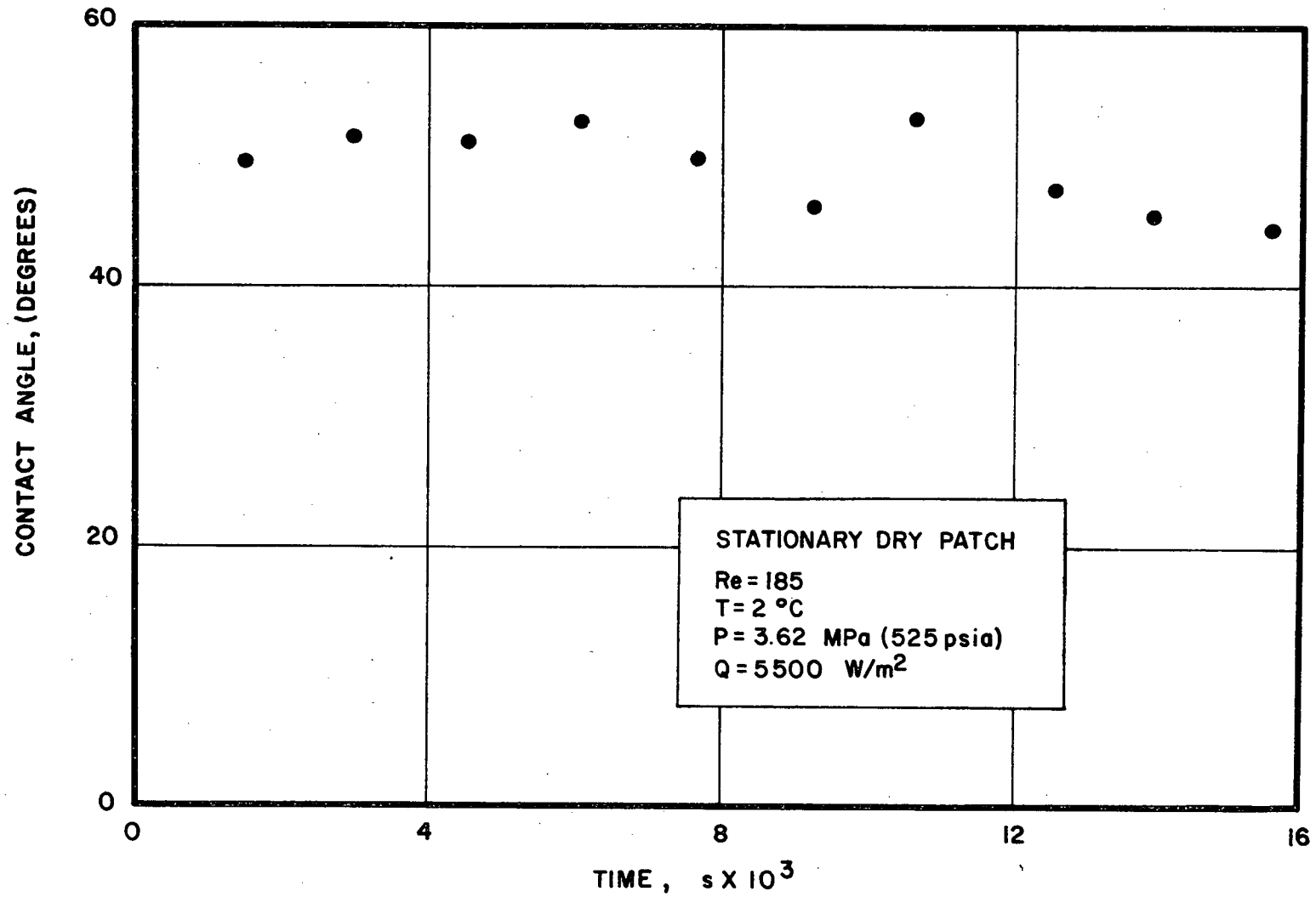


Figure 12 Contact angle variation with time, (Ref. 1)

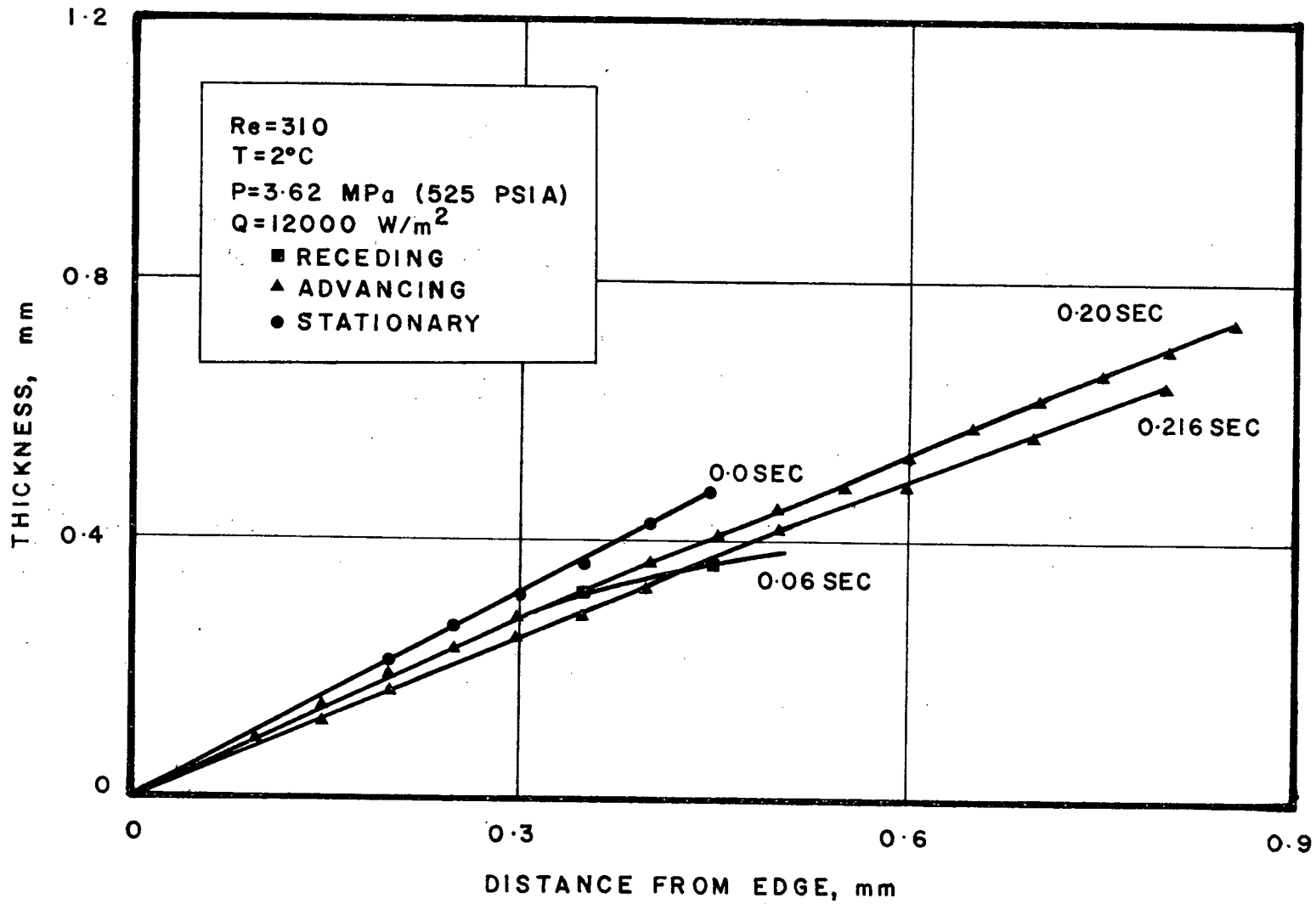


Figure 13 Film profiles for different times, (Ref. 1)

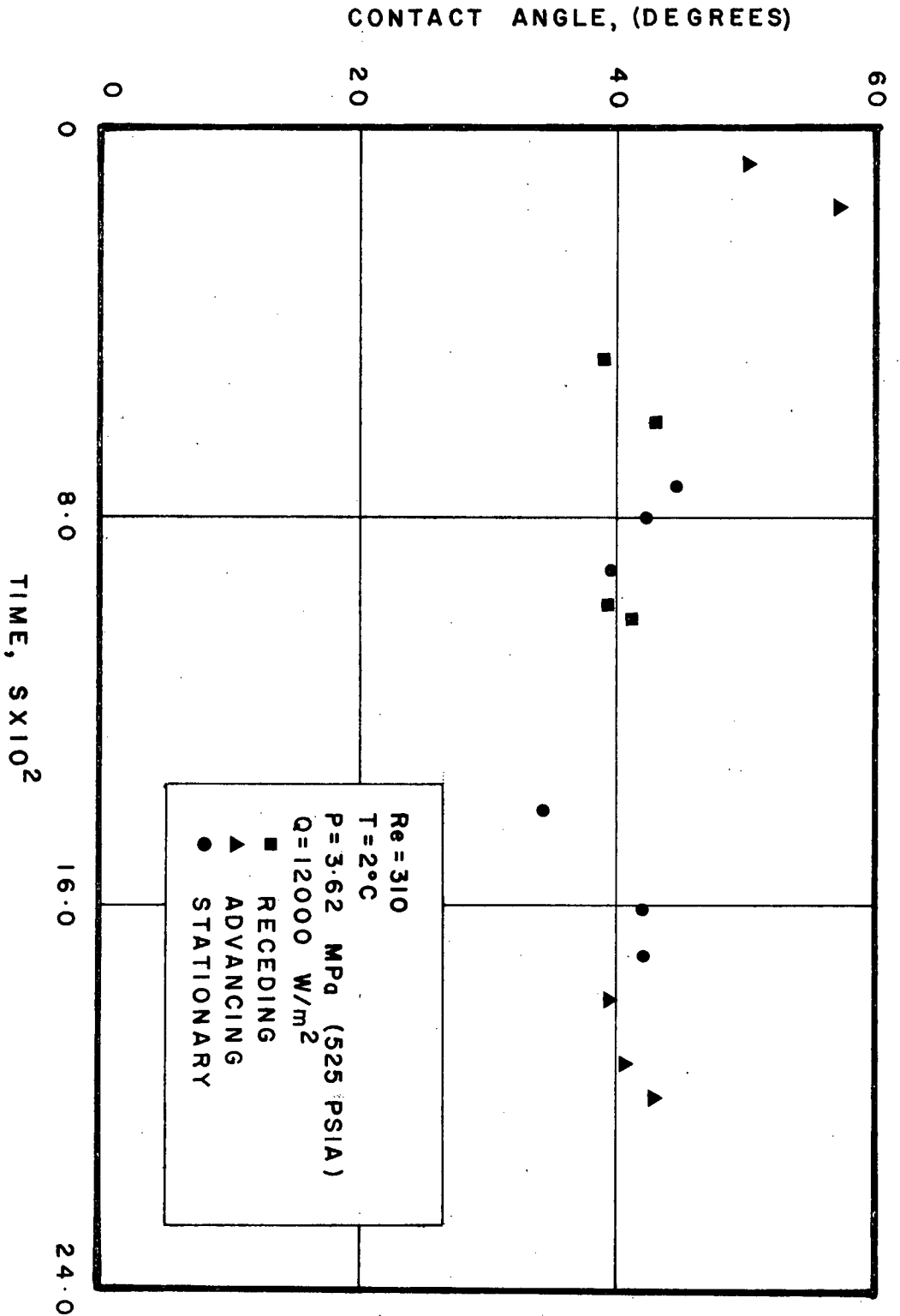


Figure 14 Contact angle variation with time, (Ref. 1)

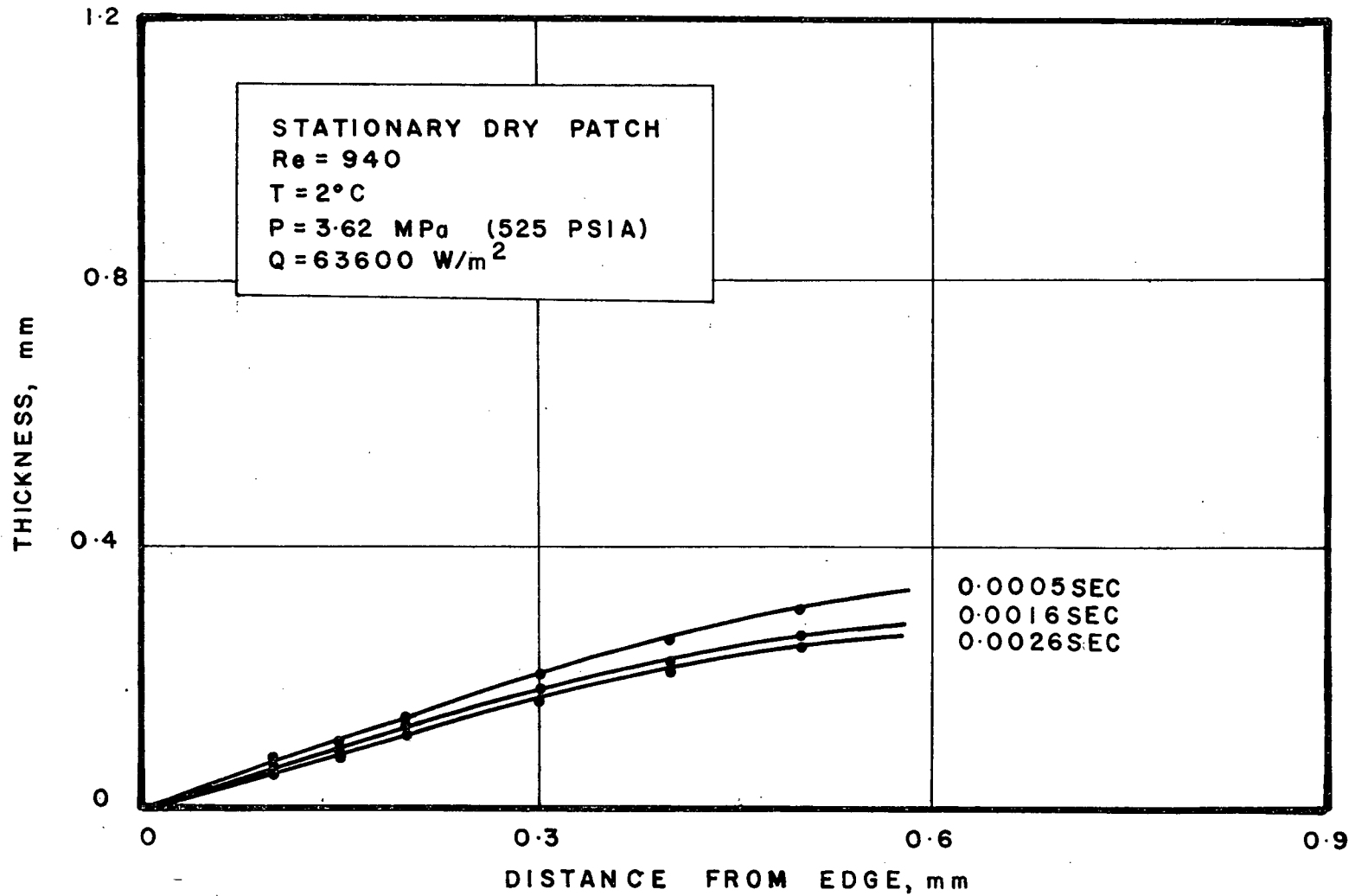


Figure 15 Film profiles for different times, (Ref. 1)

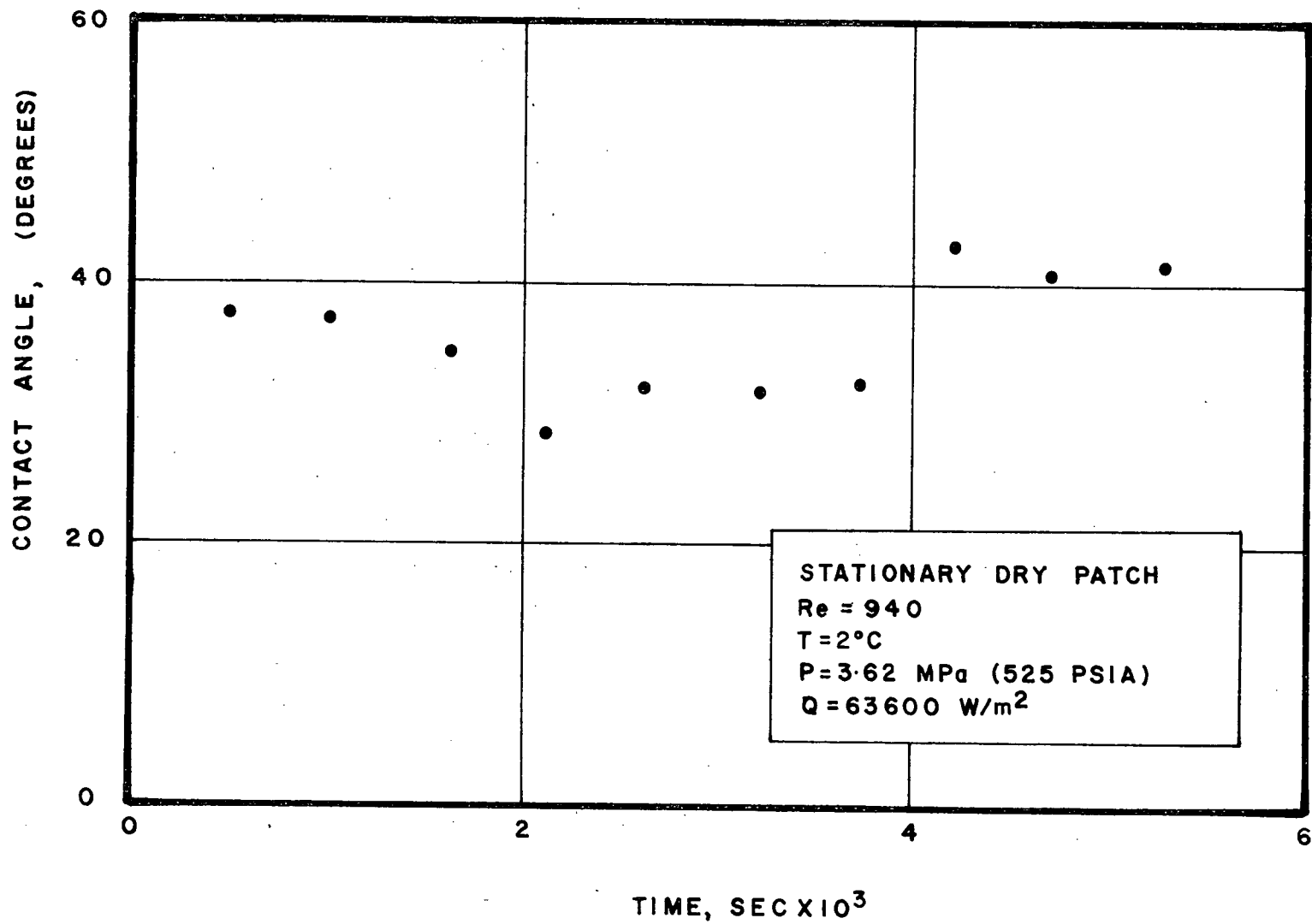


Figure 16 Contact angle variation with time, (Ref. 1)

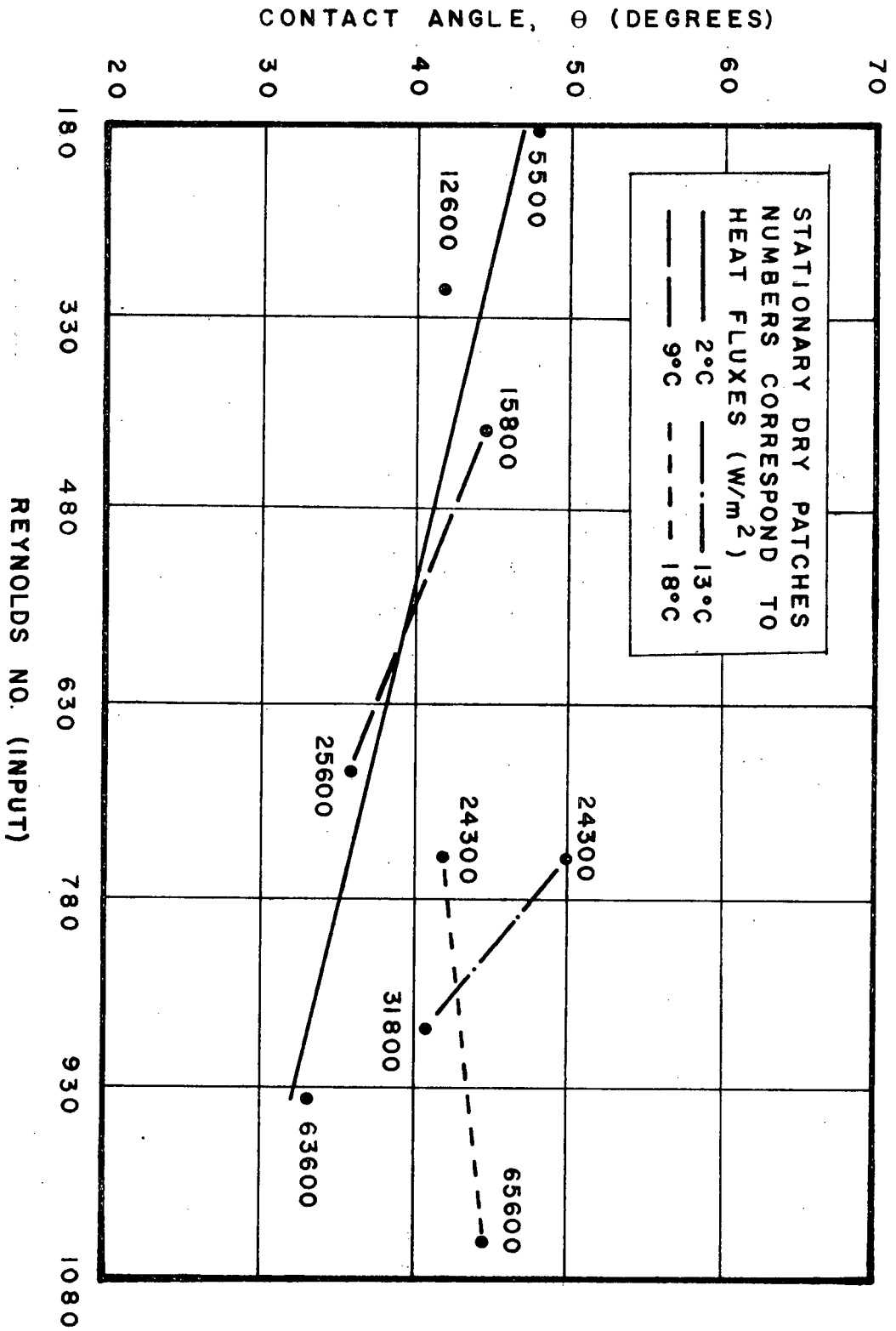


Figure 17 Average contact angle versus Input Reynolds No.

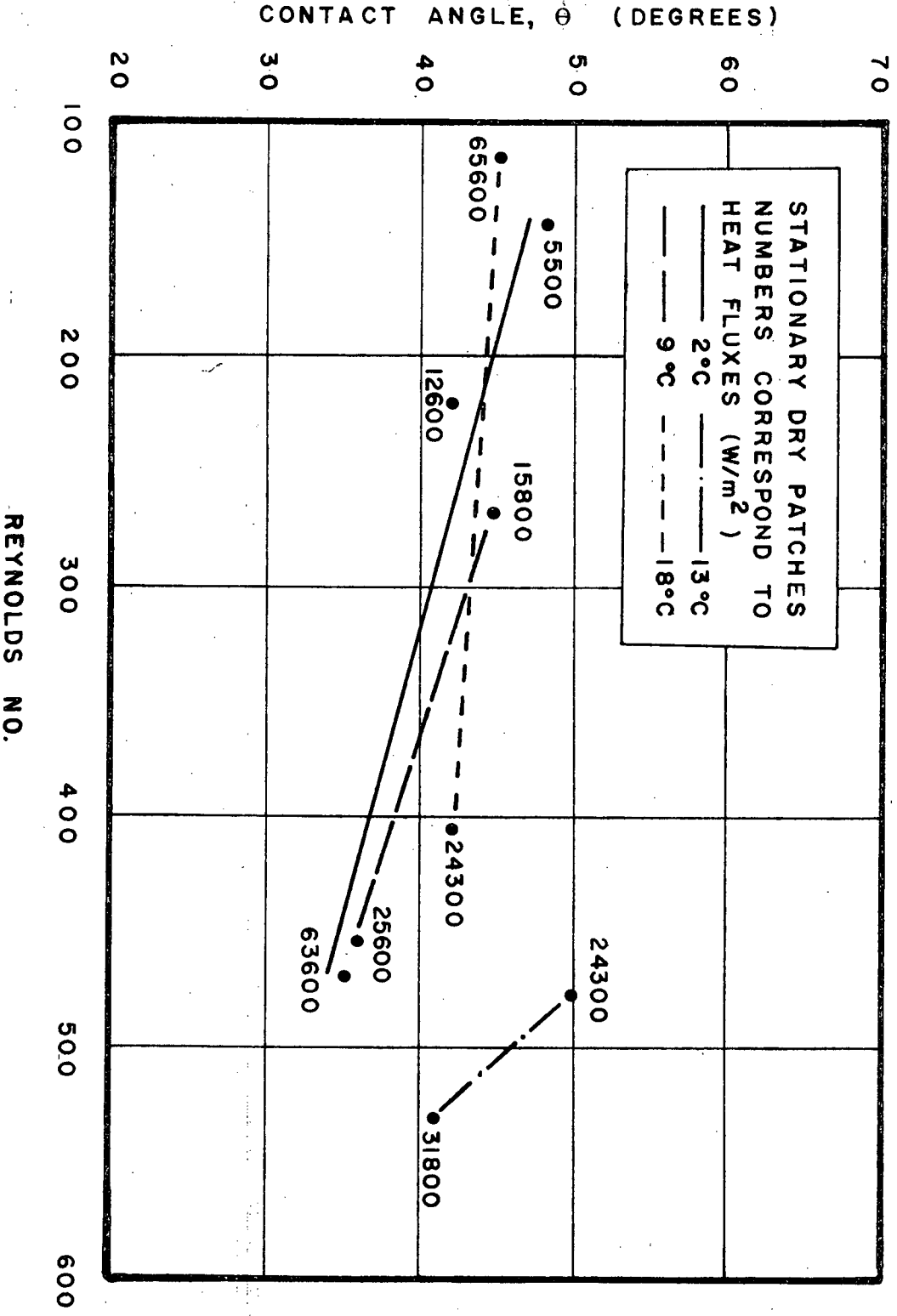


Figure 18 Average contact angle versus Local Reynolds No.

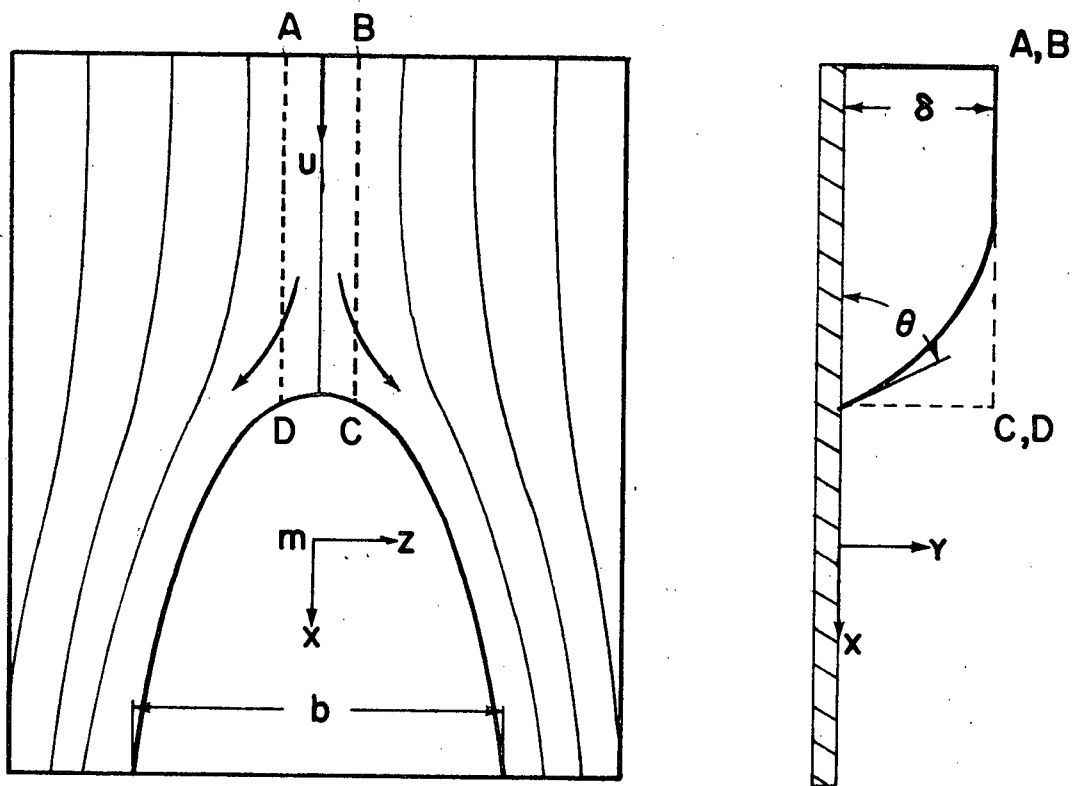


Figure 19 Scheme of a two dimensional flow around a dry patch.
The dash lines indicate the control volume used

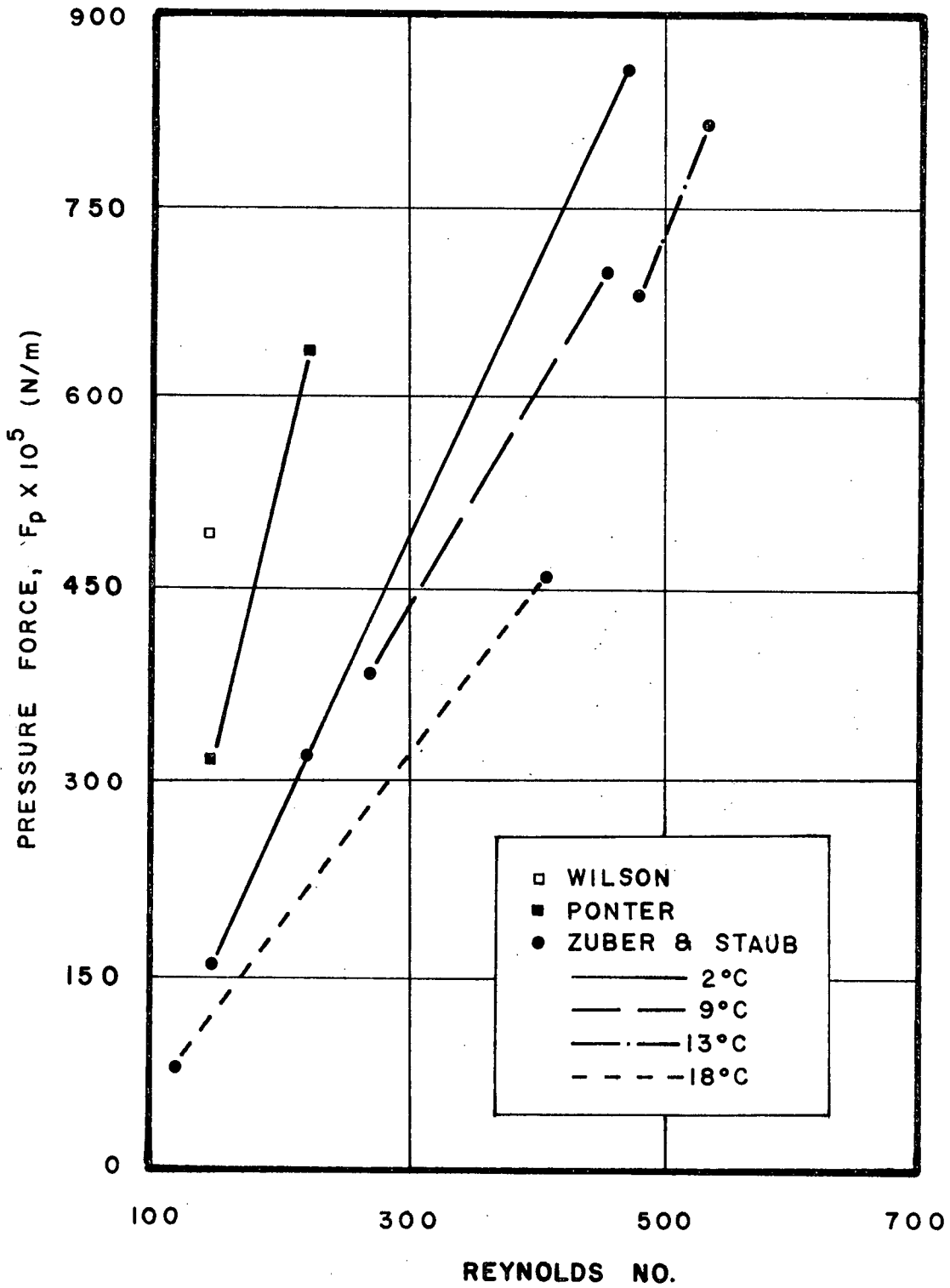


Figure 20 Pressure forces according to different models

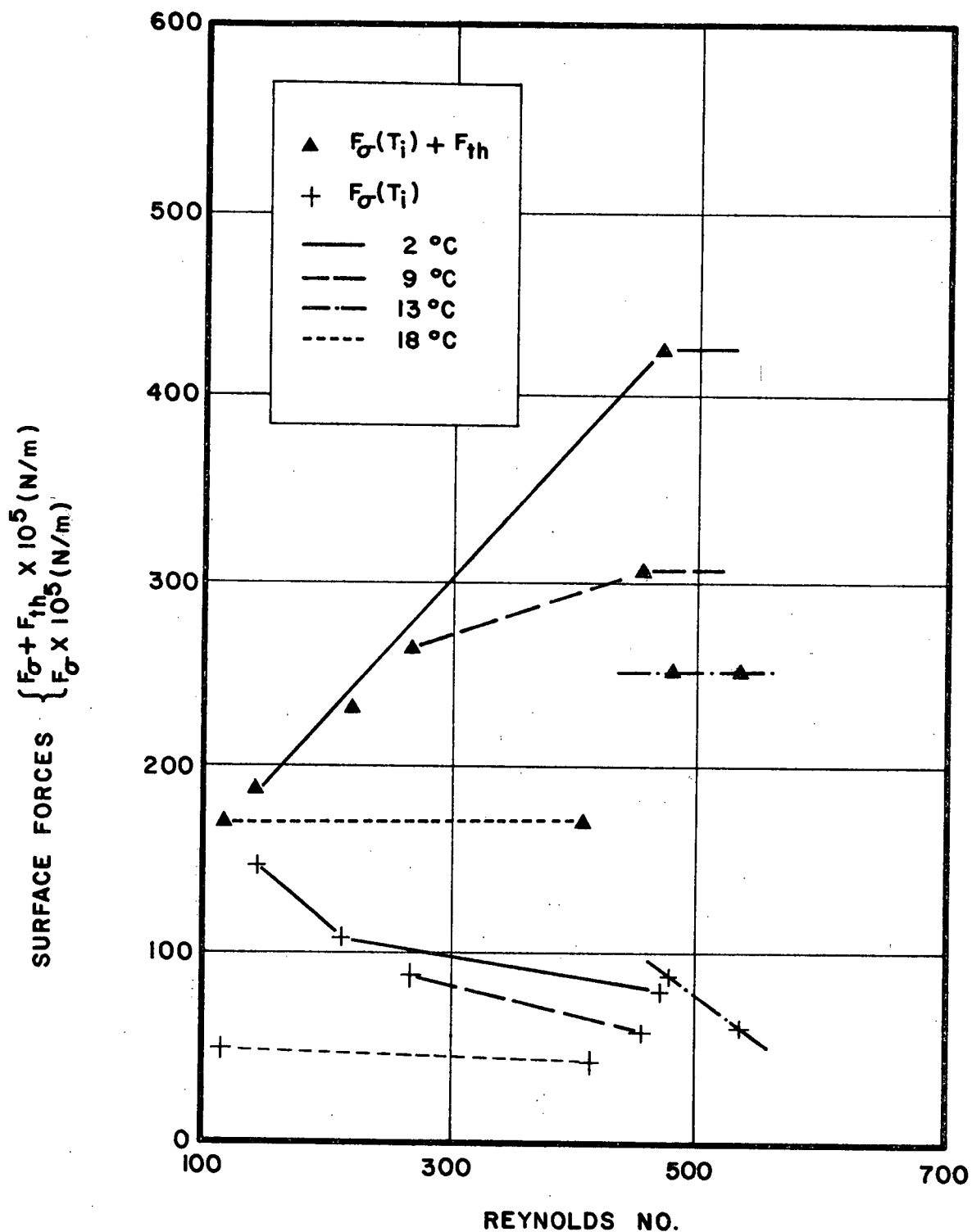


Figure 21 Comparison of the total surface force ($F_{\sigma} + F_{th}$) according to Zuber and Staub with the surface force without thermal effects (F_{σ})

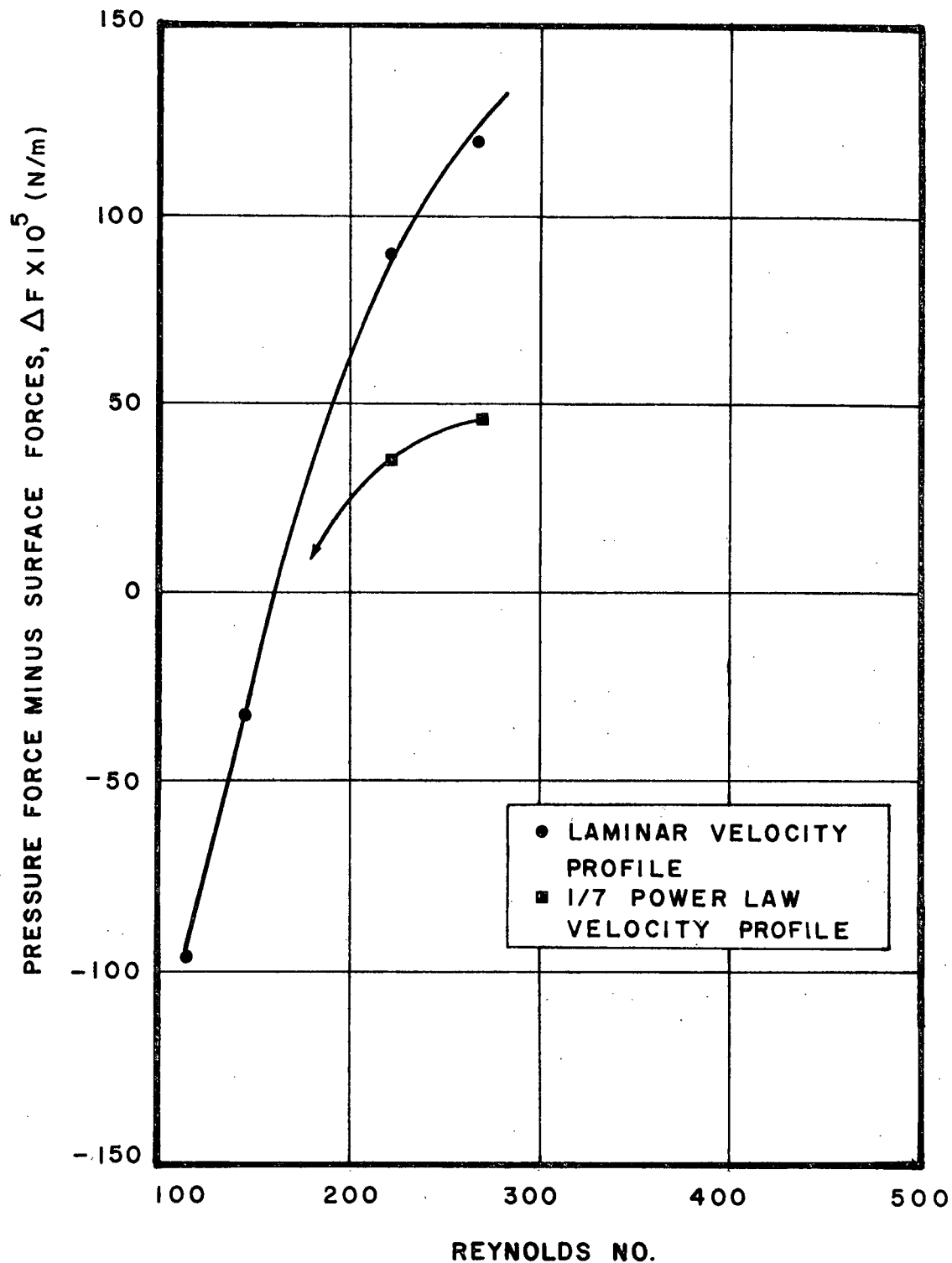


Figure 22 Difference between pressure force and surface force according to Zuber and Staub model for low Re (circles). Difference between pressure force and surface forces when the 1/7 power law is used as a velocity profile (squares)

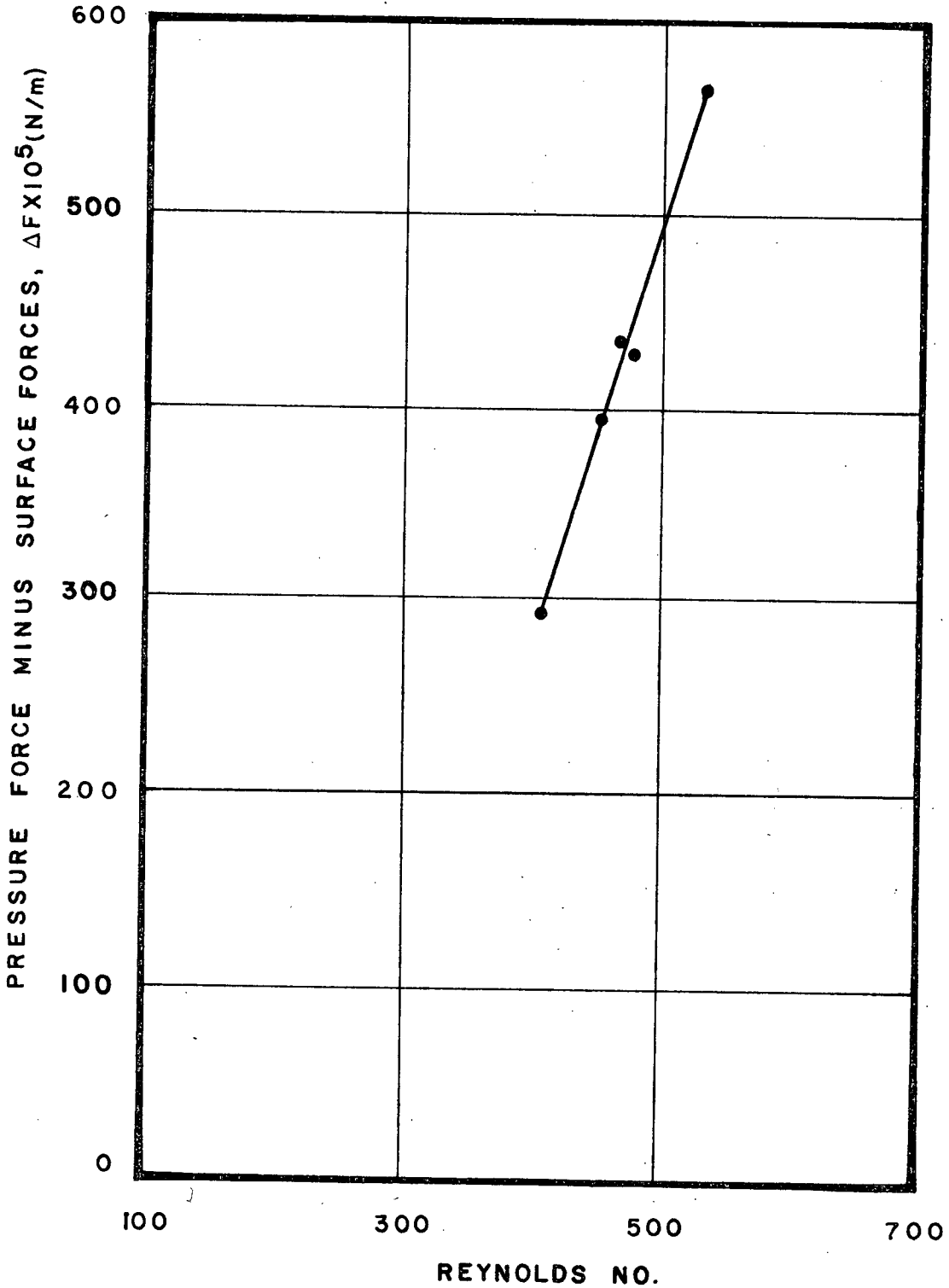


Figure 23 Difference between pressure force and surface forces for high Re

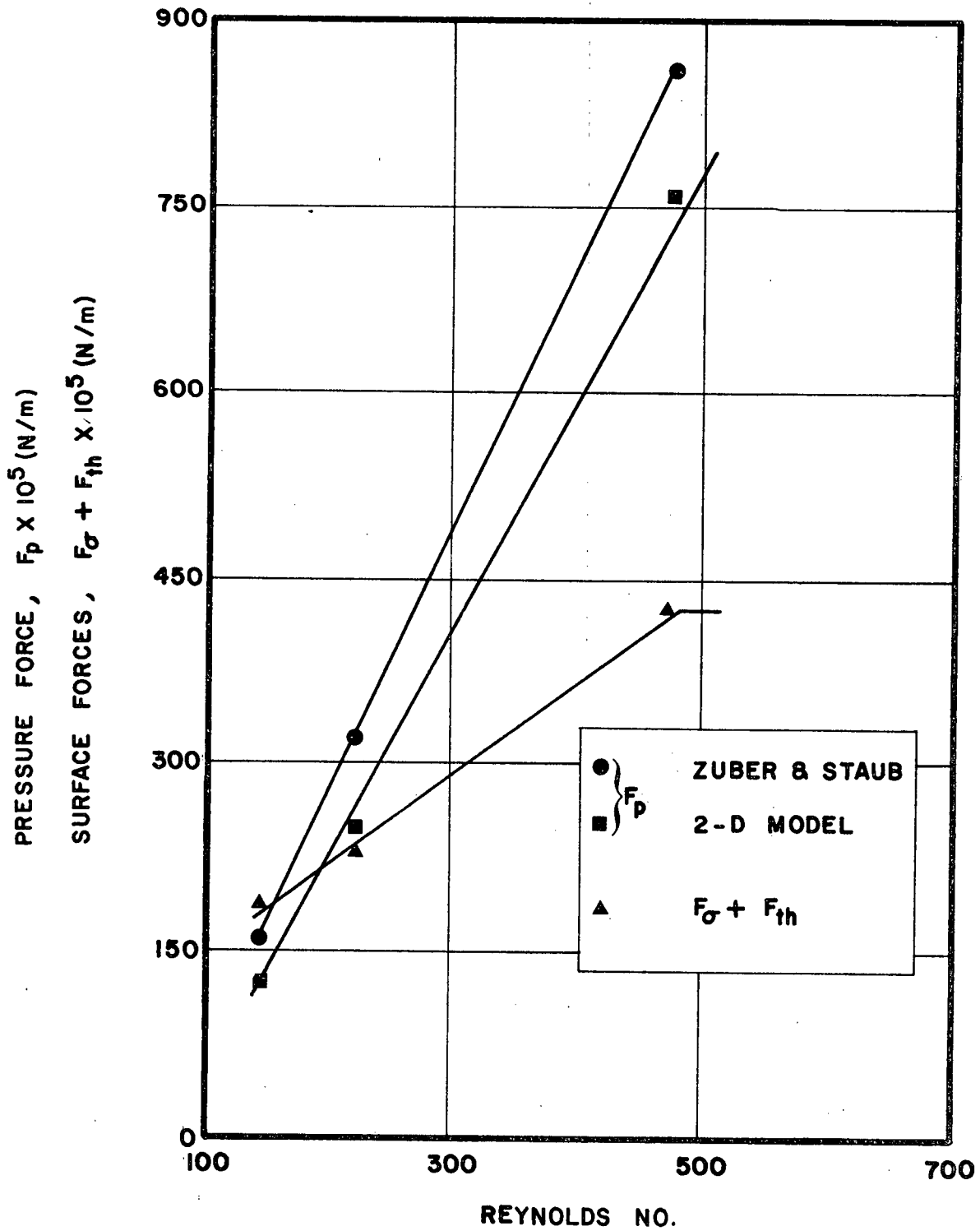


Figure 24 Comparison of the pressure force according to the two dimensional model with Zuber and Staub criterion. Inlet temperature = 2°C

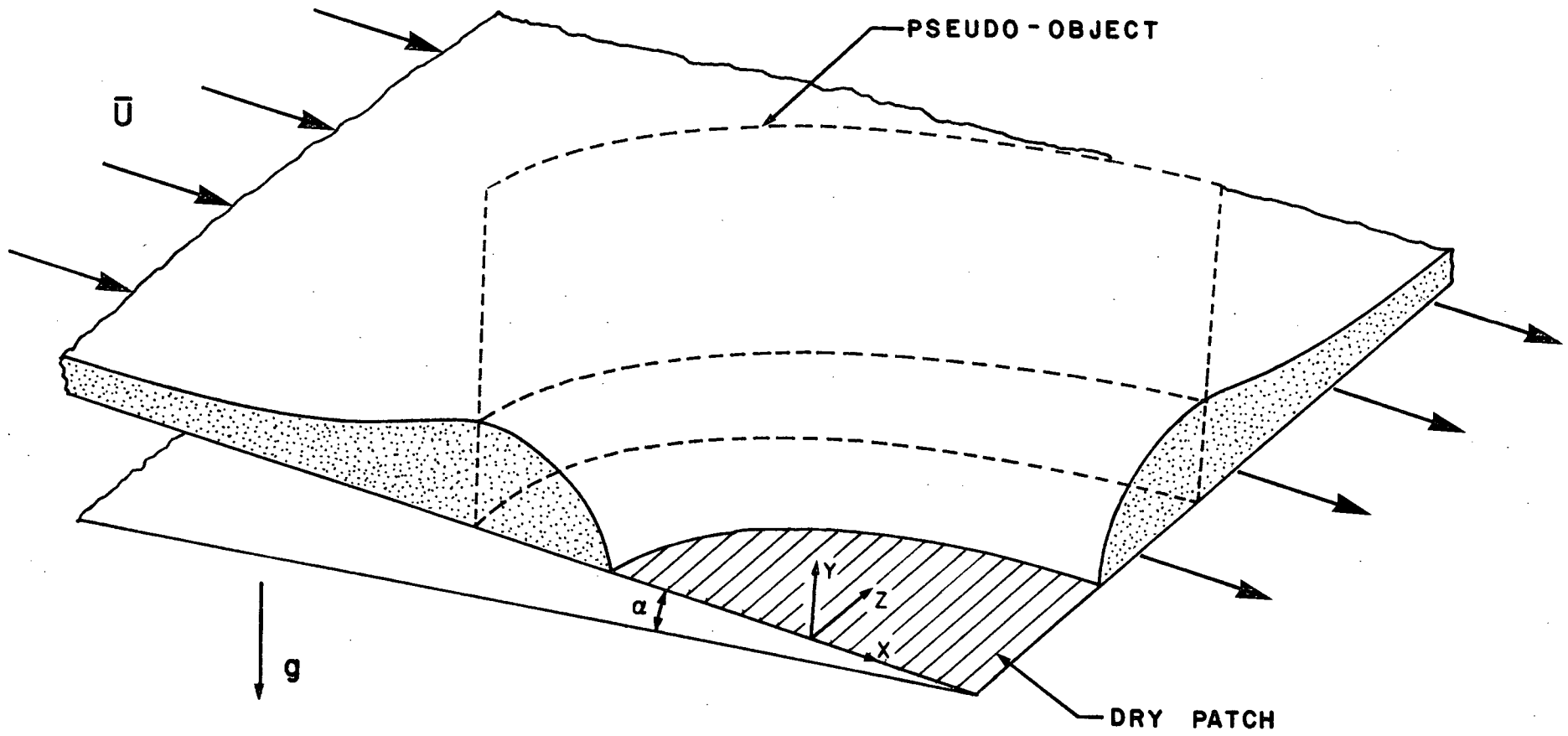


Figure 25 Scheme of the film surface profile in the vicinity of a dry patch on an inclined plate

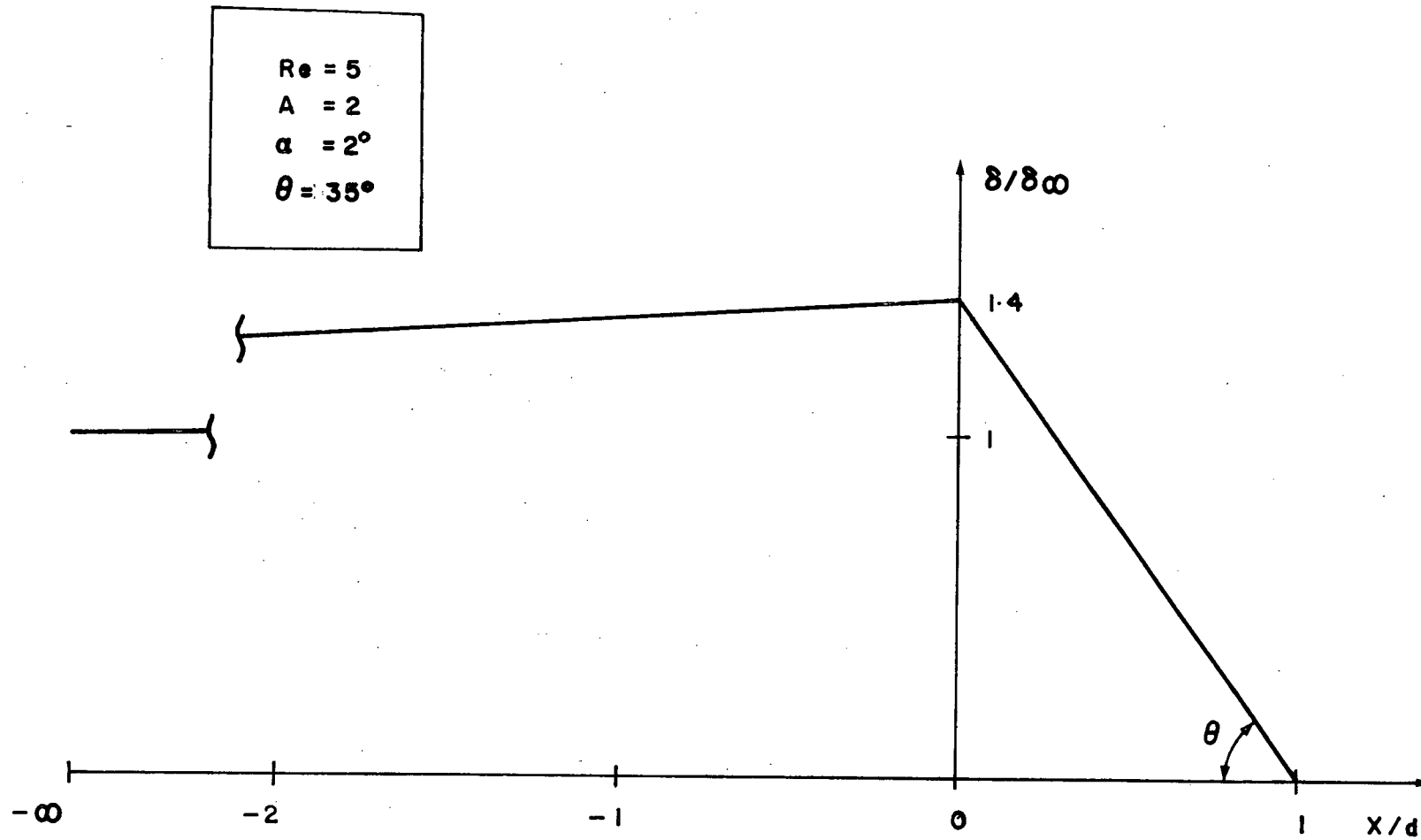


Figure 26 Film thickness profile according to model described in Chapter 5

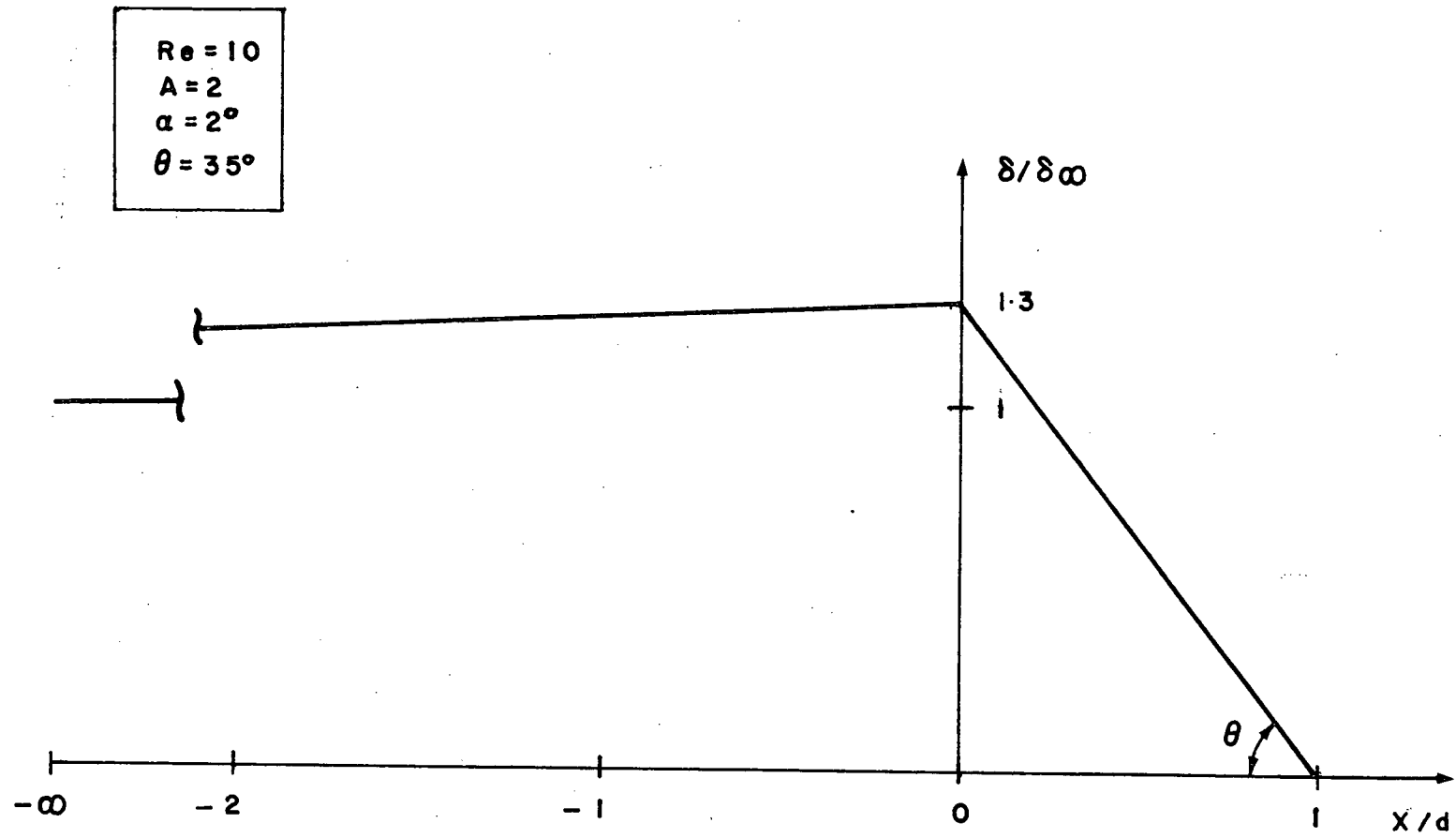


Figure 27 Film thickness profile according to model described in Chapter 5

REFERENCES

1. McAdam, D.W. "An Experimental Investigation of Dry Patch Formation and Stability in Thin Liquid Films," Ph.D. Thesis, The University of British Columbia, 1975.
2. Norman, W.S., McIntyre, V. "Heat Transfer to a Liquid Film on a Vertical Surface," Trans. Inst. Chem. Eng., 38, 301, 1960.
3. Norman, W.S., Binns, D.T. "The Effect of Surface Tension Changes on the Minimum Wetting Rates in a Wetted-Rod Distillation Column," Trans. Inst. Chem. Eng., 38, 294, 1960.
4. Hewitt, G.F., Lacey, B.M.C. "The Breakdown of the Liquid Film in Annular Two Phase Flow," Int. J. Heat and Mass Transfer, 8, 781, 1965.
5. Hartley, D.E., Murgatroyd, W. "Criteria for the Breakup of Thin Liquid Films Flowing Isothermally Over Solid Surfaces," Int. J. Heat and Mass Transfer, 7, 1003, 1964.
6. Zuber, N., Staub, F.W. "Stability of the Dry Patch Formed in Liquid Films on Heated Surfaces," Int. J. Heat and Mass Transfer, 9, 897, 1966.
7. Ponter, A.B., Davies, G.A., Ross, T.K., and Thornley, P.G. "The Influence of Mass Transfer on Liquid Film Breakdown," Int. J. Heat and Mass Transfer, 10, 349, 1967.
8. Thompson, T.S., Murgatroyd, W. "Stability and Breakdown of Liquid Films in Steam Flow with Heat Transfer," Internal Report, Queen Mary College, London, 1970.
9. Fulford, G.D. "Advances in Chemical Engineering," Academic Press, 5, 151, 1964.

10. Bird, R.B., Stewart, W.E., Lightfoot, E.N. Transport Phenomenon, John Wiley and Sons, Inc., 1960.
11. Benjamin, T. Brooks. "Wave Formation in Laminar Flow Down an Inclined Plane," J. Fluid Mech., 2, 554, 1957.
12. Castellana, F.S., Bonilla, C.F. "Velocity Measurements and the Critical Reynolds Number for Wave Initiation in Falling Film Flow," ASME, 70-HT-32, 1970.
13. Nusselt, W. Z. ver Deut. Inf., 60, 541, 1916.
14. Dukler, A.E., Bergelin, O.P. "Characteristics of Flow in Falling Liquid Films," Chem. Eng. Progress, 43, 557, 1952.
15. Cook, R.A., Clark, R.H. "The Experimental Determination of Velocity Profiles in Smooth Falling Liquid Films," Canadian Journal of Chem. Eng., 49, 412, 1971.
16. Reynolds, A.J. Turbulent Flows in Engineering. John Wiley and Sons, 1974.
17. Kapitza, P.L. J. Exp. Theor. Phys. U.S.S.R., 18, 3, 1948.
18. Levich, V.G. Physicochemical Hydrodynamics. Prentice-Hall, Inc., 1962.
19. Tailby, S.R., Portalski, S. "The Hydrodynamics of Liquid Films Flowing on Vertical Surfaces," Trans. Inst. Chem. Eng., 38, 324, 1960.
20. Bankoff, G.S. "Stability of Liquid Flow Down and Heated Inclined Plate," Int. J. Heat and Mass Transfer, 14, 377, 1971.
21. Bankoff, G.S. "Minimum Thickness of a Draining Liquid Film," Int. J. Heat and Mass Transfer, 14, 2143, 1971.
22. McPherson, G.D. "Axial Stability of the Dry Patch Formed in Dryout of a Two-Phased Annular Flow," Int. J. Heat and Mass Transfer, 13, 1133, 1970.

23. Wilson, S.D.R. "The Stability of a Dry Patch on a Wetted Wall," Int. J. Heat and Mass Transfer, 17, 1607, 1974.
24. Hsu, Y.Y., Simon, F.F., Lad, J.F. "Destruction of a Thin Liquid Film Flowing Over A Heated Surface," Chem. Eng. Symposium Series, 61 (No. 57), 138, 1965.
25. Simon, F.F., Hsu, Y.Y. "Thermocapillary Induced Breakdown of a Falling Film," NASA TN D-5624, 1970.
26. Mariy, A.H., El-Shirbini, A.A., Murgatroyd, W. "The Effect of Waves on the Motion of the Triple-Phase Front of a Dry Patch Formed in a Thin Motivated Liquid Film," Int. J. Heat and Mass Transfer, 17, 1141, 1974.
27. Barnett, P.G. "An Experimental Investigation to Determine the Scaling Laws of Forced Convection Boiling Heat Transfer," AEEW R-443, 1965.
28. Thompson, R. and Macbeth, R.V. "Boiling Water Heat Transfer Burnout in a Uniformly Round Tube," A.E.E.W. - R356, 1964 .
29. Johnson, R.E., Jr. and Dettre, R.H. "Wettability and Contact Angles," Surface & Colloidal Science, 2, 1969.
30. Johnson, R.E., Jr. and Dettre, R.M. "Contact Angle Hysteresis," Advances in Chemistry Series, 43.
31. Ponter, A.B., *et al.* "The Measurement of Contact Angles Under Equilibrium and Mass-Transfer Conditions," Int. J. Heat and Mass Transfer, 10, 733, 1967.
32. Huh, Chun and Scriven, L.F. "Hydrodynamic Model of Steady Movement of a Solid-Liquid-Fluid Contact Line," Journal of Colloid and Interface Science, 35, 85, 1971.
33. Dussan, V.E.B. and Davis, S.M. "On the Notion of a Fluid-Fluid Interface Along a Solid Surface," J. Fluid Mech., 65, 71, 1974.

34. Ponter, A.B., *et al.* "The Measurement of Contact Angles Under Conditions of Heat Transfer When a Liquid Breaks on a Vertical Surface," *Int. J. Heat and Mass Transfer*, 10, 1633, 1967.
35. Vallentine, H.R. *Applied Hydrodynamics*, Butterworths, 1967.
36. Lamb, M. *Hydrodynamics*, Dover, 1945.
37. Schlichting, M. *Boundary Layer Theory*, McGraw-Hill, 1968.
38. Hele-Shaw, M.S. *Trans. Inst. Nav. Archit*, 11, 25, 1898.

APPENDIX A

EVALUATION OF THE SHEAR FORCE AND BODY FORCE

FOR A KAPITZA VELOCITY PROFILE

The body force per unit width applied over a control volume of length $n\lambda$ and thickness h is

$$F_B = \int_0^h \int_0^{n\lambda} \rho g dx dy = \rho g \int_0^{n\lambda} h_0 + 0.46 h_0 \sin(kw - \omega t) dx$$

For $t = 0$

$$F_B = \rho g h_0 n\lambda$$

The shear force per unit width applied on a control volume whose length is $n\lambda$ is

$$F_S = \int_0^{n\lambda} \mu \left(\frac{\partial u}{\partial y} + \frac{\partial v}{\partial x} \right)_{y=0} dx$$

For thin films

$$\frac{\partial u}{\partial y} \gg \frac{\partial v}{\partial x}$$

For $t = 0$

$$\begin{aligned}
\int_0^{n\lambda} \mu \left(\frac{\partial u}{\partial y} \right)_{y=0} dx &= \int_0^{n\lambda} 3 u_0 \left[\frac{1+0.6 \sin kx - 0.3 \sin^2 kx}{h_0 + h_0 0.46 \sin kx} \right] dx \\
&= \frac{3 u_0}{h_0} \left[\int_0^{n\lambda} \frac{1}{1 + 0.46 \sin kx} dx + \int_0^{n\lambda} \frac{0.6}{1 + 0.46 \sin kx} dx \right. \\
&\quad \left. - \int_0^{n\lambda} \frac{0.3 \sin^2 kx}{1 + 0.46 \sin kx} dx \right] . \quad \dots (1)
\end{aligned}$$

Each integral of Equation 1 is solved below. First integral

$$\int_0^{n\lambda} \frac{1}{1 + 0.46 \sin kx} dx = \frac{\lambda}{2\pi} \int_0^{2\pi n} \frac{1}{1 + 0.46 \sin z} dz$$

where

$$z = \frac{2\pi}{\lambda} x .$$

Then

$$\begin{aligned}
\frac{\lambda}{2\pi} \int_0^{2\pi n} \frac{1}{1 + 0.46 \sin z} dz &= \frac{\lambda}{2\pi} \left[\frac{2}{\sqrt{1 - 0.46^2}} \arctan \frac{\tan n\pi + 0.46}{\sqrt{1 - 0.46^2}} \right. \\
&\quad \left. - \frac{2}{\sqrt{1 - 0.46^2}} \arctan \frac{0.46}{\sqrt{1 - 0.46^2}} \right]
\end{aligned}$$

$$\begin{aligned}
&= \frac{\lambda}{2\pi} \left[\frac{2}{\sqrt{1-0.46^2}} \left(n\pi + \arctan \frac{0.46}{\sqrt{1-0.46^2}} \right) \right. \\
&\quad \left. - \frac{2}{\sqrt{1-0.46^2}} \arctan \frac{0.46}{\sqrt{1-0.46^2}} \right] \\
&= \frac{n\lambda}{\sqrt{1-0.46^2}} .
\end{aligned}$$

The second integral can be split in two known integrals, that is

$$\begin{aligned}
0.6 \frac{\lambda}{2\pi} \int_0^{2n\pi} \frac{\sin z}{1+0.46 \sin z} dz &= \frac{0.6}{0.46} \frac{\lambda}{2\pi} \left[\int_0^{2n\pi} dz - \int_0^{2n\pi} \frac{1}{1+0.46 \sin z} dz \right] \\
&= \frac{0.6}{0.46} n\lambda \left[1 - \frac{1}{\sqrt{1-0.46^2}} \right] .
\end{aligned}$$

The third integral can be expressed as

$$- \frac{0.3}{0.46} \frac{\lambda}{2\pi} \int_0^{2n\pi} \left[\sin z - \frac{\sin z}{1+0.46 \sin z} \right] dz ,$$

One integrated is equal to

$$\frac{0.3}{0.46^2} n\lambda \left[1 - \frac{1}{\sqrt{1 - 0.46^2}} \right] .$$

Adding the three integrals and multiplying them by $n\mu \frac{3u_0\lambda}{h_0}$ the final result is equal to

$$n\mu \frac{3u_0}{h_0} \lambda \cdot 0.783 \quad . \quad . \quad . \quad . \quad (2)$$

The factor 0.783 represents the value of the function Φ defined by Kapitza [17] and is considered close enough to 0.8 used in his analysis. Φ was determined by Kapitza through a graphical method and the numerical constants that appear in the velocity profile are estimated with some small error. Multiplying and dividing by u_0 , the RHS of Equation (2) is:

$$n\mu \frac{3u_0^2}{h_0} \Phi \frac{\lambda}{u_0}$$

equal to

$$\rho g h_0 u_0 \frac{\lambda n}{u_0}$$

from Kapitza's analysis and equal to $\rho g h_0 n \lambda$.

Then $F_S = F_B$ and the assumption of undamped flow is equivalent to the equality of shear force and body force, both forces integrated over a distance = to a wavelength.

APPENDIX B

DEVELOPMENT OF THE SIMPLIFIED NAVIER-STOKES

EQUATIONS USED IN CHAPTER 5

In the case of a three dimensional steady incompressible flow flowing along an inclined plate that forms an angle α with the horizontal Navier-Stokes equation and the continuity equation are expressed as follows:

$$u \frac{\partial u}{\partial x} + v \frac{\partial u}{\partial y} + w \frac{\partial u}{\partial z} = - \frac{1}{\rho} \frac{\partial p}{\partial x} + \nu \left(\frac{\partial^2 u}{\partial x^2} + \frac{\partial^2 u}{\partial y^2} + \frac{\partial^2 u}{\partial z^2} \right) + g \sin \alpha \quad \dots (1)$$

$$u \frac{\partial v}{\partial x} + v \frac{\partial v}{\partial y} + w \frac{\partial v}{\partial z} = - \frac{1}{\rho} \frac{\partial p}{\partial y} + \nu \left(\frac{\partial^2 v}{\partial x^2} + \frac{\partial^2 v}{\partial y^2} + \frac{\partial^2 v}{\partial z^2} \right) - g \cos \alpha \quad \dots (2)$$

$$u \frac{\partial w}{\partial x} + v \frac{\partial w}{\partial y} + w \frac{\partial w}{\partial z} = - \frac{1}{\rho} \frac{\partial p}{\partial z} + \nu \left(\frac{\partial^2 w}{\partial x^2} + \frac{\partial^2 w}{\partial y^2} + \frac{\partial^2 w}{\partial z^2} \right) \quad \dots (3)$$

$$\frac{\partial u}{\partial x} + \frac{\partial v}{\partial y} + \frac{\partial w}{\partial z} = 0 \quad \dots (4)$$

The system of coordinates has its origin in the bottom of the plate, the x, z plane is parallel to the plate and the y-axis is perpendicular to them. To know the relative importance of the different terms in

the latter equations some suitable characteristic magnitudes are selected as units. Let u_1 , v_1 , w_1 , L , δ_∞ , and $\rho g \cos \alpha \delta_\infty$ denote these characteristic reference magnitudes, where u_1 , v_1 and w_1 are the reference velocities in x, y and z direction; L represents the size of the object in z, x directions and δ_∞ is the thickness at infinity, then

$$u^* = \frac{u}{u_1}, \quad v^* = \frac{v}{v_1}, \quad w^* = \frac{w}{w_1}$$

$$x^* = \frac{x}{L}, \quad y^* = \frac{y}{\delta_\infty}, \quad z^* = \frac{z}{L}, \quad p^* = \frac{p}{\rho g \cos \alpha \delta_\infty}.$$

The reference velocity u_1 , can be taken as the average velocity

$$\bar{u} = \frac{g \sin \alpha \delta_\infty^2}{3\nu}$$

that corresponds to the one-dimensional problem. These dimensionless ratios are of the order of one. If they are introduced into the continuity Equation (4)

$$\frac{\bar{u}}{L} \frac{\partial u^*}{\partial x^*} + \frac{v_1}{\delta_\infty} \frac{\partial v^*}{\partial y^*} + \frac{w_1}{L} \frac{\partial w^*}{\partial z^*} = 0 \quad \dots (5)$$

If w_1 is considered of the same order as \bar{u}

$$\frac{\bar{u}}{L} \left\{ \frac{\partial u^*}{\partial x^*} + \frac{v_1}{\left(\frac{\bar{u}\delta_\infty}{L}\right)} \frac{\partial v^*}{\partial y^*} + \frac{\partial w^*}{\partial z^*} \right\} = 0 \quad \dots \dots (6)$$

Since the term between brackets is of the order of one, v_1 has to be of the order of

$$\frac{\bar{u}\delta_\infty}{L} .$$

Introducing the dimensionless ratios into the x component Navier-Stokes equations

$$\begin{aligned} \frac{\bar{u}^{-2}}{L} \left\{ u^* \frac{\partial u^*}{\partial x^*} + v^* \frac{\partial u^*}{\partial y^*} + w^* \frac{\partial u^*}{\partial z^*} \right\} &= -g \frac{\delta_\infty \cos \alpha}{L} \frac{\partial p^*}{\partial x^*} + \\ &+ \nu \left\{ \frac{\bar{u}}{L^2} \frac{\partial^2 u^*}{\partial x^{*2}} + \frac{\bar{u}}{\delta_\infty^2} \frac{\partial^2 u^*}{\partial y^{*2}} + \frac{\bar{u}}{L^2} \frac{\partial^2 u^*}{\partial z^{*2}} \right\} + g \sin \alpha \dots \dots (7) \end{aligned}$$

$$\begin{aligned} \left(\frac{\bar{u}^{-2}}{L}\right) \left(\frac{\delta_\infty^2}{\bar{u}\nu}\right) \left\{ u^* \frac{\partial u^*}{\partial x^*} + v^* \frac{\partial u^*}{\partial y^*} + w^* \frac{\partial u^*}{\partial z^*} \right\} &= -g \frac{\delta_\infty \cos \alpha}{L} \left(\frac{\delta_\infty^2}{\bar{u}\nu}\right) \frac{\partial p^*}{\partial x^*} \\ &+ \left\{ \left(\frac{\delta_\infty^2}{L^2}\right) \frac{\partial^2 u^*}{\partial x^{*2}} + \frac{\partial^2 u^*}{\partial y^{*2}} + \left(\frac{\delta_\infty^2}{L^2}\right) \frac{\partial^2 u^*}{\partial z^{*2}} \right\} + g \sin \alpha \left(\frac{\delta_\infty^2}{\bar{u}\nu}\right) . \end{aligned}$$

But \bar{u} can be expressed as a function of the thickness of the film and of the angle,

$$\bar{u} = \frac{g \sin \alpha \delta_{\infty}^2}{3\nu} ,$$

then

$$\begin{aligned} \left(\frac{\bar{u}\delta_{\infty}}{\nu}\right)\left(\frac{\delta_{\infty}}{L}\right) \left\{ u^* \frac{\partial u^*}{\partial x^*} + v^* \frac{\partial u^*}{\partial y^*} + w^* \frac{\partial u^*}{\partial z^*} \right\} &= -3 \cotan \alpha \left(\frac{\delta_{\infty}}{L}\right) \frac{\partial p^*}{\partial x^*} \\ &+ \left\{ \left(\frac{\delta_{\infty}^2}{L}\right) \frac{\partial^2 u^*}{\partial x^{*2}} + \frac{\partial^2 u^*}{\partial y^{*2}} + \left(\frac{\delta_{\infty}^2}{L}\right) \frac{\partial^2 u^*}{\partial z^{*2}} \right\} + 3 \dots \dots (8) \end{aligned}$$

As the thickness of the film is much smaller than a characteristic size of the obstacle

$$\frac{\delta_{\infty}}{L} \ll 1 .$$

If a modified Reynolds number $= \left(\frac{\bar{u}\delta_{\infty}}{\nu}\right)\left(\frac{\delta_{\infty}}{L}\right)$ is defined such that is $\ll 1$, and if

$$\cotan \alpha \cdot \frac{\delta_{\infty}}{L}$$

is assumed of order of one, (true for small α) Equation 8 reduces to

$$-3 \frac{\partial p^*}{\partial x^*} + \frac{\partial^2 u^*}{\partial y^{*2}} + 3 = 0 .$$

Converting back to dimensional units

$$-\frac{3L}{\rho g \delta_{\infty} \cos \alpha} \frac{\partial p}{\partial x} + \frac{3\nu}{g \sin \alpha} \frac{\partial^2 u}{\partial y^2} + 3 g \sin \alpha = 0 .$$

After rearrangements

$$-\frac{1}{\rho} \frac{\partial p}{\partial x} + \nu \frac{\partial^2 u}{\partial y^2} + g \sin \alpha = 0 . \quad \dots (9)$$

Equation (9) is valid with the conditions

$$\left(\text{Re} \frac{\delta_{\infty}}{L} \right) \ll 1$$

$$\alpha \sim \frac{\delta_{\infty}}{L} .$$

If the dimensionless ratios are replaced in the y component of the Navier-Stokes equations.

$$\frac{\delta_{\infty}}{L} \left(\frac{\bar{u}}{L} \right) \left\{ u^* \frac{\partial v^*}{\partial x^*} + v^* \frac{\partial v^*}{\partial y^*} + w^* \frac{\partial v^*}{\partial z^*} \right\} = -g \cos \alpha \frac{\partial p^*}{\partial y^*}$$

$$+ \nu \left(\frac{\bar{u} \delta_{\infty}}{L} \right) \left(\frac{1}{\delta_{\infty}^2} \right) \left\{ \frac{\delta_{\infty}^2}{L} \frac{\partial^2 v^*}{\partial x^{*2}} + \frac{\partial^2 v^*}{\partial y^{*2}} + \frac{\delta_{\infty}^2}{L} \frac{\partial^2 v^*}{\partial z^{*2}} \right\} - g \cos \alpha .$$

Dividing by $g \cos \alpha$

$$\left(\frac{\delta_\infty}{L}\right) \left(\frac{\bar{u}^{-2}}{L g \cos \alpha}\right) \left\{ u^* \frac{\partial v^*}{\partial x^*} + v^* \frac{\partial v^*}{\partial y^*} + w^* \frac{\partial v^*}{\partial z^*} \right\} = - \frac{\partial p^*}{\partial y^*}$$

$$+ v \left(\frac{\bar{u} \delta_\infty}{L}\right) \frac{1}{\delta_\infty^2 g \cos \alpha} \left\{ \frac{\delta_\infty^2}{L} \frac{\partial^2 v^*}{\partial x^{*2}} + \frac{\partial^2 v^*}{\partial y^{*2}} + \frac{\delta_\infty^2}{L} \frac{\partial^2 v^*}{\partial z^{*2}} \right\} - 1 .$$

.(10)

The first factor in the left hand side of Equation 10, can be regarded as

$$\left(\frac{\delta_\infty}{L}\right) \left(\frac{\bar{u}^{-2}}{L}\right) \left(\frac{1}{g \cos \alpha}\right) = \left(\frac{\delta_\infty}{L}\right)^2 \frac{\bar{u}^{-2}}{\delta_\infty} \frac{1}{g \cos \alpha} = \left(\frac{\delta_\infty}{L}\right)^2 \frac{\bar{u}}{\delta_\infty} \tan \alpha \frac{\delta_\infty^2}{3v} .$$

Replacing $\tan \alpha$ by its approximate value $= \frac{\delta_\infty}{L}$, then

$$\left(\frac{\delta_\infty}{L}\right) \left(\frac{\bar{u}^{-2}}{L}\right) \left(\frac{1}{g \cos \alpha}\right) \approx \left(\frac{\delta_\infty}{L}\right)^2 \left(\frac{\bar{u} \delta_\infty}{v}\right) \frac{\delta_\infty}{L} \ll 1 .$$

Likewise the first factor in the second term of the right hand side of Equation 10,

$$v \frac{\bar{u} \delta_\infty}{L} \frac{1}{\delta_\infty^2 g \cos \alpha} = \left(\frac{g \sin \alpha \delta_\infty^2}{3v}\right) \left(\frac{v \delta_\infty}{L}\right) \frac{1}{\delta_\infty^2 g \cos \alpha}$$

$$\approx \tan \alpha \frac{\delta_\infty}{L} \ll 1 .$$

Finally for $\frac{\delta_\infty}{L} \ll 1$ Equation 10 transforms into

$$0 = - \frac{\partial p^*}{\partial y^*} - 1 .$$

Converting back to dimensional units

$$\frac{1}{\rho} \frac{\partial p}{\partial y} = - g \cos \alpha . \quad \dots (11)$$

with the restrictions

$$(\text{Re}) \left(\frac{\delta_\infty}{L} \right) \ll 1$$

$$\tan \alpha \sim \alpha \sim \frac{\delta_\infty}{L} .$$

The z component of the Navier-Stokes equations transforms into

$$\begin{aligned} \frac{\bar{u}^2}{L} \left\{ u^* \frac{\partial w^*}{\partial x^*} + v^* \frac{\partial w^*}{\partial y^*} + w^* \frac{\partial w^*}{\partial z^*} \right\} &= - \frac{g \delta_\infty \cos \alpha}{L} \frac{\partial p^*}{\partial z^*} \\ + v \frac{\bar{u}^2}{\delta_\infty^2} \left\{ \left(\frac{\delta_\infty}{L} \right)^2 \frac{\partial^2 w^*}{\partial x^{*2}} + \frac{\partial^2 w^*}{\partial y^{*2}} + \left(\frac{\delta_\infty}{L} \right)^2 \frac{\partial^2 w^*}{\partial z^{*2}} \right\} \end{aligned}$$

Multiplying left hand side and right hand side by

$$\frac{\delta_\infty^2}{v \bar{u}}$$

$$\frac{-2}{L} \left(\frac{\delta_\infty^2}{\nu \bar{u}} \right) \left\{ u^* \frac{\partial w^*}{\partial x^*} + v^* \frac{\partial w^*}{\partial y^*} + w^* \frac{\partial w^*}{\partial z^*} \right\} = - \frac{g \delta_\infty \cos \alpha}{L} \frac{\delta_\infty^2}{\nu \bar{u}} \frac{\partial p^*}{\partial z^*}$$

$$+ \left\{ \left(\frac{\delta_\infty}{L} \right)^2 \left[\frac{\partial^2 w^*}{\partial x^{*2}} + \frac{\partial^2 w^*}{\partial z^{*2}} \right] + \frac{\partial^2 w^*}{\partial y^{*2}} \right\} .$$

After rearrangements and with the assumptions that

$$\left(\text{Re} \frac{\delta_\infty}{L} \right) \ll 1 , \quad \tan \alpha \sim \frac{\delta_\infty}{L} ,$$

$$- 3 \frac{\partial p^*}{\partial z^*} + \frac{\partial^2 w^*}{\partial y^{*2}} = 0 .$$

Converting to dimension units

$$\frac{1}{\rho} \frac{\partial p}{\partial z} = \nu \frac{\partial^2 w}{\partial y^2} . \quad \dots (12)$$

APPENDIX C

PROPERTIES OF CARBON DIOXIDE

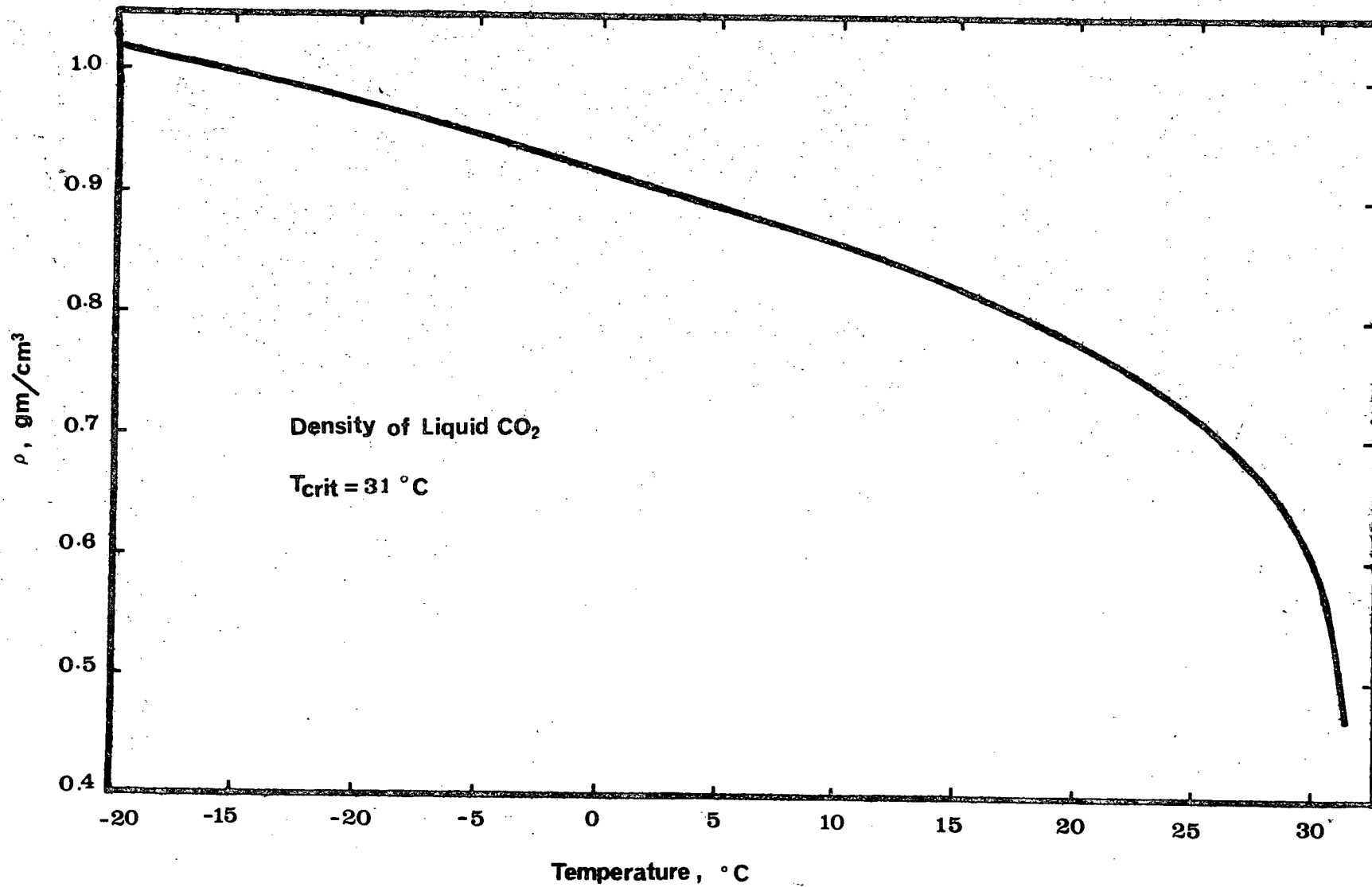


Figure 28 Density of Liquid CO₂

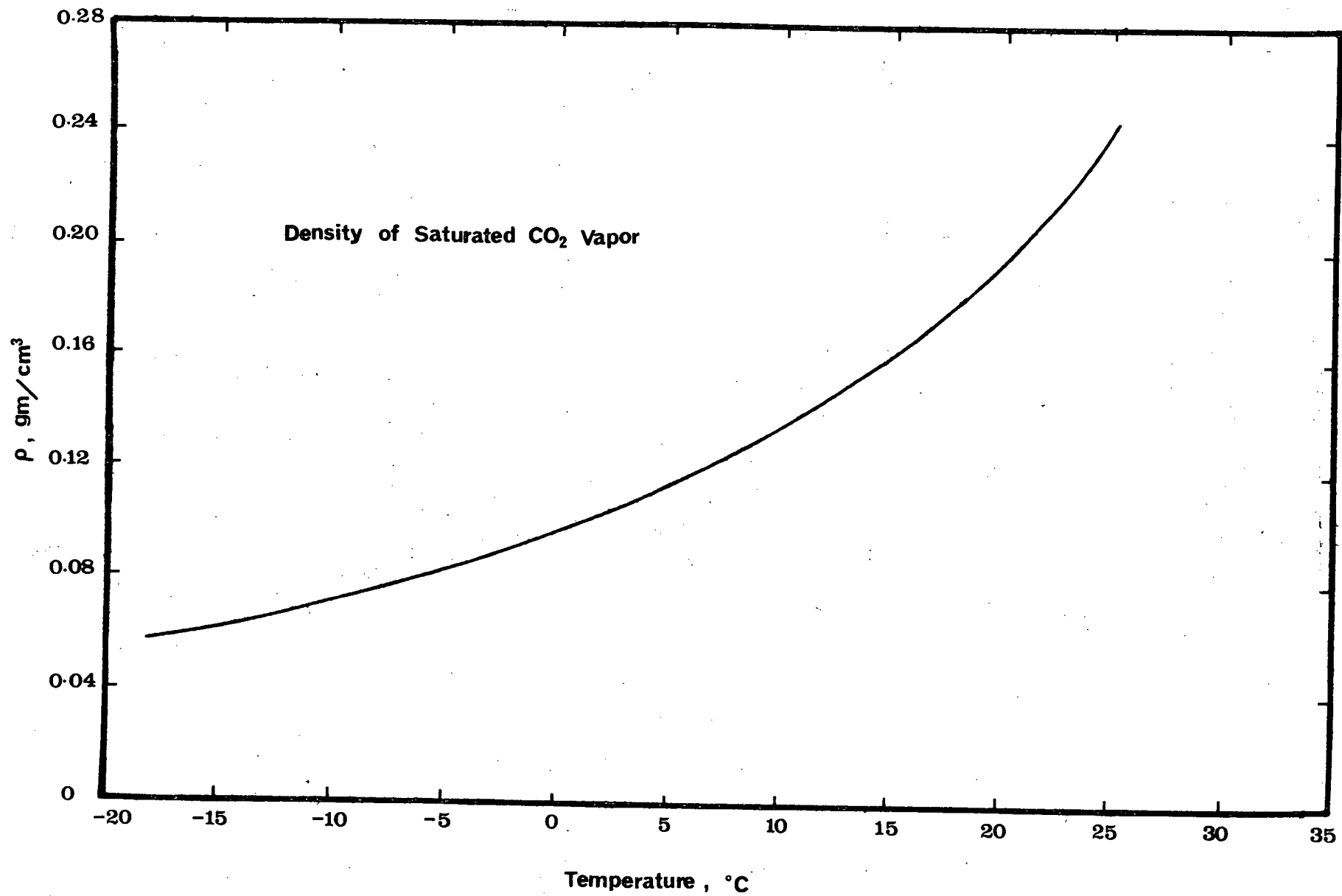


Figure 29 Density of Saturated CO₂ Vapor

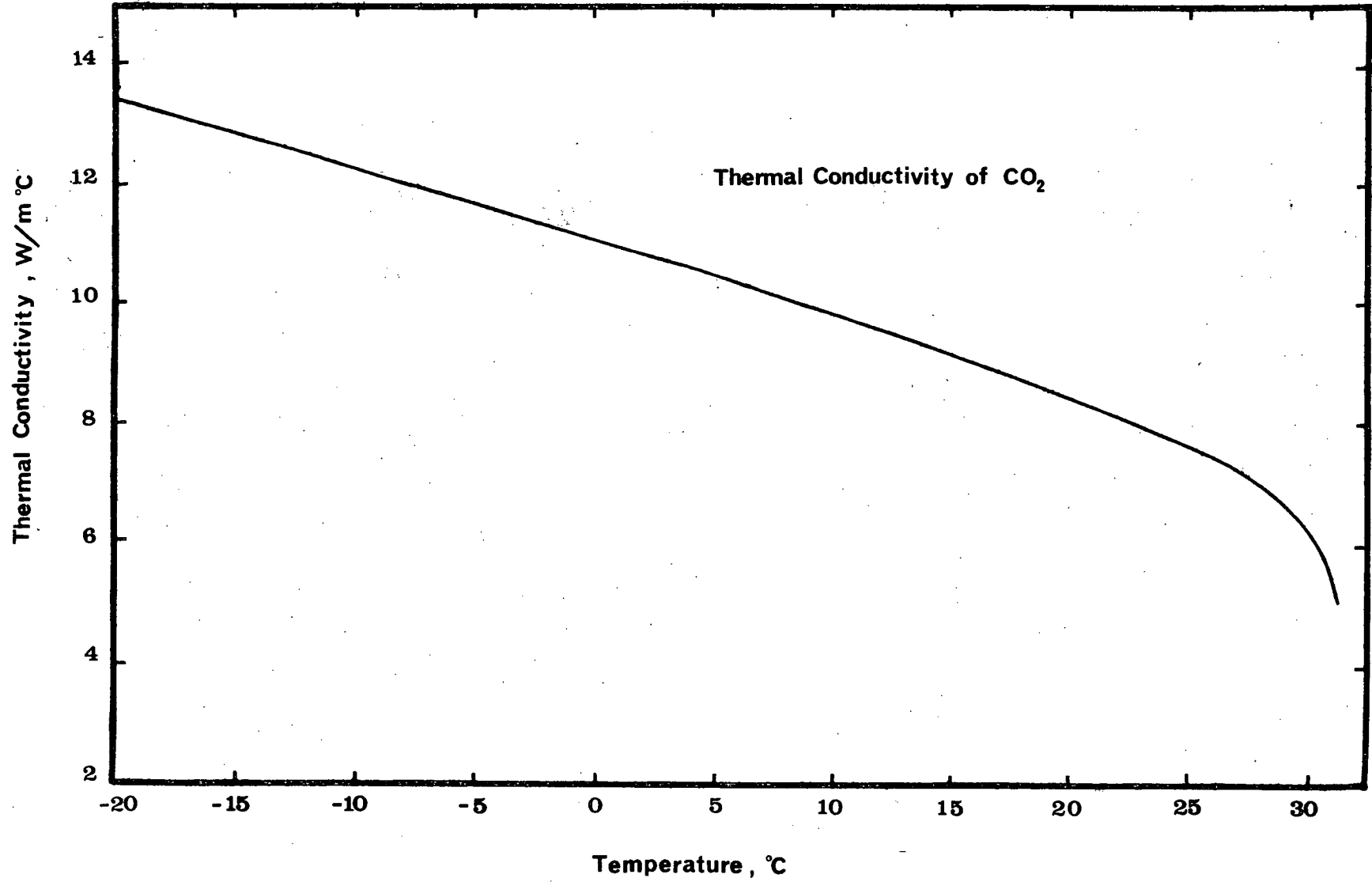


Figure 30 Thermal Conductivity of CO₂

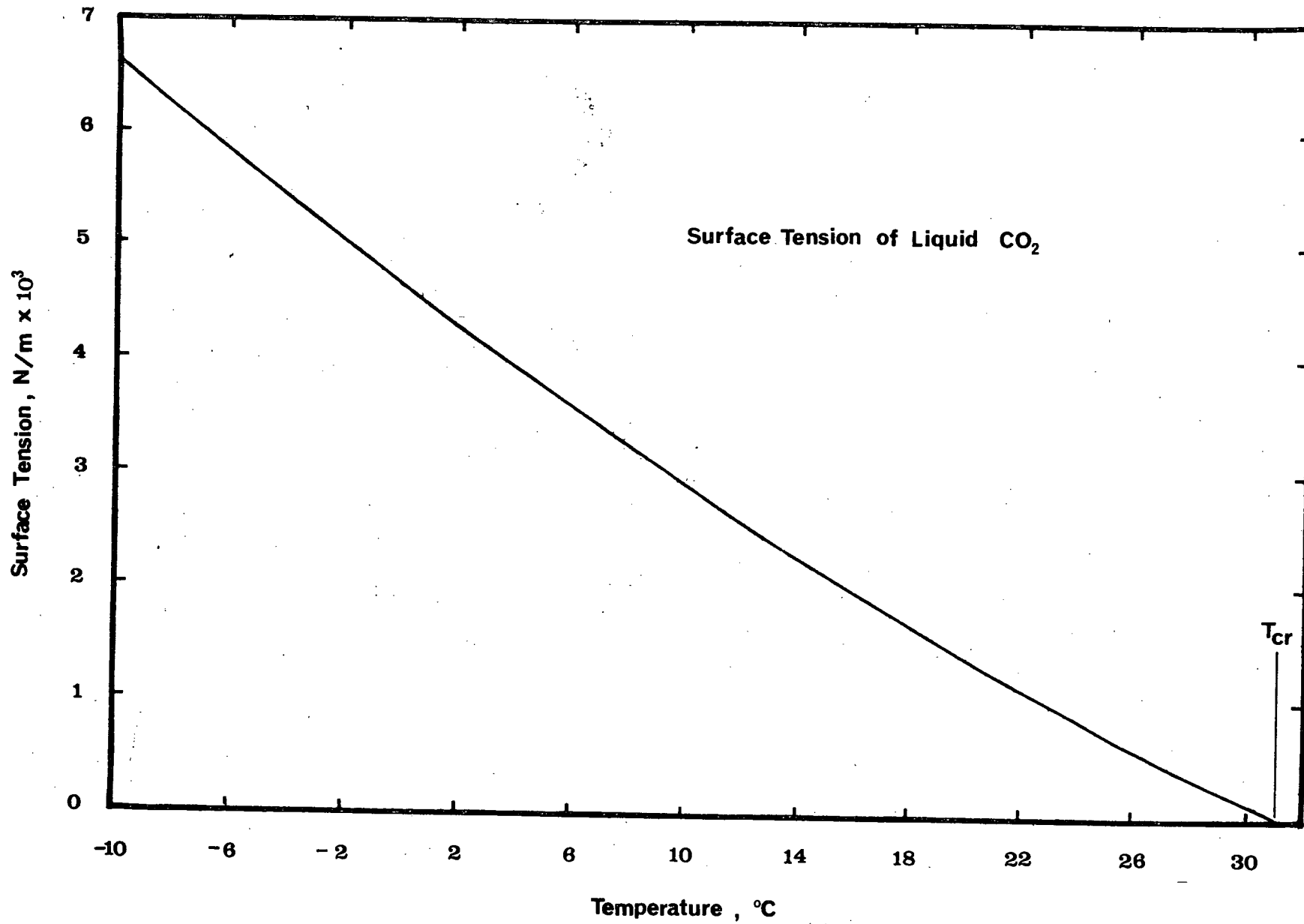


Figure 31 Surface Tension of Liquid CO₂

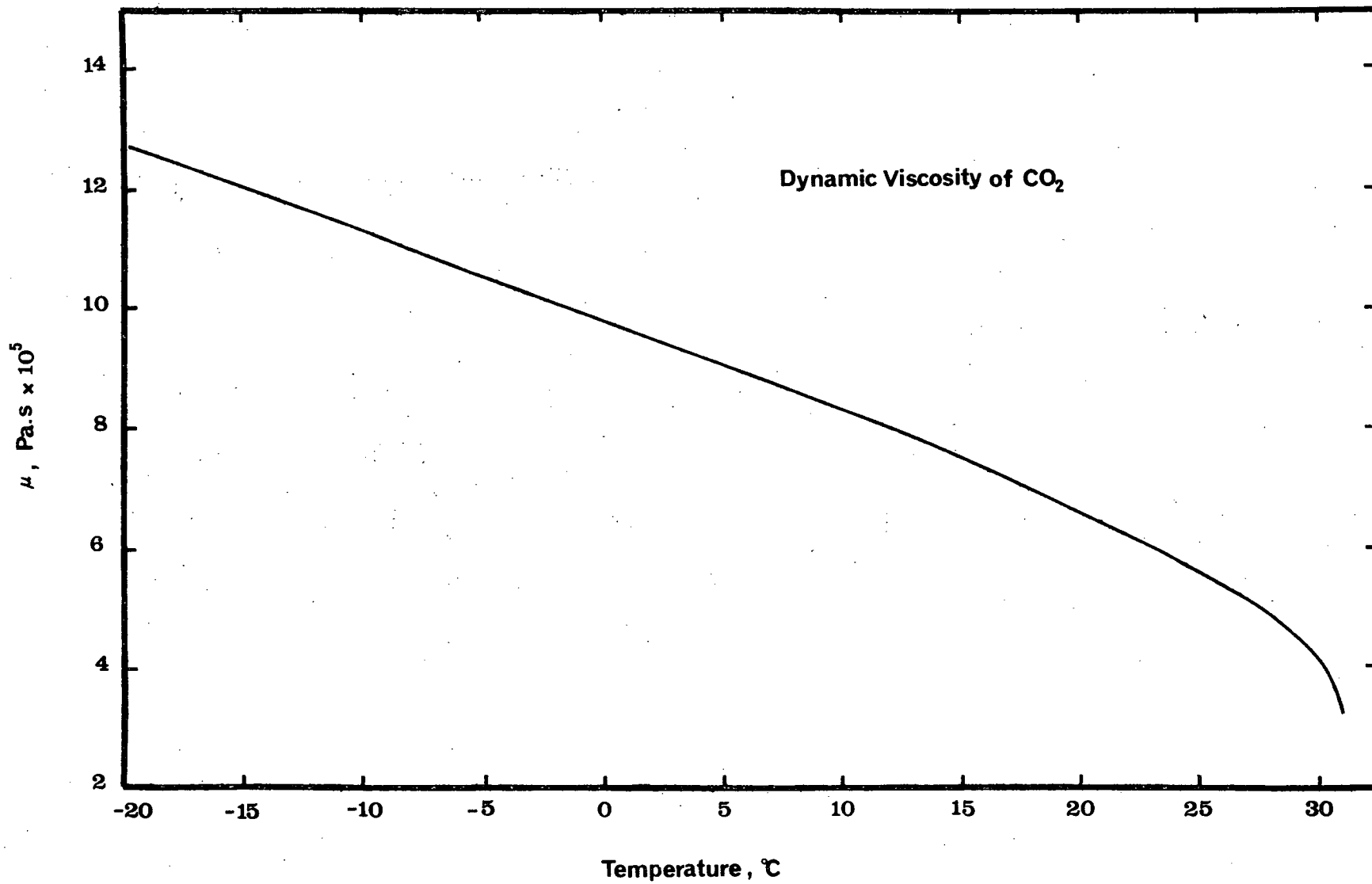


Figure 32 Dynamic Viscosity of CO₂

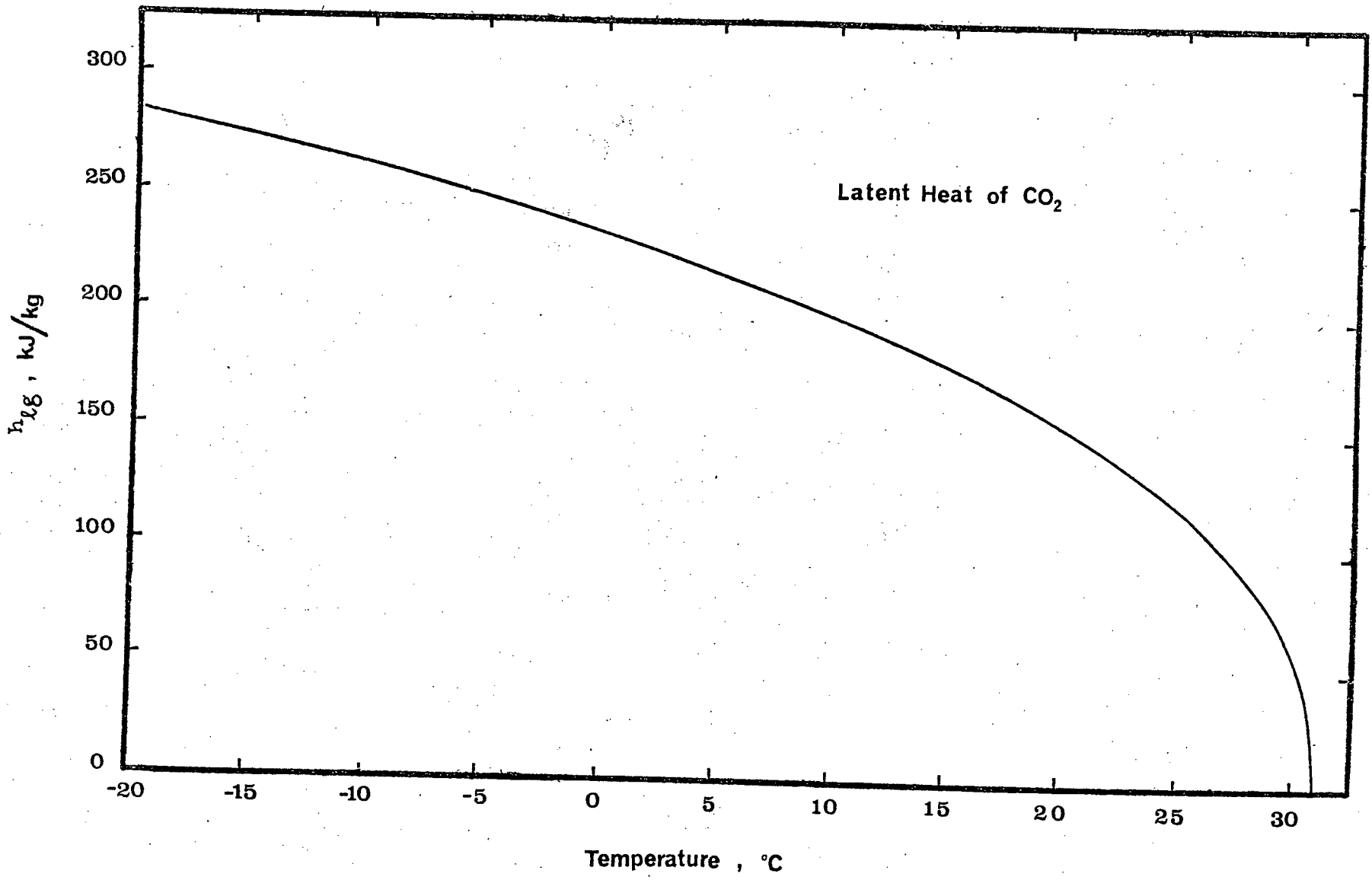


Figure 33 Latent Heat of CO₂

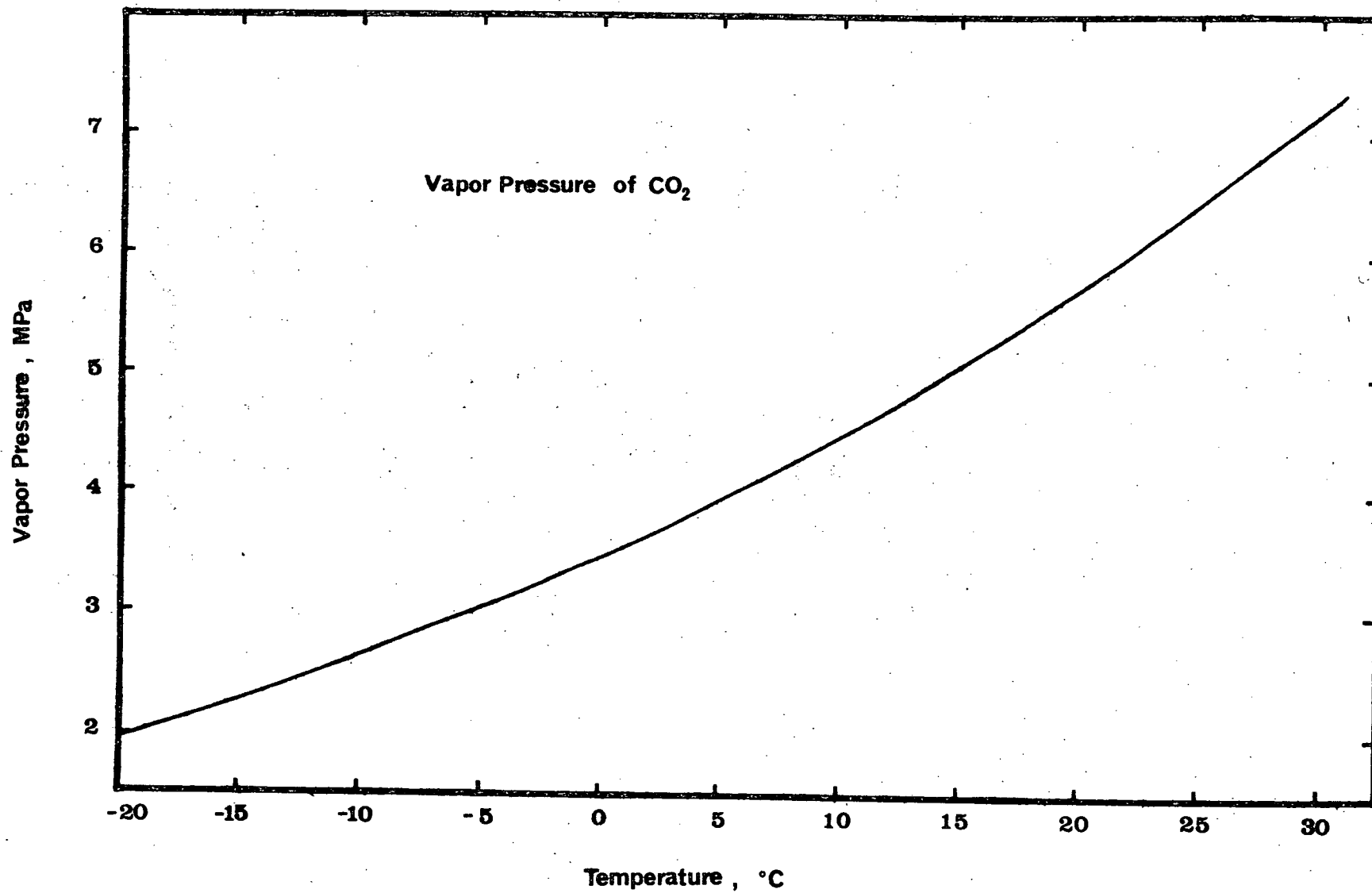


Figure 34 Vapor Pressure of CO₂